Silicon Nanowires: Monolithic Fabrication in Thick Silicon Layers and Nanomechanical Testing

by

Zuhal Tasdemir

A Thesis Submitted to the

Graduate School of Engineering

in Partial Fulfillment of the Requirements for

the Degree of

Doctor of Philosophy

in

Mechanical Engineering

Koc University

April 2015

Koc University

Graduate School of Sciences and Engineering

This is to certify that I have examined this copy of a Ph.D. thesis by

Zuhal Tasdemir

and have found that it is complete and satisfactory in all respects,

and that any and all revisions required by the final

examining committee have been made.

Committee Members:

B. Erdem Alaca, Ph.D. (Advisor)

Yusuf Leblebici, Ph.D.

Arda Yalcinkaya, Ph.D.

Demircan Canadinc, Ph.D.

Selim Hanay, Ph.D.

Antonia Neels, Ph.D.

Date: 10 April 2015

KEYWORDS

Nanowire

Mechanical properties

Micro-/Nano-fabrication

Top-to-bottom fabrication

Single crystal silicon

Bending

AFM- based bending testing

Large deformation

Beam theory

Finite element analysis

Stress measurement at the atomic scale

High resolution X-ray diffraction (HRXRD)

ABSTRACT

Nanowires have gained prominence in the fields of nanoelectronics and nano electromechanical systems thanks to continuous miniaturization of components and their utilization in day-to-day applications. Unique properties are exhibited by nanoscale structures due to quantum size confinement and an extremely large surface-to-volume ratio compared to their bulk-counterparts. Hence, mechanical characterization of these novel nanostructures is crucial in order to fulfill reliability requirements of these devices. A significant work still lies ahead in the mechanical domain due to challenges encountered inconsistent nanowire fabrication, manipulation, alignment and attachment in a test setup.

The primary aim of this study is to develop a top-down fabrication approach allowing monolithic fabrication of silicon nanowires in a thick silicon layer, either a silicon wafer or the device layer of an SOI substrate. This will ensure a good level of control on nanowire dimensions and orientation along with a permanent attachment to surrounding support structures. The second aim of this study is to characterize the mechanical integrity of resulting nanowires through a high-resolution testing approach.

For these purposes a fabrication technology is developed based on high-resolution lithography, directional etching, sidewall passivation and controlled undercut through deep reactive ion etching. Resulting nanowires exhibit widths (in-plane dimensions) between 20-80 nm, where a thickness (out-of-plane dimension) of 100 nm is demonstrated over very deep (10 μm) trenches etched in silicon. A wide range of aspect ratios with nanowire lengths ranging from 200 nm to 12 μm is achieved.

Following the successful demonstration of the fabrication approach, three-point bending experiments are conducted on silicon nanowires using atomic force microscopy. Tests are conducted under ambient conditions by using a PeakForce Quantitative Nanomechanical Property Mapping module. Both elastic and fracture behavior of

nanowires are captured. Results interpreted through analytical and numerical tools indicate the existence of a tensile intrinsic stress within nanowires.

This work provides a significant contribution to the monolithic fabrication of silicon nanowires where crystalline orientation, location and dimensions are solely determined by the layout design. Although an etch depth of 10 μm is demonstrated, guidelines are as well provided to increase the depth to 50 μm and beyond. The developed technology is unique and has important implications for future integration of nanowires with microsystems.

ÖZET

Günümüzde elektronik cihazlarda kullanılan elemanların sürekli küçülmeye gitme eğiliminin sonucu olarak küçük boyutlardaki malzemelerin fiziksel özelikleri merak edilmeye başlanmıştır. Malzemelerin küçük ölçekteki özellikleri- özellikle nanometre boyutlarında- büyük ölçekteki özelliklerinden son derece farklı olduğu gözlemlenmiştir. Bu farklılık nano ölçekte kendini göstermeye başlayan quantum kısıtlama etkisi ve yüksek yüzey alanı- hacim oranı etkisinden kaynaklanmaktadır. Nanotellerin elektonik ve elektromekanik alanlarında kullanılan aletlere küçülme ve performans arttırımı getirmesi umut edilirken bu küçük fonksiyonel birimlerin güvenilirlik ve dayanıklılık testlerinin yapılması gerekmektedir. Özellikle mekanik alanındaki güvenilirlik çalışmaları karşılaşılan bazı zorluklar sebebiyle literatürde çok az yer almaktadır. Bu zorluklar tutarlı nanotel numune üretimi, numune manipulasyonu, numune-test düzeneği hizalaması ve nanotelin test düzeneğine tutturulması şeklinde özetlenebilir.

Bu çalışmanın başlıca amacı tümden-gelim üretim yöntemi kullanılarak kalın bir silisyum tabakası ya da SOI alttaşının cihaz katmanı ile silisyum tel ile yekpare bir şekilde üretilmesidir. Bu yöntem ile nanotel boyut ve yönelim kontrolü, aynı zamanda da kalıcı olarak nanotelin yine silisyumdan yapılma tutanaklara yekpare olarak bağlanması sağlanmaktadır. Çalışmanın diğer bir amacı da önerilen üretim yöntemiyle üretilen nanotellerin yüksek çözünürlüklü test yöntemiyle mekanik bütünlük karakterizasyonu çalışmasını yapmaktır.

Bu amaçla ilk olarak yüksek çözünürlüklü litografi, yönlü aşındırma, yanduvar etkisizleştirme ve derin- yönlü iyon aşındırma ile kontrollü dip oyuğu yöntemleri kullanılarak nanotel üretim teknolojisi geliştrildi. Üretimi tamamlanan nanotellerin ebatları genişlik olarak 20 nm ile 80 nm arasında, kalınlık ise 100 nm olarak ölçülmüştür. Üretilen nanoteller 10 mikrometre derinlik üzerinde havada salınmaktadır. Uzunluk olarak ise 200 nanometreden 12 mikrometreye kadar geniş bir aralık taranmıştır.

Üretim yönteminin başarılı bir şekilde tamamlanmasını takiben, üretilen nanoteller üzerinde atomik- kuvvet mikroskobu kullanılarak üç-nokta-bükme deneyleri yapılmıştır. Ölçümler ortam şartlarında sayısal nano-mekanik özellik modülü kullanılarak gerçekleştirilmiştir. Nanotellerin elastik ve kırılma davranışları incelenmiştir. Sonuçlar analitik ve nümerik araçlarla tahlil edilip sonuç olarak üretim sırasında nanoteller içerisine hapsedilen iç gerilim stresleri olduğu gözlemlenmiştir.

Bu çalışma, silisyum nanotellerin boyutlarının, kristal yönelimlerinin, alttaş üzerindeki konumlarının sadece üretim serim tasarımı kullanılarak üretilmesi konusunda varolan bilgiye katkı sağlamaktadır. Aşındırma derinliğinin 10 mikrometre olarak gösterilmesinin yanısıra 50 mikrometre ve daha fazlası için gereken tasarım kriterleri de öngörülmüştür. Geliştirilen teknoloji eşsiz olup, gelecek nanotel- mikrosistem entegrasyonu uygulamaları açısından önemli bir yere sahiptir.

ACKNOWLEDGEMENTS

First and foremost, I would like to express my sincerest appreciation and thanks to my advisor, Associate Professor B. Erdem Alaca, who was abundantly helpful, and offered invaluable assistance, support and guidance, without his continuous motivation, this thesis would not be complete. Deepest gratitude is also due to the members of my thesis committee, Professor Yusuf Leblebici, Associate Professor Arda Yalçınkaya, Associate Professor Demircan Canadinç, Assistant Professor Selim Hanay, and Dr. Antonia Neels.

I would like to convey thanks once more to Professor Yusuf Leblebici, for hosting me in his laboratory (LSM) at EPFL, Switzerland for over a year. Great LSM people, Melinda Mischler, Tuğba Demirci, Ömer Çoğal, Selman Ergünay, Kerem Seyid, Mustafa Kılıç, Gülperi Özsema, Clemans Nyffeler, Jury Sandrini, Kadir Akın and Mahsa Shoaran (thanks for your support during my last days in Lausanne), Kiarash Gharibdoust, Jonathan Narinx, Can Baltacı, Vladan Popovic, Cosimo Aprile, lastly Dr. Davide Sacchetto for his great help and support in the first days in the cleanroom. I need to present my deepest appreciation to CMi staff, Dr. Zdenek Benes, Dr. Cyrille Hibert, Dr. Didier Bouvet, Joffrey Pernollet, Anthony Guillet, Guy Clerc, Patrick Madliger, Gatera Kumuntu, Adin Ferhatovic without whose knowledge and assistance the micro-nanofabrication part of this study would not have been successful. I would like to express my sincerest thanks to those beautiful people I happened to have the chance to get to know and work with in the same cleanroom: Xiaolong Wang, Ioulia Tzouvadaki, Valentin Flauraud, Dmitry Ovchinnikov, Daniel Toth, Elmira Shahrabi, Ryan Schilling, Jian Zhang, Francesca Puppo and Michele De Marchi for his fruitful comments and his ineffable help. Of course my friends in Lausanne, outside the labs, Laili Batooli, Dr. Özlem İpek, İrem Boybat, Merve Gürel, Emine Can, and Oliver Peric (thanks for being the best work-mate ever!), thanks for being with me in good and bad times.

I would like to express my deepest thanks to my MCL-groupmates at Koç, both current and previous and also my great friends, Dr. Jamila Kalantarova, (Dr. to be) İlknur

Eruçar, (Dr. to be) Zeynep Ülker, and (Dr. to be) Emine Güven Mayorov. Thanks for being patient with me in this tough road to becoming a Ph.D.!

Finally, I would like to express my love and gratitude to my beloved family, for their understanding and endless love through the duration of my study…

This work is supported by Tubitak under grant no. 112E058 and Koc University-Istanbul Rotary Club Fundamental Research Seed Fund Program.

TABLE OF CONTENTS

LIST OF TABLES

LIST OF FIGURES

Chapter 1 : Introduction

This chapter outlines the background (Section 1.1) and context/problem (Section 1.2) of the research. Section 1.3 describes the significance and contribution of this Ph.D. research work. Section 1.4 includes an outline of the remaining chapters of the thesis. Finally, the conceptual framework of this research is developed in Section 1.5.

1.1. RESEARCH BACKGROUND

Since this thesis involves in great deal of small structures, it would be descriptive to begin with explaining the term "Nanotechnology". According to the US National Nanotechnology Initiate [1], nanotechnology is the science, engineering and technology conducted at the nanoscale, which is about 1 to 100 nanometers. The ideas and concepts behind this new field of study firstly were laid foundations by Physics Noble Laureate, Richard Feynman, the father of nanotechnology. He gave many important far-sighed talks, but one of them is counted as inspiring and impressive speech which opens new gates into the current physics and scientific thought back to then is the talk he gave on December 29th, 1959 at the annual meeting of the American Physical Society at the California Institute of Technology (Caltech), then it was published in Caltech Engineering and Science journal in 1960 [2]. It is literally an invitation to enter a new field of physics, smaller world, titled as "There's Plenty of Room at the Bottom". In this speech, Feynman tried to convince the audience the possibility of making things "smaller" with the very strong supportive scientific facts. He visualized the things that can be done with the known physical knowledge and encouraged scientists to work on this new field of making things smaller. Furthermore, additional advantages of making things smaller are given to the audience inspiring scientists to study on this new field.

Unbelievably, almost all visionary ideas he suggested on that speech came true in today's scientific world. Storing the information in 24 volumes of Encyclopedia

Britannica onto the head of a pin area came true in 1985 by a Stanford graduate student named Thomas H. Newman. Furthermore, building a miniature motor no bigger than 1/64 inch cube constructed by William McLellan on November 28, 1960, that tiny motor weighs 250 micrograms and generates one millionth of a horsepower. Additionally, he put forward the idea of making the electron microscope more powerful on the same talk. Later on, two types of high resolution electron microscopes were invented: the transmission (TEM) in the year of 1960s and the scanning tunneling (STM) electron microscope in 1970s and the most modern microscope today in 1986, atomic force microscope (AFM) by Binning, Quate, and Gerber and made them earn the Nobel Prize for Physics for the their great development. So, the idea he gave in 1956, manipulating ad controlling individual atoms and molecules became realistic after the invention of these high resolution microscopes. The term of 'nanotechnology' firstly used by Norio Taniguchi in a conference, 1974 [3] to describe some micromachining processes having tolerances and accuracy on the order of several nanometers. However, the term had not been used until 1981 again. K. Eric Drexler used the term in his book [4], [5] finally popularized it. Since then, nanotechnology has developed rapidly and now it is widely accepted as the most significant technological frontier. For example, in the field of electronics, foundries currently develop technologies to fabricate integrated circuits components and structural features with a critical dimension down to 10- nanometers range. These dimensions are at least 1000 times smaller than typical biological cells. Materials and devices at the nanoscale have vast amount of potential for innovation in almost every industrial applications that will have a great impact on the everyday life of the society. It has been accepted as "the next industrial revolution" [6]–[16].

The reason behind the nanotechnology being the next industrial revolution is lying on the fact that when the dimensions of a material are reduced to the nano-scale, unique properties appear, due to the quantum size confinement in nanoclusters and an extremely large surface-to-volume ratio relative to bulk materials and thus high amount of particles (atoms/molecules) existing at reactive boundary surfaces. Scientists have already found

out unusual nano-scale materials with superior durability, electric conduction, heat conduction, thermal resistance, abnormal magnetic properties, etc. [17]–[33].

Nanowires (NWs), being one of the exciting type of the nanomaterials, have been heavily studied owing to their remarkable mechanical, optical, electrical and other properties [33]. These properties facilitate building of new sensor systems, opto-electronics, nano-electro-mechanical systems (NEMS)[34], [35], [35]–[38]. Having such vast and charming applications of NWs, the study of their properties turns out to be exceptionally critical and essential. There have been two ways of study in the literature so far; one is numerical simulation and modelling, the other one is experimental methods. In order to reveal the unknown properties of NWs, one should usually rely on the experimental methods. However, doing experiments at small scale raises some challenges, including the fabrication of samples as well as controlling the process parameters, handling small samples from a place to another and also even if the fabrication is completed well, in the next step, which is the measurement, there occur many problems, such as accuracy, building a new setup for holding small samples as well as reading out the small electrical or mechanical outputs. Although experimental studies provide a great deal of meaningful knowledge on the properties and performance of NWs, due to extremely small dimensions of nanostructures, implication of these experiments require vast amount of time, energy, manpower and intensive economic resource.

The main advantage of atomistic simulation study is to gain insight about the deformation mechanism of the NWs- for instance the dislocation movement observation under the loading. However, the existence of defects at the nanoscale great impact the behavior of NWs since relative amount of defects becomes highly comparable in the overall volume of the sample at the nano-scale. Although defects can be added into the model, the amount and the distribution of these defects inside the sample based on the assumptions usually, from the bulk material behavior. The true understanding of the properties and behavior of NWs could only be obtained through experimental methods. By experiments, it only becomes possible to get information about the real performance.

It also should be noted that the sample preparation technique becomes the real factor which influence the presence of defects inside the material, therefore experimental results should be evaluated as being case-specific, and it cannot be generalized for various NWs fabricated by different methods. An experimental study which reveals both mechanical behavior and deformation mechanism at the nano-scale is still rare in the literature.

In such a context, an experimental study of the NWs becomes highly necessary. There have been a number of studies about the mechanical characterization of NWs relying on AFM for bending, compression and nano-indentation [39]–[55]. However, the measurement results all lack consistency. These differences could be attributed to the randomness due to using different processed samples and/or to the measurement setup accuracy issues at the nano-scale. In this thesis, we aim to overcome these experimental problems and reveal a fundamental understanding of the mechanical properties of NWs.

1.2. RESEARCH PROBLEM

It has been stated so far that the NWs possess great mechanical, electrical, optical, thermal and many other properties, which enabled them to be under-studied and widely applied. Extensive amount of experiments have been carried out to shed light into the mechanical behavior of NWs, however they all lack consistency due to sample preparation and measurement challenges. Therefore, significant work still needs to be conducted to obtain an extensive understanding and knowledge of the properties and behavior of NWs. Additionally, the presence of defects inside the NWs have shown to dominate the overall performance and behavior of NWs but unfortunately, no quantitative study has been carried out up to now. Based on these circumstances, the questions aimed to be addressed in this thesis can be stated as follows:

- By which method should we fabricate nanowires which permits reliable mechanical measurement free from end-effects and in a controlled way?
- What are the mechanical properties and behavior of NWs under AFM-based bending loading?

- What is going on inside the structure of NWs after the fabrication and under loading? Which kind of deformation mechanism is responsible for the failure? Eventually, could we control the presence of the defects inside NWs?

1.3. SIGNIFICANCE AND CONTRIBUTIONS

A number of contributions have been achieved though this thesis, which are listed as below:

- A first micro-nanofabrication technique has been developed based on the top-down approach for a single suspended silicon NW with ultra-deep trench.
- A first fabrication of the single suspended silicon nanowire down to dimension of 30 nanometers has been achieved having a trench depth of 10 μm, allowing easy handling and loading for *in-situ* experiments.
- A first complete AFM bending test has been accomplished on the samples fabricated, revealing both process-related and nano-sized effects on the mechanical properties.
- A first deformation mechanism study on the atomic scale based on high resolution X-ray diffraction (HRXRD), revealing internal stress present inside the sample at the atomic level and/or during the loading.

1.4. THESIS OUTLINE

In this section, a brief outline of the chapters for the remainder of the thesis is presented.

In *Chapter 1*, the research background and problem are presented and discussed. The current knowledge and understanding of the problem has been discussed. Contributions of the study conducted have been stated.

In *Chapter 2*, a contemporary literature review is presented. This chapter begins with an overview of the unusual properties of NWs and their various applications demonstrating superior performance over their bulk-counterparts.

In *Chapter 3*, the emphasis will be on the fabrication technology developed for the NWs. The continuing sections reveal an understanding of the fabrication technology developed by means of several high-tech tools such as scanning electron microscope (SEM) and focused ion beam (FIB).

In *Chapter 4*, this chapter mainly focuses on the mechanical characterization of the samples fabricated. It begins with the bending experiment carried out with AFM, the results obtained and it continues with the preliminary HRXRD measurement result on the NWs fabricated.

In *Chapter 5*, the emphasis will be on the verification and the validation of the measurement results obtained in Chapter 4. Process related internal stress will be speculated quantitatively.

In *Chapter 6*, this chapter solely discusses the process flow developed for the micro-system- NW integration at the Center of MicroNanoTechnology Center (CMi) in Switzerland.

In *Chapter 7*, major conclusions, limitations and recommendations of this research will be presented.

1.5. FRAMEWORK OF THIS THESIS

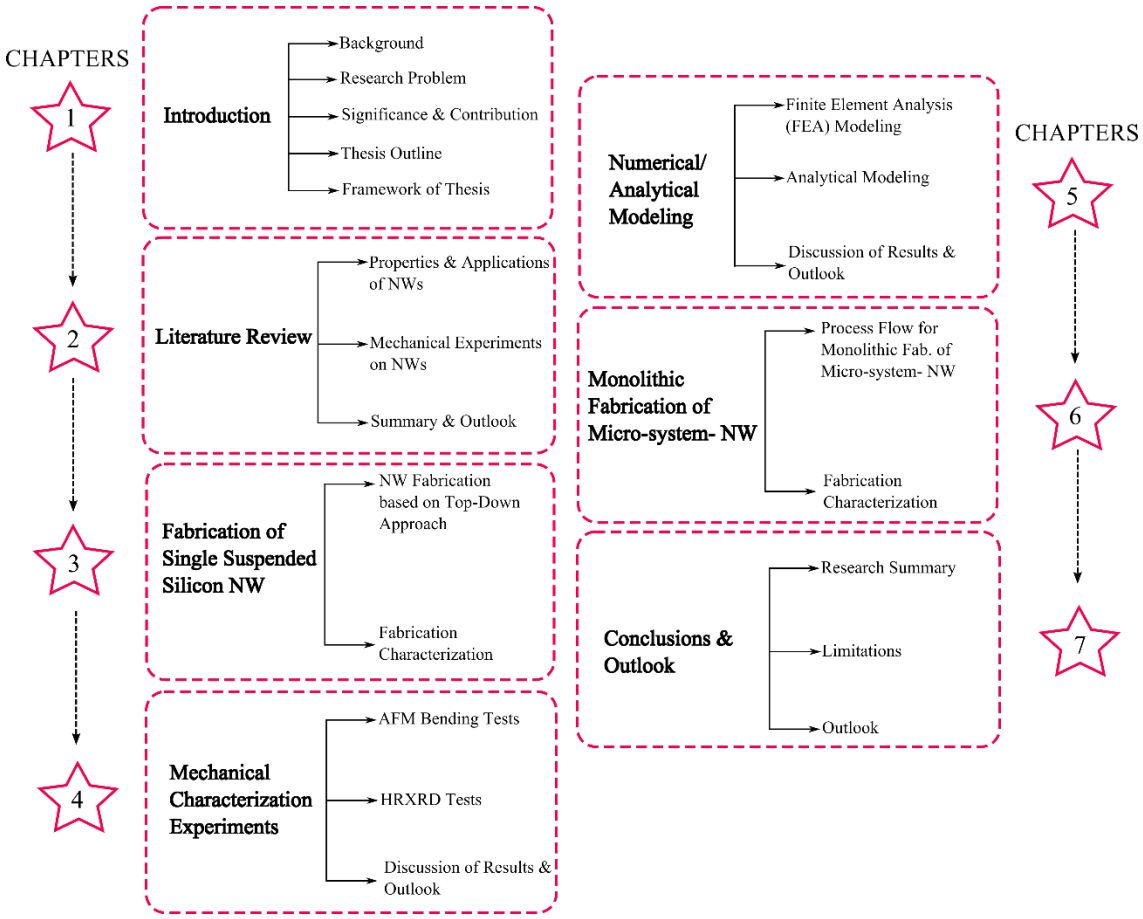

Chapter 2 : Literature Review

This chapter presents an overview on the various applications and striking properties of NWs, Section 2.1. In the later sections, studies done on the NWs will be summarized, beginning with studies done on NWs revealing unique properties, Section 2.2 and finalized with the various experimental techniques employed to characterize mechanical properties of NWs, Section 2.3.

2.1. AN OVERVIEW ON NANOWIRES

NWs have known to be intriguing structures for the past several decades. It has been popular after a few years later when the carbon nanotubes were discovered in 1991. NWs are generally termed as 1D- structures since two of their dimensions are in the nanoscale regime, giving them unusual electrical and optical properties due to quantum confinement effects [33], [56], [57]. However, unlike other 1D structures such as quantum dots, the length of NWs could extend to a few hundred micrometers which allow them easily connect to the outside macro-world [58]. No other materials can be produced with these high aspect ratios. This high aspect ratio also gives them a high surface-to-volume ratio making NWs superior structures for chemical or biological sensors since there exists a high percentage of atoms/molecules lying at reactive boundary surfaces [59]–[64].

Having superior mechanical, electrical and optical properties have enabled NWs to become ideal building blocks of opto-electronics, sensors systems, and nanoelectromechanical systems [37], [65], [66]. For instance, based on vibration of nanowires at very high frequency range, 7 zepto-gram mass resolution is achieved corresponding to the mass of 30 Xenon atoms in 2006 [67]. After six years, another ultra-high resolution nanomechanical mass sensor has been developed reaching a single proton mass limit [68]. Xiang *et al.* [69] showed that semiconducting nanowires are potential

alternatives to MOSFETs due to their unique electronic structure and reduced carrier scattering caused by 1D- quantum confinement effects. To reveal mechanical properties of NWs, great amount of experimental work including *in-situ* SEM/TEM measurements has been carried out despite a common consensus [17]–[22]. Recently, AFM-based mechanical measurements have been conducted as well due to the ease in the force exertion by the small-scale AFM tip which is in similar dimensions with the nanowires [76]. Richter *et al.* [77] found out that the properties of nanomaterials can be tuned by controlling defect and flaw densities. Seo *et al.* [78] reported that the defect-free Au NWs show superplasticity on tensile deformation. However, today's nanomechanical research on 1D- structures is still incomplete due to the difficulty in manipulating and testing these structures with current experimental techniques.

2.2. ENHANCED PROPERTIES OF NANOWIRES

As aforementioned in Section 2.1, unique properties emerge when materials are scaled down to the nanoscale due to quantum size confinement and an extremely large surface-to-volume ratio relative to their bulk counterparts. Up to now, scientists have reported many enhanced properties of NWs such as superior mechanical durability, electric conduction, heat conduction, thermal resistance and so on. Some of these properties will be presented as below:

2.2.1. Mechanical Properties:

The scaling effect in mechanical properties of materials; the change in mechanical properties of materials was firstly shown by Galileo Galilei in the year of 1638. He mentioned in his final book named "Dialogue Concerning Two New Sciences" which is translated to English in the year of 1914 for the first time, that on smaller scales, gravity becomes less and less important and he exemplifies this as large wooden rods will break while all the shorter ones will be strong enough to support something more than their own weight; "this which I have said about the ability to support itself must be understood to apply also to other tests; so that if a piece of scantling will carry the weight of ten similar

to itself, a beam having the same proportions will not be able to support ten similar beams" [79]. First experimental evidence on scale dependence for a brittle solid - cast iron in this case – was then provided by da Vinci, where higher strength with reduced sample volume was reported along with the observation of significant statistical distribution [80]. Back to date, in 1920, Griffith, have stated that wires or fibres might be expected to be stronger than large ones, as there must be some additional restriction on the size of the flaws. He also stated that "sufficiently fine wires, this effect should be enormously greater than is observed in ordinary cases since a fiber consisting of a single line of molecules must possess the theoretical molecular tensile strength" [81]. Statistical foundations were laid out by the seminal work of Weibull in 1939 [82]. In the year of 1947, N. Davidenkov *et.al* [83] in Journal of Mechanics showed the influence of size on the brittle strength of steel by performing tension tests on various samples of steel. The results suggested that 10% decrease in diameter resulted in 30% increase in brittle strength, or in another words, ultimate tensile strength of steel. Some recent work done by researchers on various NWs including metal NWs such as Au [72], [84], Ag [85]; also some metal oxides NWs [86]–[88] and semiconducting NWs such as Si [70], [89], Ge [90]. These studies highlighted the importance of size on strength of materials catalyzing the manta of "smaller is stronger!"

2.2.2. Electrical Properties:

NWs have been widely employed as active channels in field effect transistors (FETs) with expectation to be the next building blocks for high frequency integrated electronics, i.e., memory element, logic gates [91], [92]. Moselund *et al.* [93] showed that SiNWs based tunneling FETs yielding an I_{on}/I_{off} current ratio of around 10^6. Another study done by Xie *et al.* [94] has proved that a nanowire-nanopore sensor for the local electrical potential detection of DNA could be achieved by combining the solid-state nanopores with SiNWs FET. Several semiconductor devices such as junction diodes, memory cells and switches, transistors, inverter, and many others have been fabricated using NW junctions. Effective contact between nanowires and electrodes is crucial for

obtaining nanoscale electronic devices, so it has shown by Sakurai et al. [95] that Ga doped ZnO nanowires make better electrical contact. Based on SiNW with the cross section of 10 nm by 30 nm, high performance SiNW n- and p-based FETs are reported having high on/off ratio, low drain-induced barrier lowering [96].

2.2.3. Magnetic Properties:

Due to small scale, NWs with high surface-to-volume ratio thus less atomic coordination through the nanostructure itself and less degree of bonding result in more localized electronic states in addition to narrower bands and larger density of states thus imposing novel magnetic behaviors [97]. Moreover, some materials which are formed in NWs i.e., Pd and Pt NWs, are found to be ferromagnetic up to room temperature, suggesting some promising applications in memory-effect related spintronics [98].

2.3. MECHANICAL EXPERIMENTS ON NANOWIRES

As mentioned in the previous section, NWs have found immense applications in various fields. Thus, understanding the mechanical and physical properties of NWs is crucial for both scientific and technological point of view. Once we understand how the properties are governed inside these small materials, we will have the chance to tune the properties according to a specific guideline. So far, many experimental studies have been conducted, however, although experimental methods provide realistic and meaningful information of the mechanical behavior of NWs, due to their extremely small dimensions of NWs, the application and manipulation of these experiments involve huge challenges in terms of sample fabrication, handling the small scale sample and also small-scale measurement setup with high resolution. Experimental questions that need to be addressed are listed as follows:

- How to fabricate small dimensions of samples with good geometric tolerances?
- How to measure the dimensions of small samples that cannot be imaged with conventional optical methods?
- How to measure and apply small forces with high dynamic range?
- How to manipulate and grip small specimens?

2.3.1. Tensile Experiments:

Tensile testing at the macro scale have been studied in great detail and there are already some standards, i.e., ASTM standards, about how to perform these test in this scale. However, the techniques at the macro scale cannot be simply scaled down to micro /nano-scale due to issues addressed before.

Tensile testing is performed by stretching and pulling the sample where load is applied uniaxially and the resulting stress and strain state is nominally uniform in the specimen. The interpretation of the data is fairly straightforward since the data can be processed directly. As a downside of this method, the application has many problems such as specimen manipulation and gripping without any end effects between the sample and the testing device, actuation and force-displacement measurement with high sensitivity and accuracy [99], [100]. To eliminate the problems of alignment and gripping, co-fabrication of the specimen together with the testing devices has been proposed by M.A. Haque and M.T.A. Saif [101]. They co-fabricated and performed tensile testing of thin metal films with a thickness of 30 nm. H.D. Espinosa *et al.* reviewed the state-of-the-art of mechanical characterization of 1-D nanostructures and pointed out that the biggest challenge is the handling of extremely small specimens [102]. Therefore, micro-and nano-manipulators together with high resolution imaging systems are widely employed to locate, attach, transfer and manipulate these small specimens to the desired testing

platform. Many in-situ SEM/TEM experiments have been conducted with the help of the micro- and nano-manipulators [103], [104].

On the other hand, compression tests are very similar to tension tests in terms of loading situation. Compression type of test is mainly used to study the buckling behavior of NWs. Buckling behavior of NWs such as SiNWs [105], [106] have been investigated.

2.3.2. Bending Experiments:

Due to the ease of manipulation, force exertion and alignment, bending type of tests are mostly employed to study mechanical properties of materials [47], [107]–[110]. This method involves bending of the beam which can be in cantilever or double-clamped configurations by exerting force on the beam directly with the help of a wedge or AFM tips. These tests are used to determine the reliability and elastic properties of Si-based MEMS systems [106] as well as to find the plastic deformation properties of single crystals [111] and also biological materials [112]. Stiffness of the support, substrate properties and contribution of the indenter stress field and positioning of the indenter itself are considered during modelling of the actual stress present in the beam during the loading [113].

2.4. SUMMARY AND SCIENTIFIC MOTIVATION

Mechanical tests at small length scale is an attractive field of research and technology since it provides an answer how materials differ at small scale when compared to their bulk-counterparts. As mentioned in previous sections, many studies have been conducted to study mechanical properties of NWs so far. However, literature still lacks a consistent set of data for NWs. Difficulties arise in terms of sample clamping, precise manipulation and alignment and accurate measurement of the response, e.g. force, displacement.

Furthermore, sample fabrication is also problematic. Fabrication at the nano-scale is not yet controllable so even the samples fabricated in the same batch differ greatly from

each other. These differences may be attributed to fabrication induced geometric inaccuracies and also defects inside the material nanostructure induced by fabrication process or at a later stage. To fill this gap, sample fabrication is to be carried out in a repeatable fashion and also measurement is to be carried out without any support effect.

Chapter 3 : Fabrication of Single Suspended Silicon Nanowires

This chapter details all fabrication work done at the class 100 cleanroom facilities of EPFL, Switzerland namely The Center of MicroNanoTechnology (CMi).

Fabrication process flow for single suspended silicon nanowire with an ultra-deep trench will be presented, this will be followed by the fabrication characterization by high resolution electron microscopes: scanning electron microscope (SEM) and focused ion beam (FIB).

3.1. SINGLE SUSPENDED SILICON NANOWIRE WITH ULTRA-DEEP TRENCH

In this part of the study, we explore the limits of batch fabrication of a single silicon (Si) NW within a very thick Si layer with two objectives contradicting the aforementioned approach [114]. First, NW is not formed in a separate Si layer, but 'carved' from the same Si crystal, which will later (Chapter 6) form the rest of the microscale device. Second, it is aimed to keep the Si NW at the wafer surface for the ease of processing such as doping and contact formation. Hence, one can pursue a unique set of surface processes apart from the comparatively straightforward MEMS fabrication, as Si NW does not remain buried at the bottom of a thick Si layer.

To achieve this set of objectives, we revisit the well-known SCREAM (Single Crystal Reactive Etching and Metallization) process [115], [116] that played an important role in the surface micromachining of electrostatic devices. The backbone of SCREAM was formed by an important sidewall passivation step, which would provide protection during isotropic release etch. The approach allows versatility with new combinations of materials [117]. Thinking along similar lines, one can argue that the same approach

should work at the nanoscale. If one can define a nanoscale line protected with a conformal sidewall coating, one can, in principle, etch deep into the substrate without damaging the protected line of material. How deep one can etch the substrate while preserving the integrity of Si NW is an interesting question and forms the motivation of this work.

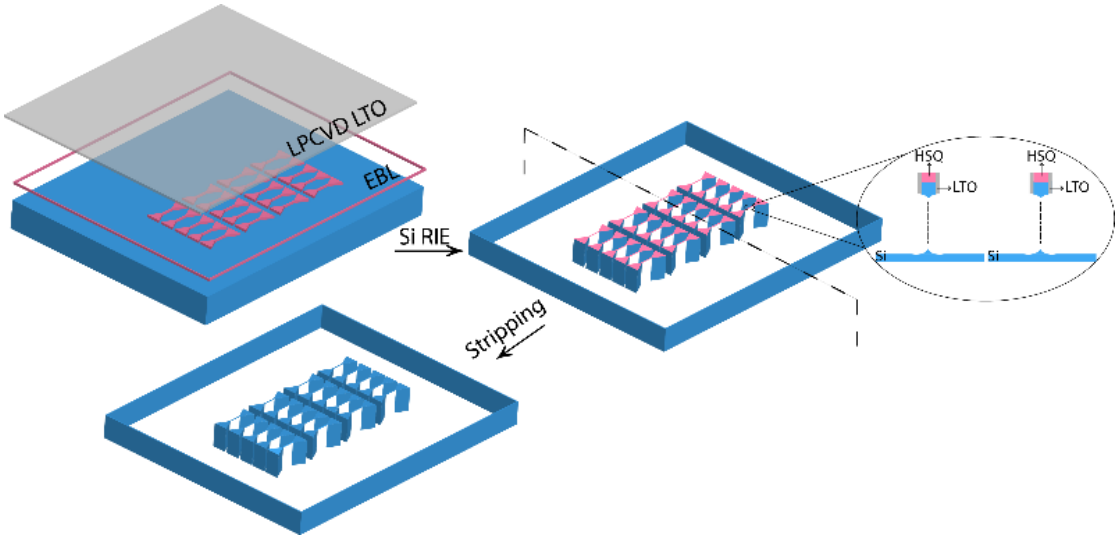

Figure 3.1. Overview of the process flow for the single suspended Si NW fabrication.

Proposed approach consists of using e-beam lithography for the patterning and LPCVD-LTO coating for the sidewalls protection during NW forming at reactive ion etching (RIE) step, Figure 3.1. It relies on high-resolution lithography to define the location of Si NW. For demonstration purposes e-beam lithography was used throughout this work. This is the only patterning in the whole process and is followed by a nanoscale etching step. A conformal coating is carried out, which is later removed from horizontal surfaces using reactive ion etching (RIE). A deep Si etch (DRIE) is then carried out constituting the most critical aspect of the fabrication process, as the etch recipe should allow adequate undercut to form a Si NW, while not attacking it chemically from its unprotected bottom surface. Finally, all protective layers are removed to release Si NW.

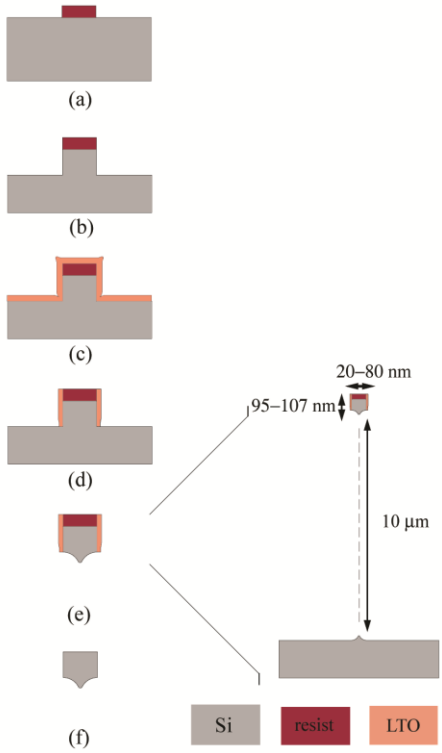

Figure 3.2. Process flow for single suspended Si NW.

The process begins with the definition of e-beam resist HSQ (Hydrogen silsesquioxane) lines on a <100>, p-type, 100-mm Si wafer with a thickness of 525±25 micrometers and a resistivity in the range 0.1-100 Ω-cm Figure 3.2.(a). Resist thickness is kept at 200 nanometers. Linewidths between 20-80 nanometers are patterned with e-beam doses of 2000-5000 $\mu C/cm^2$. This dimension directly translates into Si NW width. HSQ is then used as an etch mask for the subsequent RIE process Figure 3.2.(b), where Cl_2 gas is used with a flow rate of 50 sccm and pressure of 5 mTorr with platen RF power of 100 W and coil RF power of 800 W in Surface Technology Center (STS) Multiplex Inductively Coupled Plasma (ICP) plasma etcher. The etch depth is kept at 150 nanometers. This depth is monitored through control windows etched over the same substrate, as it is one

of the critical parameters determining the thickness of the resulting Si NW. Low-temperature oxide (LTO) is chosen as the conformal coating of Figure 3.2.(c). LTO is deposited in a Centrotherm furnace at 425 °C temperature and at a pressure of around 100 mTorr by Low Pressure Chemical Vapor Deposition (LPCVD) yielding a coating thickness of 80 nanometers. LTO is then etched from lateral surfaces in a fluoroform plasma in SPTS Advanced Plasma System (APS) ICP-based high density plasma etcher as depicted in Figure 3.2.(d). The removal of LTO is as well monitored through control windows on the same substrate. At this stage one achieves a clean, exposed Si surface, where discrete Si lines are protected by LTO on the sides and by HSQ at the top. A DRIE recipe is developed consisting of alternating steps of plasma etching and passivation Figure 3.2.(e). This recipe is optimized to produce an adequate scallop size allowing the release of Si NW at the end of the first cycle of etching. Specifics regarding the recipe can be seen in Table 1. Further cycles of etching are carried out to obtain a single Si NW over the desired trench depth. Using HSQ as the only mask material at the top it was possible to obtain a maximum etch depth of 10 micrometers. Under the conditions listed in Table 1, etching process takes about 240 seconds. Finally, both LTO and HSQ are removed by hydrofluoric acid (HF) vapor etching at 40 °C, Figure 3.2.(f). Details of the recipe development work including e-beam lithography dose calibration and also etching time is given in Appendix-A.

The minimum selectivity of HSQ over Si under the conditions given in Table 1 is estimated to be 1:50. While LTO does a better job in protecting the side walls, HSQ thickness seems to be the main limiting factor, as prolonged etching is always observed to lead to the loss of HSQ protection from the top surface. In principle, it is possible to tailor the process for etching needs deeper than 10 micrometers. For instance, one can choose to utilize a thicker HSQ layer, which, however, might jeopardize lithographic resolution. One can equally choose to utilize another mask material with a higher selectivity against Si, which, in turn, will increase process complexity. Nevertheless, using presented HSQ and LTO thicknesses one can achieve 10 micrometers without

further complications as the preliminary results indicate. This provides a considerable advantage, as a device thickness of 10 micrometers is frequently used in all-Si MEMS applications [114].

Table 3.1. Deep Reactive Etching (DRIE) Recipe Details

Priority	Gases	Flow Rate (sccm)	Pulse Time (seconds)	Source Generation Power (W)
1	C_4F_8	150	2	1800
2	SF_6	300	6.5	1800

Characterization of the Fabrication by SEM & FIB

An array of resulting Si NWs is shown in Figure 3.3.a. Opposing triangles represent supports, which are spanned by Si NWs over a wide range of widths between 20-80 nanometers. An aspect ratio (defined as length/width) range of 10- 150 is chosen leading to a Si NW length window between 200 nanometers and 12 micrometers. Furthermore, a high process yield is evident from the micrograph of Figure 3.3.a, indicating suitability for batch fabrication. Figure 3.3.b and Figure 3.3.c depict a Si NW with the smallest width of 20 nanometers, and a moderate width of 30 nanometers, respectively. Average Si NW thickness (out-of-plane dimension defined by the first RIE step of Figure 3.2.(b) is observed to be 100 nanometers (close-up provided as an inset). The reduction of 150 nanometers thickness related to RIE etch depth of Figure 3.2.(b) to 100 nanometers obtained after DRIE is an indication of isotropic etching of Si over its unprotected bottom surface. Midsection of Si NW is further thinned down to 95 nanometers, whereas near the supports Si NW thickness increases to 107 nanometers. As etching from the bottom takes place in a mass-transport-limited fashion, midsection of each SiNW is exposed to a higher isotropic etching rate due to faster diffusion away from the supports. It is to be noted that this loss of Si from the bottom would be the major limiting factor for the overall etch depth, if one used a thicker HSQ mask or a more resistant mask material for the DRIE step as discussed above. Similarly, replacing DRIE

with an isotropic release step such as a high-pressure RIE process was observed to pose significant challenges regarding Si NW height and overall etch depth [118]. Under the present conditions reported in this study, a final thickness uniformity within 10% is obtained. More data on the cross-sectional uniformity and dimensions will be provided in the upcoming FIB discussion.

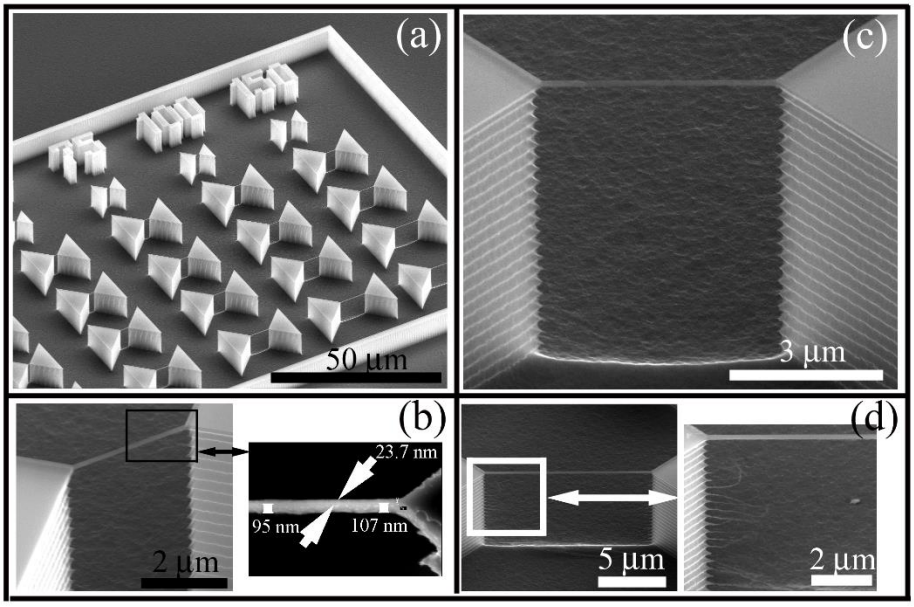

Figure 3.3. a) An array of Si NWs. Numbers at the top correspond to Si NW aspect ratios. b) Si NW with the minimum achievable width of 20 nm. Average Si NW thickness is on the order of 100 nm with a reduction towards the midsection of Si NW. c) Si NW with a width of 30 nm and an aspect ratio of 150. d) Si NW with the maximum width of 80 nm. Remnants of DRIE in the form of discontinuous Si lines are visible for this thick Si NW

The meaning of a successful recipe optimization is clear in Figure 3.3.(d) showing a Si NW with the maximum width of 80 nanometers utilized in this study. Residual Si fibers, remnants from DRIE of Figure 3.2.(e), appear for the first time at this width level, as the undercut associated with the recipe of Table 1 apparently removes all Si underneath Si NW for smaller widths. As the sum of the resist width defined by the lithography of Figure 3.2.(a) and LTO sidewall coating thickness of Figure 3.2.(d) define the maximum linewidth to be etched for a complete release of Si NW, adequate SF_6 etch time is

necessary. An array of Si NWs as reported previously [119] are observed to survive for shorter durations of SF_6 etch time than that mentioned in Table 1. Although the current recipe is shown to operate successfully up to a Si NW width of 80 nanometers, this observation raises a further opportunity to define the number and location of multiple Si NWs, if one chooses to run a combination of different durations for SF_6 etching step.

To determine exact thickness and shape of resulting Si NWs, a cross-sectional study is further carried out by using Focused Ion Beam (FIB) (FEI Nova 600 NanoLab Dual Beam- SEM/ FIB). Prior to the milling of SiNWs, they are first coated with an about 20-nanometers-thick Pt layer by atomic layer deposition (ALD). This step is necessary as it enhances contrast during scanning electron imaging and thereby increasing the quality of dimensional characterization. ALD is carried out by using (methylcyclopentadienyl) trimethylplatinum (MeCpPtMe3) and oxygen as precursors at 75 °C and at room temperature, respectively. Reaction chamber is kept at 280 °C.

Si NWs in total number of ten (10) with sizes of 20-40 nanometers in linewidth with aspect ratios of 50, 75, 100 and 150 are studied under FIB. Si NWs are cut both at the center and in the vicinity of one of the supports, indicated as AA' and BB' in Figure 3.4.(a), respectively. All Si NWs studied under FIB exhibited a rectangular cross-section with the maximum thickness at the anchors at both ends. This thickness is then observed to decrease by about 10 % towards the middle. Similar phenomenon is evident in the micrograph in the inset of Figure 3.3.b. On the other hand, the width as defined by e-beam lithography also increases by 10 % due to the backscattering effect (proximity effect) of the transmitted electron beam [120].

As an example, one can consider the 40-nanometers-wide Si NW depicted in Figure 3.4.(a). The increase of both width and thickness from the center, Figure 3.4.(b) to the support location, Figure 3.4.(c) is evident. A close-up of cross-section near the support is given in Figure 3.4.(d) as well. The existence of a 16-18 nanometers-thick Pt sheath as well as a rectangular cross-section is evident.

However, Figure 3.4 shows that cutting the nanowire in different position along the length and imaging those sections with SEM could not reveal the native oxide thickness around the silicon nanowire, which has been reported to have influence on the overall mechanical properties of nanowires at the nano-scale. Thus, we need HR-TEM imaging in order to carry out a dimensional study on the native-oxide thickness on these small scales of nanowires.

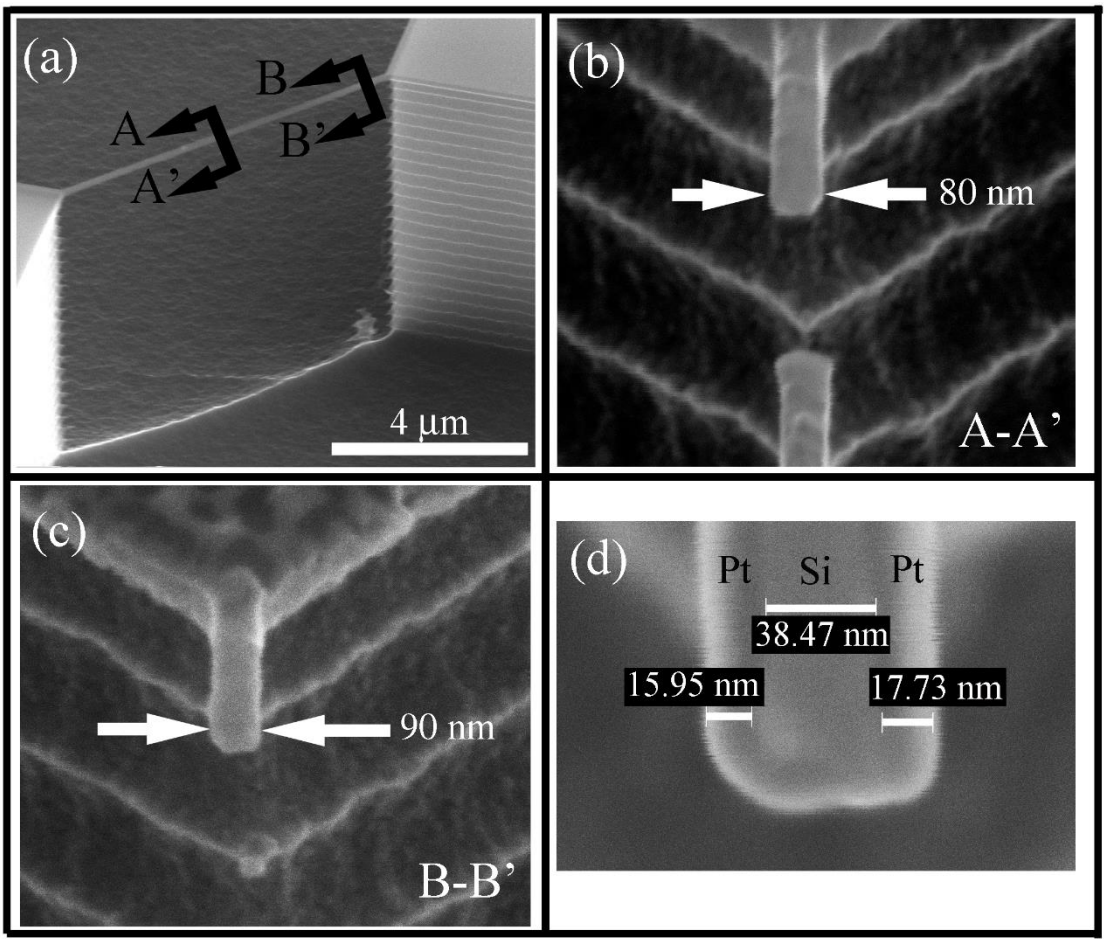

Figure 3.4. a) 40-nm-wide Si NW with cross-sections marked for FIB study. b) A FIB cut near the midsection reveals a width of 80 nm indicating a Pt coating thickness of about 20 nm. c) Cross-section near the anchor. d) A close-up showing Si core enveloped by Pt.

Chapter 4 : Mechanical Characterization Experiments

After fabrication and dimensional characterization, the mechanical integrity of silicon NWs was tested through a three-point bending experiment using an atomic force microscope, AFM (Bruker Dimension Fast Scan). AFM enables bending tests at the nanoscale with its high-resolution force measurement capability and high spatial resolution [121]–[126]. Bending tests are carried out using the quantitative nanomechanical property mapping mode (PeakForce QNM) with FastScan-A cantilevers. The cantilevers are calibrated with the thermal tuning method [127] and the correction factors are taken into account through the native AFM software [128]–[130].

This chapter presents study on the bending type structural characterization experiments, Section 4.1, and some preliminary High Resolution X- Ray Diffraction (HR-XRD) experiments, Section 4.2, conducted on the fabricated nanowires presented in Chapter 3, Section 3.1. This first part is done in close collaboration with the Laboratory for Bio- and Nano- Instrumentation (LBNI) at EPFL. The second part is carried out with X-Ray Laboratory at EMPA, Swiss Federal Laboratories for Materials Science.

4.1. AFM BENDING EXPERIMENTS

Researchers have used the scanning probe microscope (SPM) to obtain the force on the tip versus its vertical position [131]–[135]. The resulting force curves will then be analyzed to determine various types of material properties of the sample beneath the tip. However, these force curves can only provide data at one point on the sample. Later, there emerged another technique called force-volume imaging [136], with this technique, it was possible to collect force-volume curves at each pixel in an image and integrate that information to get a map of the properties across a larger sample. Although it delivers more information, it is very slow to collect the data at each and every point of the sample,

making the experiment inefficient and time-consuming and impractical. However, recently, this technique has been improved further more after the development of tapping mode imaging in 1993. In tapping mode, the cantilever is vibrated near the resonant frequency of itself while it scans across the whole sample. The tip only contacts the surface of the sample for a very short time, keeping the tapping force and measurement time low. Because the cantilever is oscillating, it experiences attractive and repulsive forces depending on its position in the cycle. A drawback to this technique is that the resonant behavior of the cantilever also act as a filter, making it impractical to reconstruct the force curves with sufficient precision to extract quantitative mechanical information. Later, in 2008, another technique developed to solve this problem, however, as downsides of it, it requires special cantilever and the operation can be complicated and the interpretation of the results is difficult. Recently, a new technique has been developed by Bruker Company called 'Peak Force QNM (Quantitative Nano Mechanics). Peak Force QNM uses Bruker's new peak force tapping technology for system feedback to deliver a number of important benefits.

The AFM experiments is carried out by using a recent and special module of Bruker Peak Force Tapping mode, called Peak Force QNM (Quantitative Nano Mechanical Mapping) as mentioned in the previous paragraph. It is designed to measure materials properties quantitatively at the nano- scale such as modulus, adhesion, deformation, and dissipation. Peak Force Tapping mode controls the force applied by the cantilever by calibration of the stiffness of cantilever in certain measurement limits which is around 15% [137]. In this mode, the Peak Force Tapping mode, since the cantilever oscillates far below the cantilever resonant frequency, the vertical motion of the cantilever using the (main) Z piezo element and relies on peak force for feedback. Peak interaction force and nanoscale material property information is collected for each individual tap.

The first challenge we came across was to find the position of the nanowire on a 4-inch wafer and then accurately place the AFM tip in the middle section of the sample, on which later on we aim to exert force and measure the max. deflection exactly at this

point. Our first approach was to see, whether it is possible to image a nanowire. If this is possible, we can easily place the tip of the cantilever in the middle of the beam, at the point of maximum deflection. Depending on the AFM cantilever used, the correct placement using only the optical image of the sample and the cantilever is very hard to accomplish.

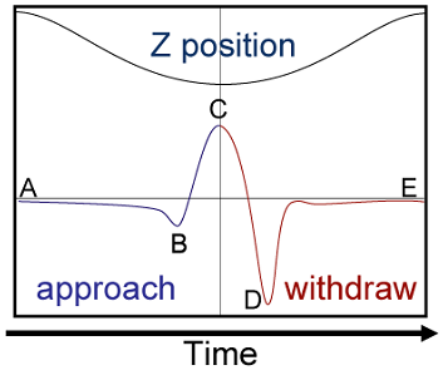

Figure 4.1. Force vs. distance curves for approach (blue) and retract (red), also called 'heartbeat'. 'B' represents the initial contact of the cantilever with the sample surface, 'C' is the point of maximum force applied, and 'D' is the adhesion [138].

Using the Z-position information, the heartbeat is transformed into a force curve, Figure 4.2. The force curve plot is analyzed to produce the peak interaction force as the control feedback signal and the mechanical properties of the sample (Adhesion, Modulus, Deformation, and Dissipation).

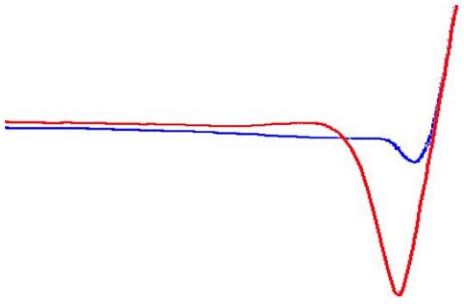

Figure 4.2. Traditional force and piezo-Z position curve [138].

4.1.1. Calibration Routine before Measurement

In order to quantify the forces and as well as other mechanical properties, calibration routine should be followed thoroughly for each cantilever used and even before every measurement session. Cantilever stiffness and deflection sensitivity should be well calibrated before beginning of the measurements.

a) Deflection Sensitivity Calibration:

Because Peak Force QNM mode ramps the Z piezo and acquires force curves, measuring deflection sensitivity requires fewer steps than the normal ramp procedure. The steps that we follow using the deflection sensitivity is explained as follows:

- Engage the tip onto a clean sapphire (especially if the cantilever stiffness is larger than 100 N/m) or onto the same wafer with the nanowires using the Peak Force QNM in Air mode.
- Activate the Ramp mode and apply force which you would like to apply onto the samples.
- Move two cursors onto the Deflection vs. Z plot, Figure 4.3.
- Arrange the cursors so that they surround the steepest portion of the graph, Figure 4.3.

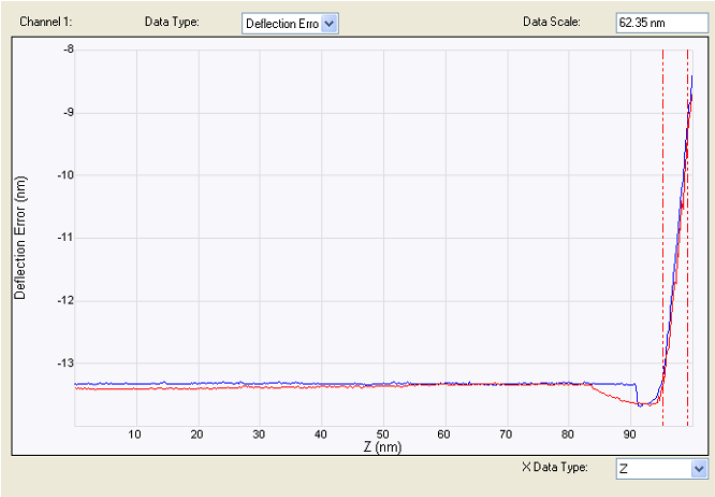

Figure 4.3. Deflection error (nm) vs. Z (nm) force curves for the measurement of deflection sensitivity.

- Select Ramp > Update Sensitivity from the software. It will automatically calculate the deflection sensitivity and open the Set Realtime Channel Sensitivities window, Figure 4.4.
- By clicking on the OK on this window, Figure 4.4., deflection sensitivity value will be updated.

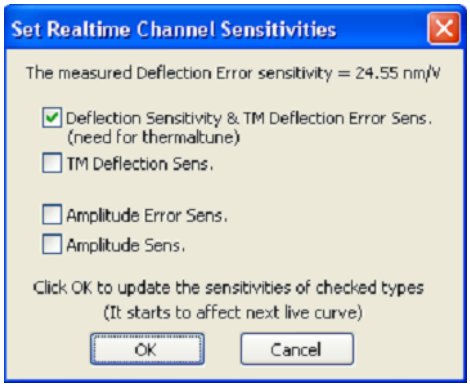

Figure 4.4. Deflection sensitivity calibration window.

b) Cantilever Stiffness Calibration by Thermal Tuning:

The spring constant of the cantilever should be calibrated as accurately as possible since it is used to determine the force applied in the ramping mode by the software. The steps followed will be listed below:

- Select thermal tune frequency range (either 1-100 KHz, or 5-2000 KHz) according to the cantilever which you are going to work with.
- Click Acquire data in the thermal tune panel.
- Zoom in onto the region around the peak and click Lorentzian (air) button to select the Lorentzian model to fit the data. The equation used to fit the filtered data is :

$$A(\vartheta) = A_0 + \frac{C_1}{(\vartheta - \vartheta_0)^2 + C_2} \qquad (4.1)\ [138]$$

where: $A(\vartheta)$ is the amplitude as a function of frequency, ϑ,

A_0 is the baseline amplitude,

ϑ_0 is the center frequency of the resonant peak,

C_1 & C_2 are Lorentzian fit parameters.

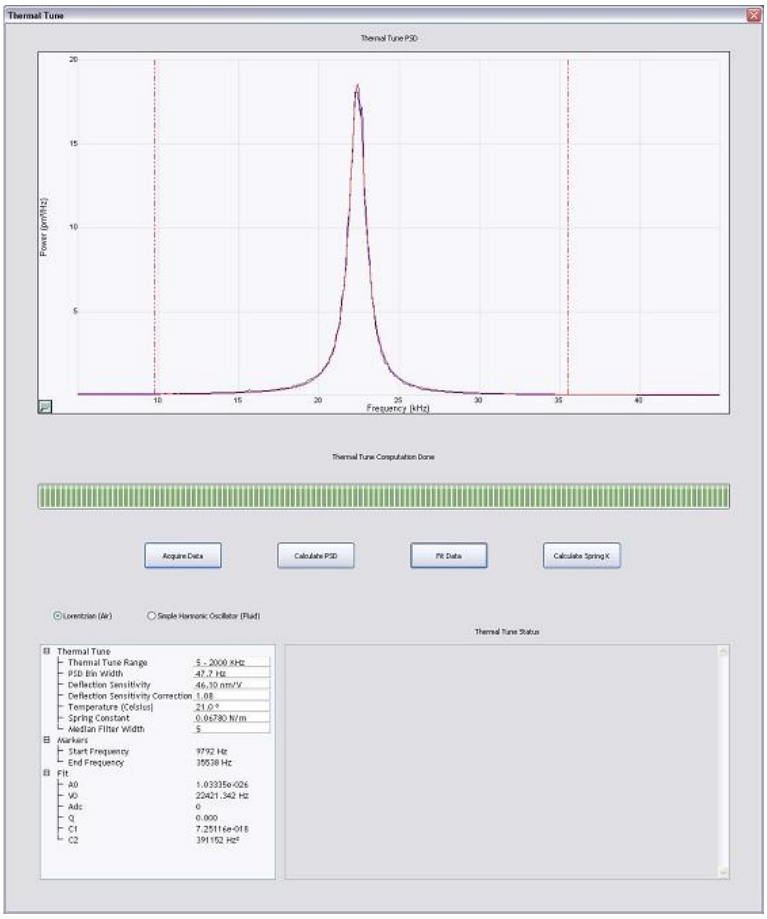

Figure 4.5. Thermal tune panel in the Peak Force QNM operating software.

- Drag cursors from both sides to bracket the bandwidth over which the fit is to be performed.
- Adjust the cursors position good enough to get the best fit at the thermal peak.
- Input the cantilever temperature.

- Click calculate spring constant button.
- You will be asked whether you want to accept the calculated value of the spring constant, k. By clicking OK, the recent calculated spring constant will be updated in the Cantilever Parameters window.

4.1.2. Imaging Nanowires with QNM

During the imaging, the primary purpose is to be able to make sure that we position the AFM tip in the middle section of the nanowire both in length and in width. We zoomed in gradually on the spot in the middle section to confirm that the tip was well positioned in the center of the wire then we raised the maximal force step by step and observed a bending of the beam. The tapping mode images shown in Figure 4.6 below depict a nanowire with width of 80 nm and the length of 12 µm. On the subfigures we can as well observe the imaging of the AFM tip's sidewall, which makes the nanowire appear wider. These images prove us that we could successfully tap onto the nanowire.

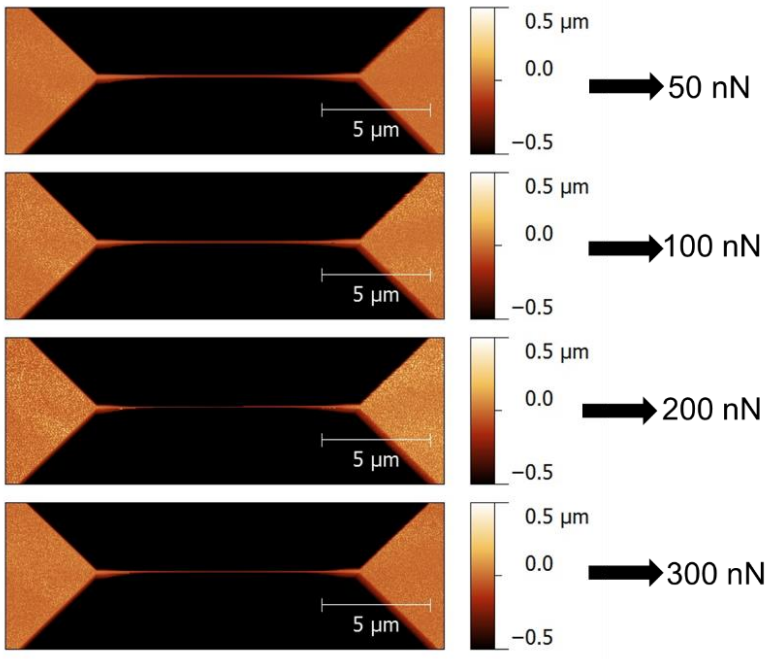

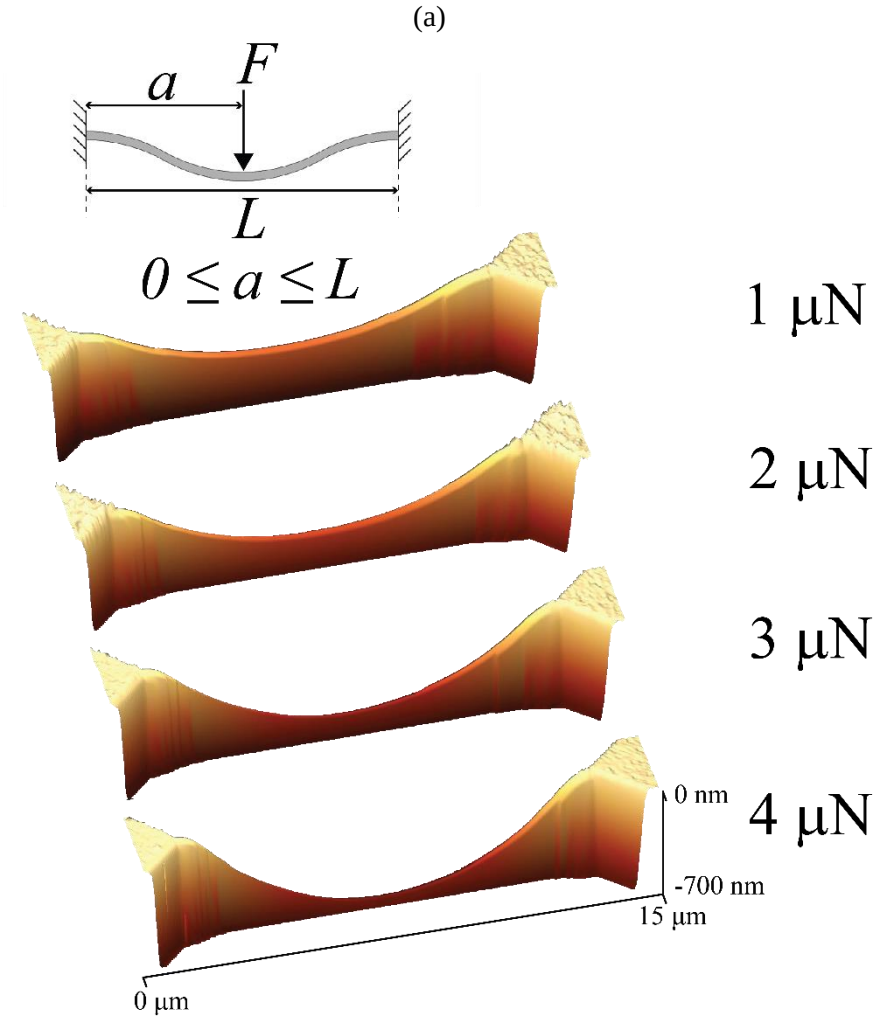

Figure 4.6. (a) AFM Tapping mode images showing bending of the nanowire maximum in the middle section where the tip is well-positioned exerting force, observing an increase in the deflection when there is an increase in the force, (b) A series of three-dimensional AFM images of a SiNW in PeakForce QNM mode. Each image is constructed as a superposition of multiple loading steps at constant force, where the point of the application of load is scanned along the entire length of SiNW.

We confirmed the nanowire width by analyzing the profile across the nanowire; only the points of maximum height correspond to the nanowire width. We started the experiments with a softer AFM cantilever (ScanAsyst-Air). The imaging of the nanowires was done across the length of the nanowire. The scan angle has been adjusted for every

experiment. After the first proof of concept with the ScanAsyst-Air, we used an AFM tip with an order of magnitude higher spring constant than the expected stiffness of the wires (FastScanA), Figure 4.7 and Table 4.1.

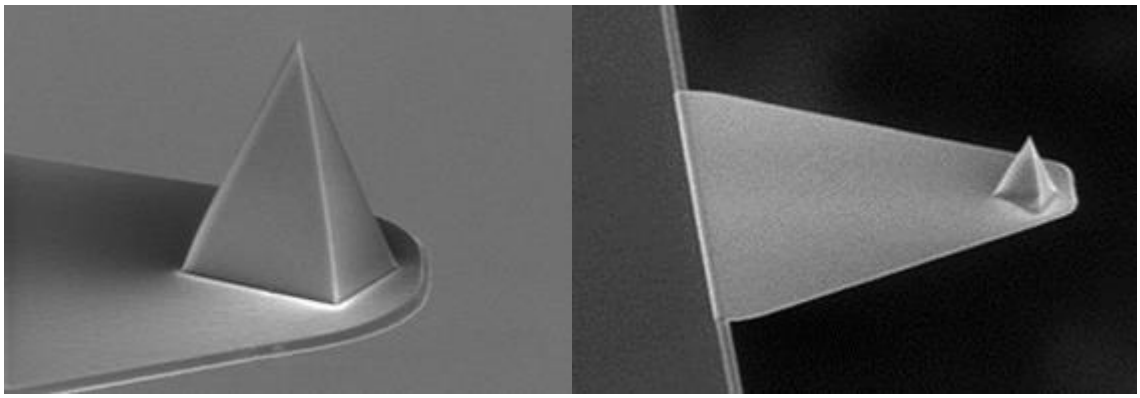

(a) (b)

Figure 4.7. Close-up SEM images of the AFM tip used – Bruker FastScanA- in the experiments (a) tip only (b) cantilever [139].

Table 4.1. Bruker FASTSCAN-A AFM cantilever specifications [139].

Geometry	Rotated (Symmetric)
Tip Height (h)	2.5- 8 μm
Front Angle (FA)	15 ± 2.5º
Back Angle (BA)	25 ± 2.5º
Side Angle (SA)	17.5º
Tip Radius (Nom)	5 nm
Tip Radius (Max)	12 nm
Tip SetBack (TSB) (Nom)	5 μm
Tip SetBack (TSB)(RNG)	0- 7 μm

During the QNM imaging, we augmented the peak force in constant steps. Moreover, after several steps, we took a reference image with the initial peak force value, in order to compare the bending behavior compared with the initial image. The results showed

that the nanowire behaves elastically and after the force is released it returns to its initial position.

4.1.3. Ramping on Nanowires

After we verify with tapping mode imaging that we are in the middle of the nanowire, we switch to the ramping mode in which we apply the force gradually to eliminate the possibility of a sudden break of the nanowire. The single force curves (ramps) are done with the FastScanA tip, Figure 4.7 and Table 4.1, on the nanowire with the width of 30 nm and a length of 4.5 µm. The applied force is raised with an increment of 100 nN as from 100 nN to 1 µN and in 500 nN steps higher from 1 µN until the breaking point. A confirmation with scanning electron microscope (SEM) is done after the breaking point to confirm that the wire is broken.

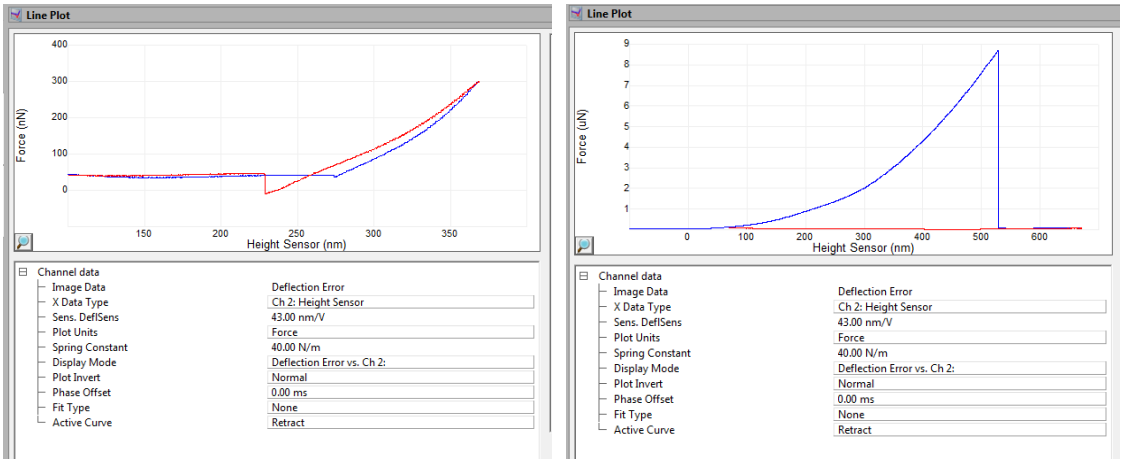

(a) (b)

Figure 4.8. Force-displacement curves for an applied force of 300 nN and (b) 8500 nN, at which failure occurs.

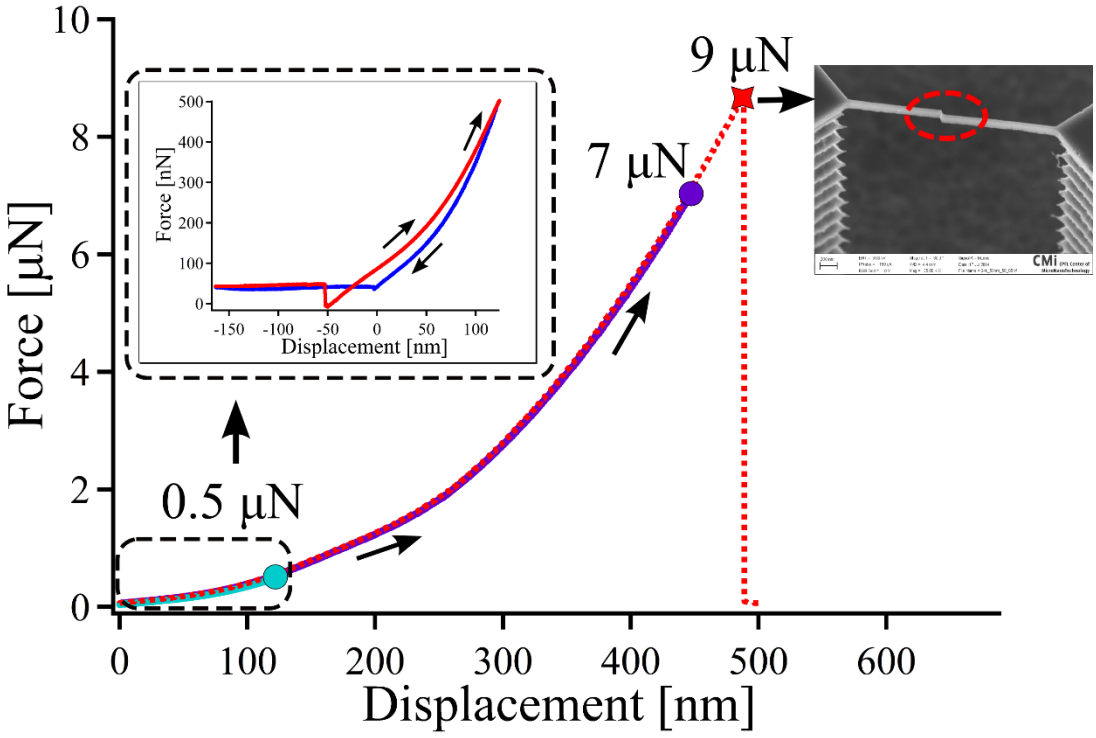

Figure 4.9. Three force-deflection curves, where SiNWs are loaded at their mid-span. Overlap of loading curves indicate elastic behavior, which is further verified by the brittle nature of fracture recorded at a load of 9 μN.

Force-displacement curve during loading and unloading is found to be identical, Figure 4.9. These identical F-d curves indicate the linear-elastic bending deformation of NWs, i.e., the NW is elastically loaded and unloaded. So, after 0.5 μN to 7 μN, and even from 7μN to 9 μN, the NW recovers to the original state after being fully unloaded. More measurement results are found in Appendix-B.

So we stopped the test after failure of the nanowire, as shown in Figure 4.8. (b) and Figure 4.9. After the failure, samples were investigated by SEM in order to verify the failure by imaging and to get more understanding of the failure type, Figure 4.10. From these SEM images, we observe that the samples are broken in the middle where the tip is placed and force is exerted. Furthermore, we get an idea of how samples are broken after

some max. force they can handle. From the images Figure 4.10. (a)- (d), we could safely deduct the conclusion of a brittle type of failure as the nanowires are broken at the instant of max. force and sudden cracking, without the observation of any necking.

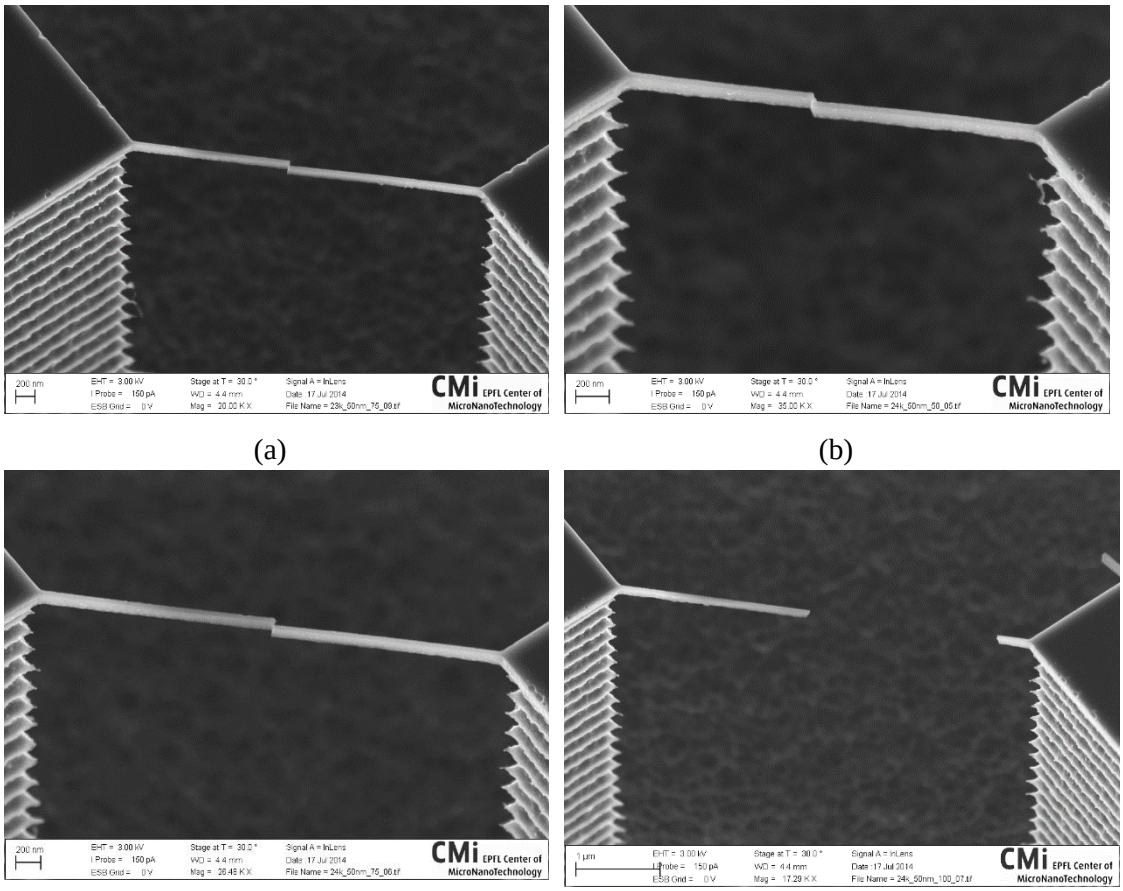

Figure 4.10. SEM images of some of the nanowires tested with AFM until failure for the nanowires having width of 50 nm and a length of (a) & (c) 3.75 µm (b) 2.5 µm, (d) 5 µm.

4.2. HIGH-RESOLUTION X-RAY DIFFRACTION MEASUREMENTS

The effect of the presence of defects inside nanostructures into resulted mechanical properties have been mentioned in *Literature Review*, Chapter 2 [77], [78].

Thus, characterization of the internal structure holds a key-role in tuning and improving the resulted mechanical properties of NWs.

The distribution of internal stress inside the silicon nanowires coming from both fabrication and the substrate used is aimed to be investigated by the powerful non-destructive method of high resolution x-ray diffraction (HRXRD) methods [140]–[142].

High resolution x-ray diffraction is a powerful technique for the study of strain measurements on the atomic level, especially in semiconductors. Unlike the other methods such as cross-sectional TEM, high resolution x-ray diffraction is a non-destructive method and also gives a quantitative information about sample's mechanical behavior [143]–[145]. Furthermore, this technique is used to measure the lattice spacing directly having a high stress sensitivity. These information is valuable for charactering material properties and evaluating the structural integrity of components [146]–[148].

The main source of the failure of NWs is usually attributed to their crystalline imperfection and residual strain. Although there have been many studies on the surface stress or residual stress effect on the mechanical properties of materials at nano-scale, the investigation of the defect effect is still rare in the literature, which is critical in enhancing NWs' performance in various applications. Generally, NWs are considered to be almost strain-free crystalline objects without defects that propagate into their structure when compared with thick planar layers of structure, where the deformation mechanism is mainly plastic involving the formation of dislocation networks. So, we could think of NWs as deformation-free on the macro-scale but not on the micro-/nano-scale. In this part of the thesis, we focus on finding a reliable answer to this question by investigating the already-fabricated SiNWs by the method of HRXRD.

The preliminary measurements for the proof-of-concept purposes is conducted at ESRF (The European Synchrotron) in Grenoble, France, in close collaboration with senior scientist Dr. Gilbert Chahine. Different design has been implemented for the measurements as the sample-to-be-tested specifications are different for the HRXRD measurements but the fabrication process flow is kept to be the same in order to detect fabrication related strain. NWs are arrayed in a number of ten as shown in Figure 4.11 (a)

and (b), to increase the magnitude of the read-out signal, resulted SEM images of the fabricated nanostructures are seen in Figure 4.11 (c) and (d). Further details are given in Appendix-C.

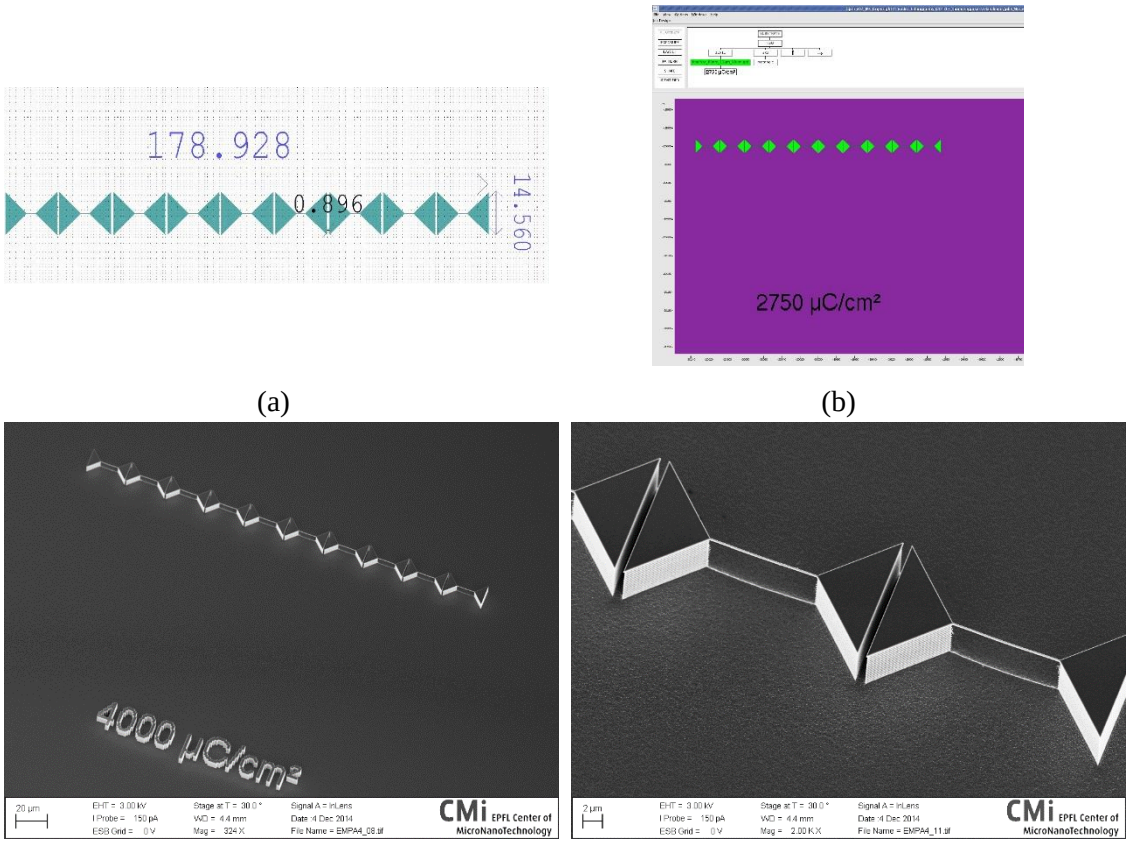

(a) (b)

(a) (b)

Figure 4.11. (a) Mask layout for the e-beam lithography (b) Processed layout ready for the exposure by e-beam lithography (c) Top-view SEM image of the resulted NWs (d) close-up SEM image of two individual NWs.

After the fabrication of the NWs, nanostructures are diced into rectangle chips by laser-dicing consisting of a few array of NWs by Dr. Antonia Neels and then samples are transported to Grenoble for the HRXRD measurements.

Sample is positioned orthogonal with respect to beam source in order to get information from the suspended NWs only not from the bulk substrate beneath, Figure 4.12 (a). Preliminary results suggest that x-ray beam could be successfully positioned on the NWs

and even more, we could get sufficient amount of signal out of the nanowires, Figure 4.12. (b) a). Intensity of the diffracted x-ray beam from the NWs can be differentiated from that coming from the triangular Si pillar at both ends, Figure 4.12. (b) b). Moreover, Reciprocal Space Mapping (RSM) demonstrate that the 2D diffraction peaks of the substrate (S) and for the SiNWs (NW) superposed with the silicon triangular pillars at both ends (P). RSM gives us information about the structure's deviation from the ideal crystalline behavior. By comparing the RSM data from the Si-pillars (in the micro-scale) and from the NWs (in the nano-scale), we could get to know defect population in between and overall deformation mechanism in these micro- and nano-scales.

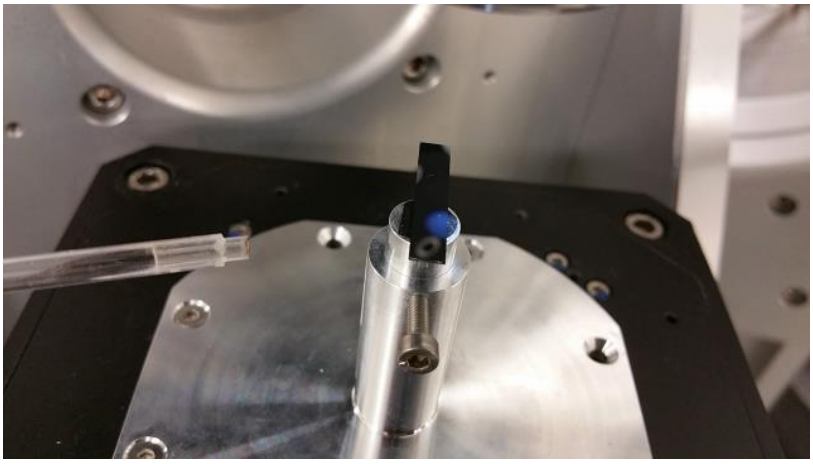

(a)

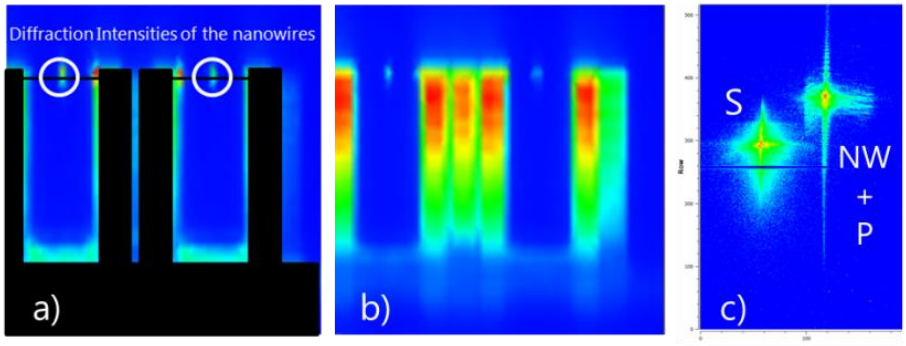

(b)

Figure 4.12. (a) Measurement setup for the HRXRD tests conducted at ESRF- Grenoble, (b) Measurement results showing a) signal output coming from NWs, b) different intensity of

signals coming from NWs and Si pillars, c) RSM of 2D diffraction of substrate and NWs+pillars.

As for the estimation of the impurities present inside the fabricated nanowires, a simple computation is carried out. The silicon substrate which we have used in the fabrication of the nanowires is a p-type doped wafer having a resistivity range of 0.1- 100 Ω- cm. The relation between resistivity and p-type dopants at the room temperature is given as in the equation 4.2 below:

$$\rho = \frac{1}{q\ p\ \mu_p} \tag{4.2}$$

The p-type dopant concentration in that resistivity range is 10^{17} cm^{-3} and 10^{14} cm^{-3}. Since the dimension of the fabricated nanowires range from 20 nm- 80 nm in diameters and 200 nm and 12 μm in length, with a rough estimation of 100 nm thickness (out-of-plane dimension). In these volume ranges of 10^{-15} cm^3 (for the smallest nanowire) - 10^{-18} cm^3 (for the biggest nanowire), the smallest wire (20 nm diameter and 200 nm length) has the possibility of 0.1 dopant atom and for the biggest nanowire (80 nm diameter and 12 μm length) 100 dopant atoms seem to be present in their volume sizes.

4.3. DISCUSSION OF RESULTS AND OUTLOOK

In short, mechanical measurements have been carried out to explore mechanical properties of nanowires. Firstly, AFM based mechanical measurements have been conducted revealing the presence of 850 MPa internal stress inside the nanowires. In the last section, HRXRD measurements have been presented to reveal the internal structure of the fabricated nanowires. This information is crucial to make a relation between the internal structure and the resulting mechanical properties of nanowires. It has been reported previously in the literature *(Chapter 2)* that the deformation mechanisms are greatly influenced by the presence of defects, i.e., defects act in the role of dislocation sources and many different deformation mechanisms are triggered from these weakest

points. Utilization of the high resolution x-ray investigation on the fabricated silicon nanowires will be further carried out to shed a light on the influence of pre-existing defects on the mechanical behavior of silicon nanowires revealing different styles of pre-existing defects including single surface defects, surface bi-defects and single internal defects. In addition to this, the information obtained from the analysis of the pre-existing defects will be used to make a correlation in the overall mechanical behavior of nanowires. The influence of the quantity, the position and also the dimension of the pre-existing defects inside the nanowires into the overall nanowires will be further investigated as the future work.

Chapter 5 : Numerical/Analytical Modeling

According to the *Literature Review*, due to its manipulation convenience, bending type of experimental testing both *in-situ* [149] or AFM bending [150]-[152] at nano-scale is broadly used in mechanical characterization of NWs. Many different type of materials have been investigated based on this type of testing including metals such as Ag [153]-[156], Au [72], [149], [157]-[159], W [160], and also some metal oxides such as ZnO [96], [161]-[171], and semiconductor NWs such as Si [71], [172], [173]. Due to its manipulation convenience, bending type of testing at nano-scale is widely used in mechanical characterization of NWs. However, it is noted that a complete description of the bending deformation of NWs is still lacking.

This chapter presents the comparison between measurements and numerical computations. Finite element analysis method is used as a tool to validate the measurements and found to be in a good agreement.

5.1. THEORETICAL BASICS FOR THREE-POINT BENDING MODEL

In this section, three-point bending model for doubly clamped beams (NWs in this case) according to the classical Euler-Bernoulli beam theory will be presented. Comparison between measurements is carried out based on the assumption that the contact area between AFM tip and sample underneath is so small that it will be safely assumed as a point load, Chapter 4, Table 4.1.

For the classical Euler-Bernoulli beam theory, the governing equation of the doubly clamped thin beam under pure bending is given as:

$$(EI)\frac{d^4v}{dx^4} = 0 \tag{5.1}$$

Where *E* is bulk Young's modulus, *v* is the beam deflection, *I* is the moment of inertia.

For the rectangular cross section NW, *I* equals $bh^3/12$, where *b* is the width and *h* is the thickness of the beam. Solving Eq. 5.1 using the usual boundary conditions of fixed-fixed end, with a constant load *F* applied at the midpoint *x=L/2* of the NW, which are the displacement and slope are zero at *x=0* and the slope at *x=L/2* is also zero due to symmetry.

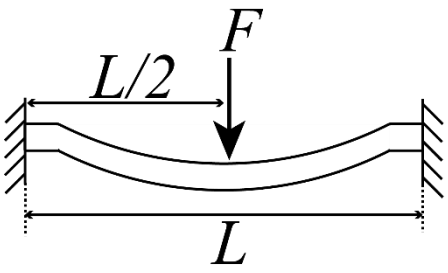

Figure 5.1. Force diagram for the double clamped NW

The force equilibrium at x=0 is;

$$-(EI)\frac{d^3v}{dx^3} = \frac{F}{2} \tag{5.2}$$

Applying the boundary conditions of;

$$v(0) = 0 \qquad \frac{dv}{dx} = 0 \; at \; x = 0 \qquad \frac{dv}{dx} = 0 \; at \; x = L/2$$

will yield a general displacement equation of:

$$v(x) = \frac{-Fx^3}{12EI} + \frac{FLx^2}{16EI} \tag{5.3}$$

Since maximum deflection occurs in the middle of the NW, replacing x with L/2 in Eq. 5.3 will yield the equation of

$$v(L/2) = \frac{FL^3}{192EI} \tag{5.4}$$

So the relationship between the applied load *F* and the resulting displacement *d* can be rewritten as

$$F = \frac{192EI}{L^3} d \tag{5.5}$$

However, because of the ultra- small scale of the nano-structures, it has been found that the classical beam theories –including Euler-Bernoulli and Timoshenko beam theories- Eq.5.5 impose some inaccuracies in the interpretation of the mechanical properties of NWs. Most of this inaccuracy results from the axial tensile force which in inherently induced inside the beam due to stretching. This effect can be safely neglected in continuum mechanics since it does not have a profound effect as the displacement is much smaller than beam's dimensions. However, at the small scale, deflection of the beam becomes comparable with the beam's dimensions and this axial tension effect has obvious effect on the bending behavior of NWs [174]. By considering this axial tensile force, the classical linear relation between force and displacement turns into a nonlinear relation as

$$F = \frac{192EI}{L^3} f(k)d \, , f(k) = \frac{k}{48 - 192 \tanh\left(\frac{\sqrt{k}}{4}\right)/\sqrt{k}} \tag{5.6}$$

Where *k* is solved from a complex transcendental equation, with the asymptotic solution given as

$$k = \frac{6s(140 + s)}{350 + 3s}, s = d^2 \frac{A}{I} \tag{5.7}$$

Where *A* is the NW cross-sectional area and *I* is the moment of inertia.

The comparison of both theories is shown in Figure 5.2. As seen from the plot, Eq. 5.5 predicts the small deformation region, that is up to around 15 nm very well but they begin to deviate for larger displacements.

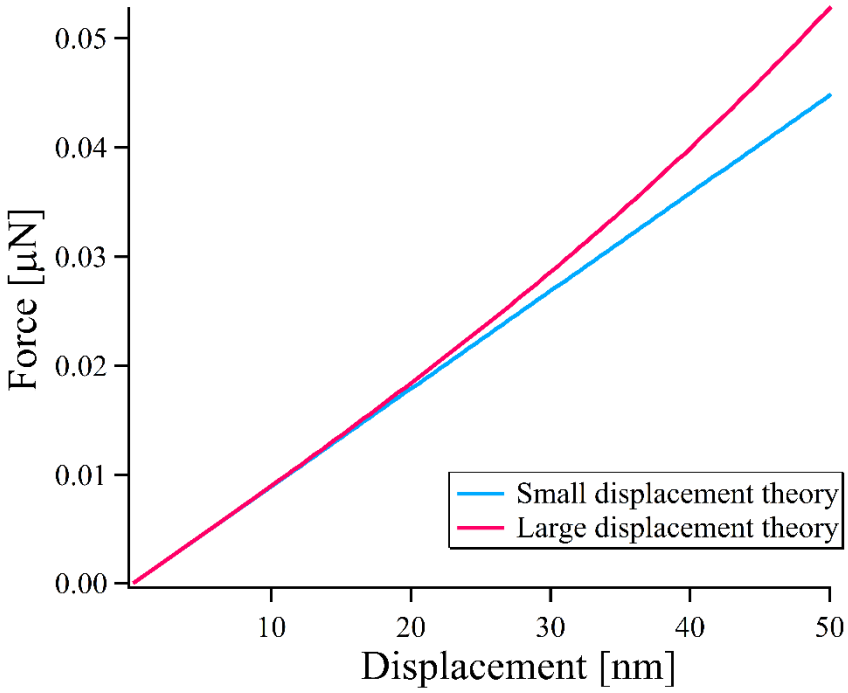

Figure 5.2. Force vs. displacement curves for both theories (Eq. 5.5 and Eq. 5.6).

5.2. CORRELATION OF MEASUREMENTS RESULTS WITH ANALYTICAL AND FEA RESULTS

Efforts have been made to correlate experimental measurements with the theoretical results. However, direct comparisons are difficult since theoretical formulations are based on the assumption that all samples are perfect, defect-free samples and free from any initial stress coming from either during fabrication process or later during measurement stages. Experimentally obtained force versus bending displacement curves conducted on four-different samples having the same geometry by applying the same forces are processed statistically to find a confidence interval (Figure 5.3). Finite

element computations have been carried out for the same force range and the resulted displacement is computed. In Figure 5.3, the comparison is made only in the elastic regime.

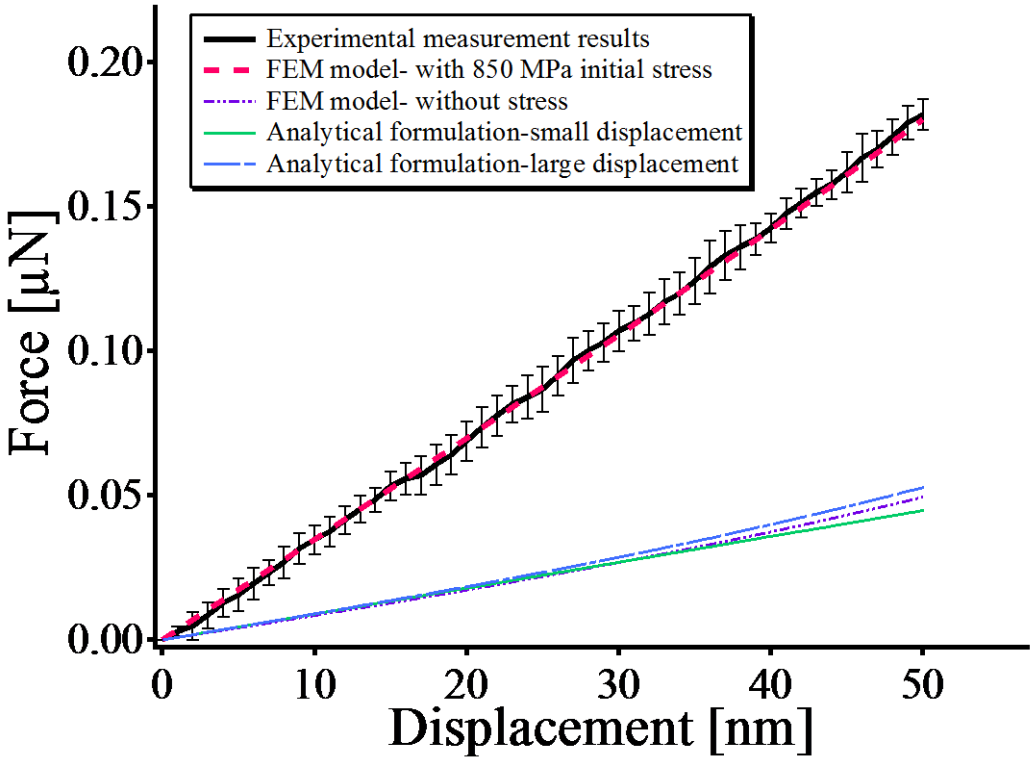

Figure 5.3. Three-point bending test results obtained on four SiNWs in the linear deformation regime. A comparison of measurements with finite element analysis indicates the existence of an intrinsic stress of 850 MPa.

The correlation is firstly done with the assumption that there is no initial stress inside the nanowires. However, it is found that this assumption does not correspond to the measurement results behavior as it can be seen in lower part of the plot, Figure 5.3. Thus, computations are carried out further with the assumption that there exists some initial stress inside the nanowires, which is possible to be induced during the microfabrication process. To find the exact numerical value of the stress, a parametric study is carried out and the exact initial stress value is found to be 850 MPa, Figure 5.4.

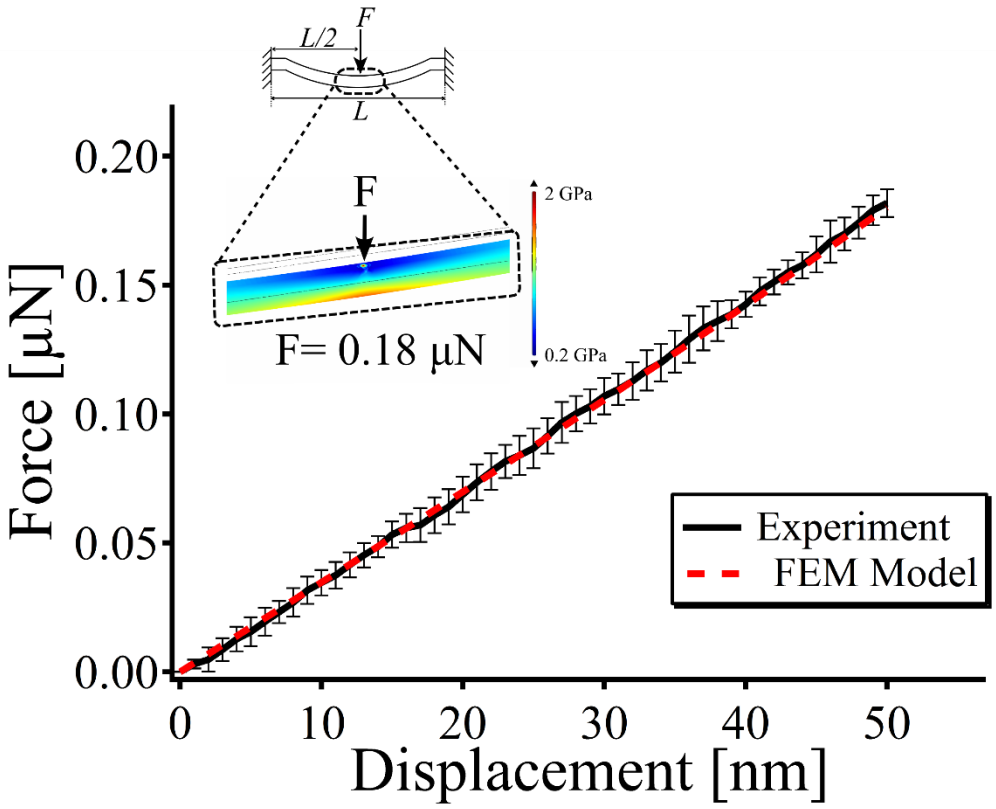

Figure 5.4. Three-point bending test results obtained on four SiNWs in the linear deformation regime. A comparison of measurements with finite element analysis indicates the existence of an intrinsic stress of 850 MPa.

Although, we get an idea about the amount of the stress trapped inside the nanowires, this stress is changing from sample to sample as the position of the nanowires on the substrate is different, process parameters vary for each samples. This results in different stress accumulation and consequently a different force-displacement behavior. Nevertheless, we could safely claim that this initial tensile stress inside the nanowires gives a stiffening effect resulting a steeper force-displacement behavior.

Furthermore, FEA computations are also carried out in order to determine the maximum stress accumulated inside the nanowires during the fracture, ultimate tensile stress, Figure 5.5. This stress value is found to be around 15-20 GPa, which is close and a bit higher than the value stated in the literature, 12 GPa [175].

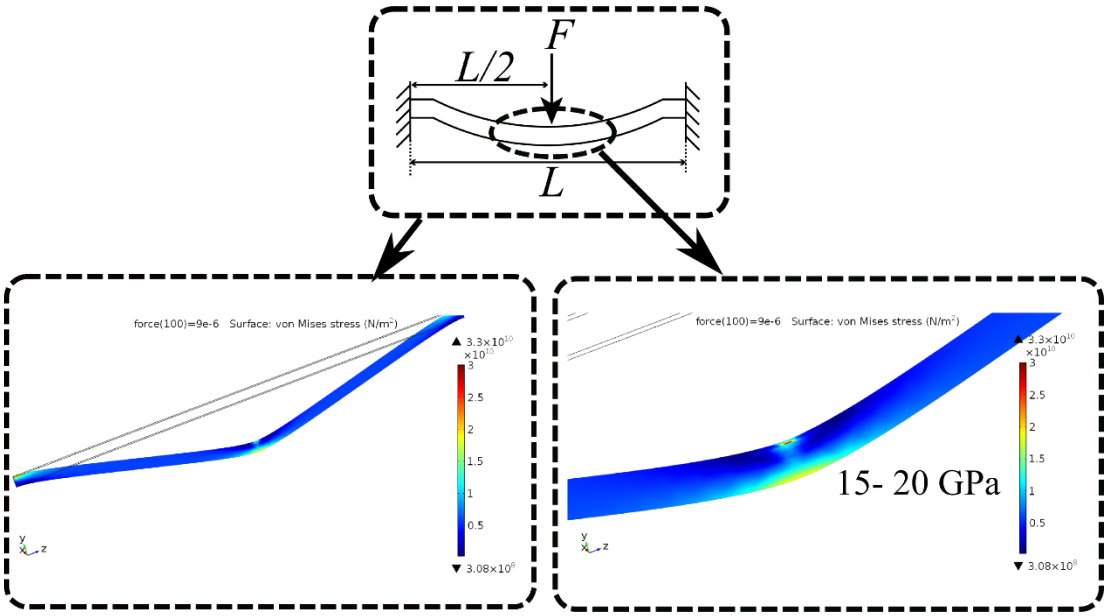

Figure 5.5. FEA simulation results showing the stress state during the fracture, stress accumulated at the fracture is computed to be around 18 GPa.

Chapter 6 : Monolithic Fabrication of Micro- System & Nanowire

This chapter presents another fabrication work conducted at the class 100 cleanroom facilities of EPFL, Switzerland namely The Center of MicroNanoTechnology (CMi).

The chapter presents a challenging process flow which includes both the single suspended nanowire from *Chapter 3* and a microsystem integrated monolithically on the same chip developed for the monolithic fabrication of SiNWs with micro-system and also the preliminary fabrication results.

6.1. MONOLITHIC FABRICATION OF MICRO- SYSTEM & NANOWIRE

Nanowires technology is developing rapidly for several decades. It adds up functionality, offering process advantages and delivering superior performance in most areas of applications. This trend is further motivated by the advantages of the 3D integration. Rather than metallic NWs, semiconductor NWs have one more advantage of being able to use in CMOS-compatible processes as they have the potential to be implemented on an existing semiconductor infrastructure. Integration on silicon is critical for nanowires to be of interest for large-scale electronic applications. Once the NWs have been fabricated, they need to be connected to the outside world to eventually become a part of an electronic circuit. However, it brings along some challenges in terms of fabrication, the high aspect ratio of these bigger objects requires development of new, nanowire-specific processing techniques. Additionally, the length and the diameter of a NW need to be controlled within tight limits not to compromise from device performance. In order to eliminate those stringent dimensional control, we aim to use top-down

approach, which employs only e-beam lithography for patterning both the smallest dimension, NW, and the bigger dimensions in the rest of the device itself.

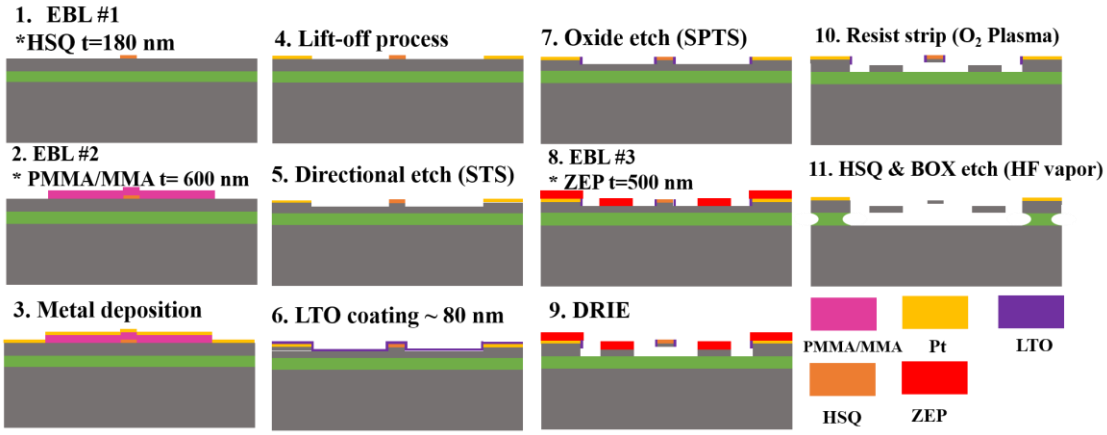

Figure 6.1. Process flow for monolithic integration of microsystem-NW.

Process requires SOI (silicon on insulator) wafer as the substrate since at later stages BOX layer will be etched away to release the MEMS moving plate. Process consist of three different resist layers and thus three exposures, all of which is done by e-beam lithography.

It begins with definition of NW linewidth by e-beam lithography using the same e-beam resist-HSQ- in single suspended NW formation in *Chapter 3*, Figure 6.1. Step 1. Then, the second layer, which is PMMA/MMA layer for the metal lift-off is exposed; in this stage metal conducting paths are defined, Figure 6.1. Step 2. In the third step, metal coating is carried out by using the Leybold Optics LAB600H metal evaporator, at first Aluminum (Al) is used but later Platinum (Pt) is observed to be an easier lift-off metal than Al so we decide to continue with Pt as metal contacts, Figure 6.1. Step 3. Right after the metal coating, wafer is put into the lift-off container and it is waited for the metal lines to be dissolved from the undesirable regions inside pure Acetone, Figure 6.1. Step 4.

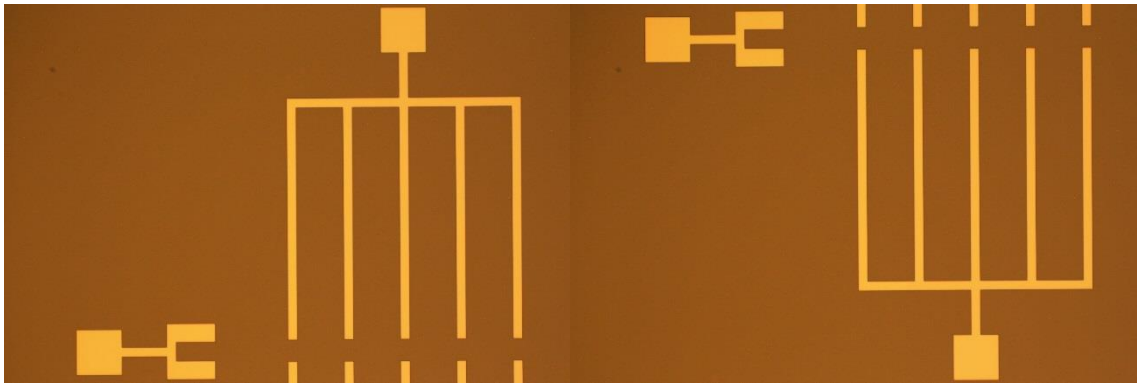

(a) (b)

Figure 6.2. Optical microscope images of the metal contact paths right after step 4 in Figure 6.1 (a) half above (b) half below of the whole structure.

After this lift-off step, the remainder of the process is very similar to the single suspended NW process as described in *Chapter 3*, Figure 3.2. So, in step 5, anisotropic silicon etching is done using STS Multiplex ICP dry etcher in order to define the thickness of the later-to-be-formed NW, Figure 6.1. Step 5. In step 6, this newly etched silicon sidewalls are protected by LPCDV LTO (low temperature oxide) deposition carried out at a temperature of 425 ºC, Figure 6.1. Step 6. Later on, oxide coating is cleaned from all lateral regions to give some space to the last exposure resist coating, Figure 6.1. Step 7. The last layer is microsystem device layer, for that we use ZEP as the e-beam resist and then exposure is done by e-beam lithography, Figure 6.1. Step 8. It is observed that ZEP is acting as a good hard mask in RIE especially in BOSCH process environment. After all the device layer is etched inside AMS 200 DSE Si dry etcher, Figure 6.1. Step 9, resist strip is carried out inside O_2 plasma asher, Figure 6.1. Step 10. In the final step, all protective layers i.e., HSQ, LTO, and also the buried oxide (BOX) layer of SOI wafer layer are stripped in a single step by a fairly dry etching method of HF vapor etching, Figure 6.1. Step 11. An overview of the metal path lines defined in step 2 of Figure 6.1, and coated in step 3 are shown in Figure 6.2 just after the lift-off step, Figure 6.1. Step 4 (a) and a closer-up to the nanowire is seen in Figure 6.2. (b).

(a)

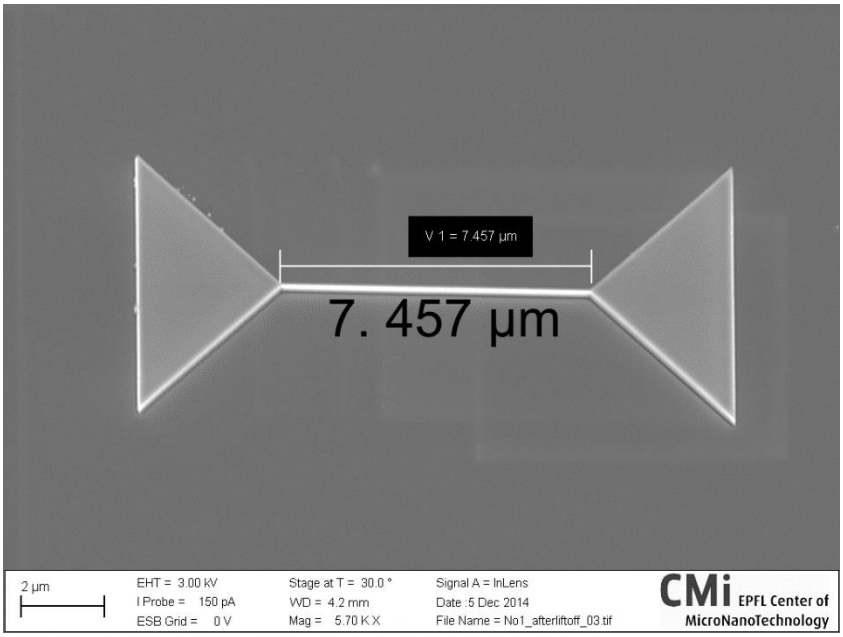

(b)

Figure 6.3. (a) SEM images right after metal lift-off, Figure 6.1 Step 4. (b) close-up SEM image of the NW shown in (a).

At the final step, the excessive HSQ remained on top of Si NW to protect it throughout the previous processes and BOX layer is etched away in the same step by a semi-dry etching method, HF vapor etching. Final images of the structures both optical microscope and SEM are seen in Figure 6.4 and Figure 6.5.

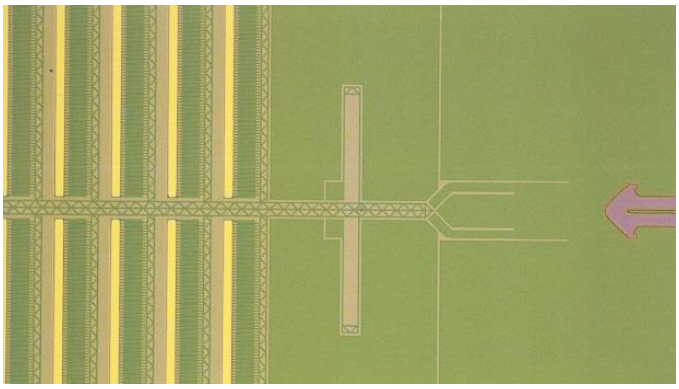

(a)

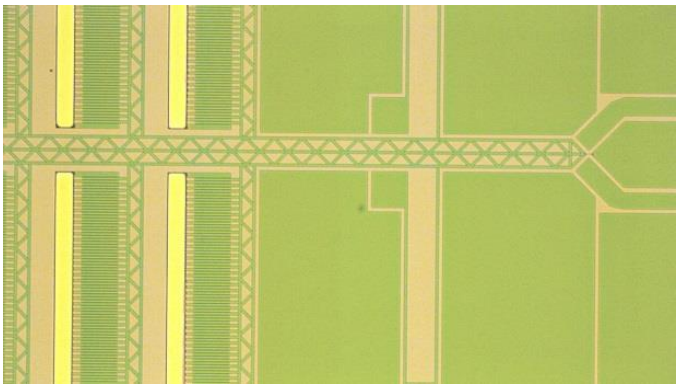

(b)

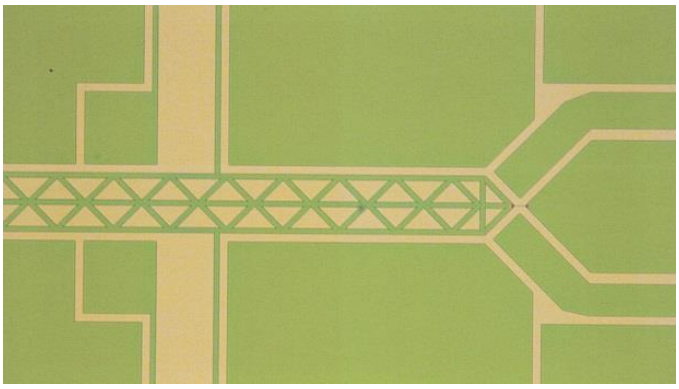

(c)

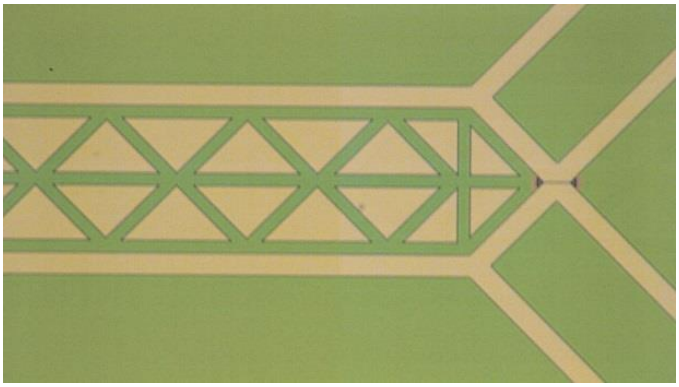

(d)

Figure 6.4. Optical microscope images of microsystem-NW structures after final step, (a) a bird eye's view image containing both NW and microsystem, (b) – (d) gradually closer look to NW- microsystem interface.

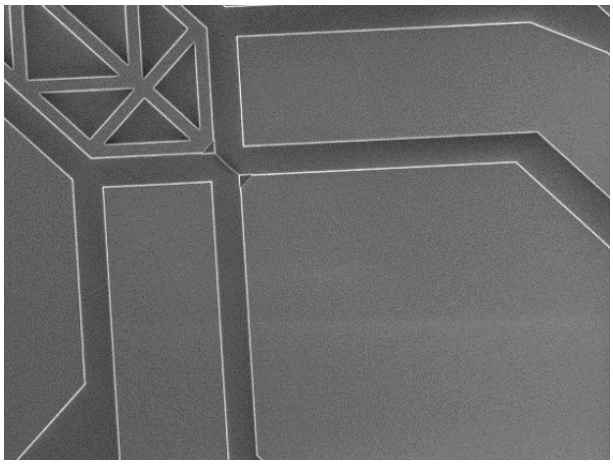

(a)

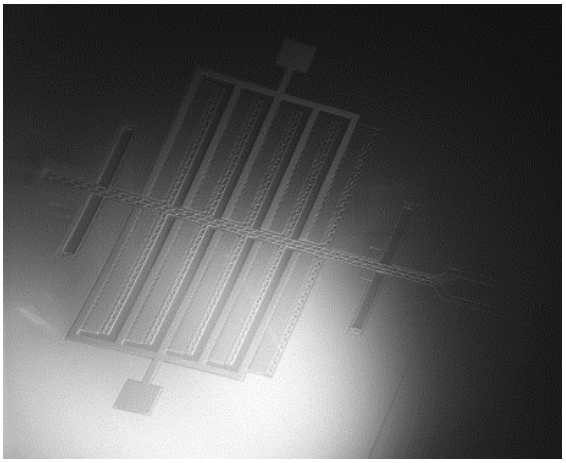

(b)

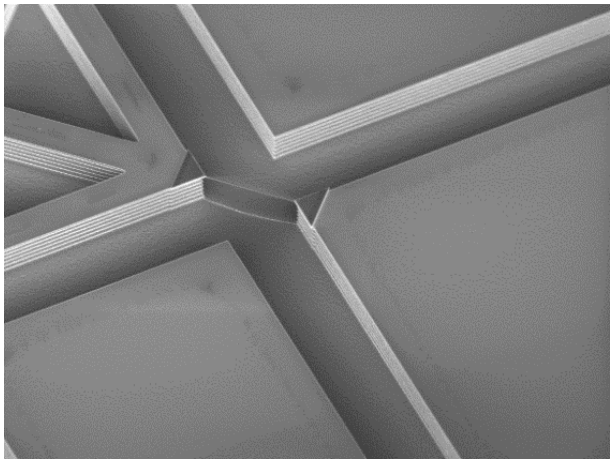

(c)

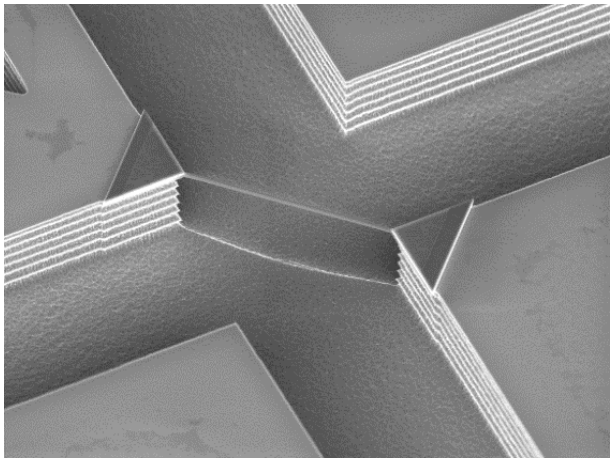

(d)

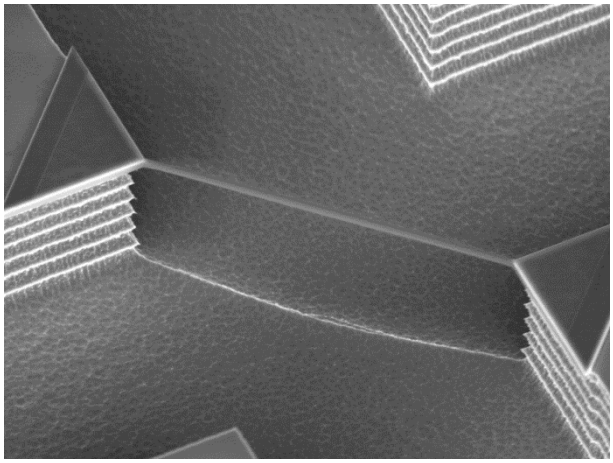

(e)

Figure 6.5. SEM images of the same samples as Figure 6.4, (a)-(b) a bird eye's view from top, (c)-(e) a closer look on the NW region with 30º tilted angle.

Chapter 7 : Conclusions & Outlook

Due to appealing and broad applications of NWs, this study has investigated the mechanical properties and deformation mechanisms of NWs, including the sample fabrication in double-clamped configuration without any support effect at the ends, and also AFM-based bending type of mechanical characterization in the elastic regime. In this chapter, an overall summary is provided in Section 7.1, and concluded with a proposed future work of plan.

7.1. RESEARCH SUMMARY

Ultimately, researchers from various disciplines are in the need for predictive models of physical phenomena. Extracting material properties across a broad length scale will give them physically-based and technologically relevant models. Understanding the fundamental response of the building blocks of complex systems with a good understanding of physical constraints will give rise to the possibility of true predictive capability and smart engineering design. If we can understand how materials deform at the nano-scale, it will be possible to push the limits of performance in many applications.

In overall, throughout this thesis, a systematic study on the mechanical properties of SiNWs has been carried out. In the first phase, sample, i.e. Si NW fabrication based on top-to-bottom approach is realized ranging in a broad dimension spectrum in diameters from 20 nm to 80 nm and in lengths of 200 nm to 12 μm. Mechanical measurement of the NW having a geometry of 30 nm to 4.5 μm has been carried out with AFM- based bending test. Results are correlated with the existing analytical formulations and FEM-tools. From the calculations, we observed that there exists an initial stress inside the NWs which make them stiffer, which analytical formulations do not take into account. Initial

stress value is implemented later inside the FEM simulation and found to correlate with measurement results very well with the value of 850 MPa. In addition, stress and defect analysis at the atomic scale has been carried out by using HRXRD technique. Due to the nano-scale size, the presence of defects appears to be one of the most influential factors in determining NW's properties. It has been reported already that the properties of NWs can be engineered by controlling defects and flaw densities. Thus, the knowledge of the defect type and quantity inside the fabricated NWs and also the knowledge of how these defects affect the overall mechanical properties will give us a complete understanding of how materials deform.

7.2. OUTLOOK

Some foreseen directions of this research are listed in the following:

- **Further characterization of the fabrication process:** In order to obtain reliable and uniform specimens, all steps of fabrication should be characterized by high resolution imaging tools, unfortunately, when we reach down to 20 nm in diameter, SEM imaging could not get us reliable information, for instance about the native oxide layer thickness around it. Thus, imaging with TEM should be carried out in the cross-sectional area of the NWs.
- **Further bending tests on different geometries of NWs:** In the scope of this thesis, only one geometry of NW has been tested. In order to carry out a scale-dependence study, the other geometry of NWs should be measured as well.
- **New analytical formulation need:** a new analytical formulation considering the initial stress should be derived and correlated with the experimental measurement and FEM results.

BIBLIOGRAPHY

[1] The national Nanotechnology, "National Nanotechnology Initiative," *JNCI Journal of the National Cancer Institute*, 2001. [Online]. Available: http://www.nano.gov/nanotech-101/what/definition.

[2] R. Feynman, "There is plenty of room at the bottom," *Eng. Sci.*, vol. 23, no. 5, pp. 22–36, 1960.

[3] N. Taniguchi and Others, "On the basic concept of nanotechnology," in *Proc. Intl. Conf. Prod. Eng. Tokyo, Part II, Japan Society of Precision Engineering*, 1974, pp. 18–23.

[4] E. K. Drexler, "Molecular Machinery and Manufacturing With Applications to Computation," 1977.

[5] E. Drexler, *Engines of Creation: The Coming Era of Nanotechnology*, vol. 3. 1987.

[6] K. Kalantar-Zadeh and B. Fry, *Nanotechnology-enabled sensors*. 2008.

[7] R. V. Burri and S. Bellucci, "Public perception of nanotechnology," *Journal of Nanoparticle Research*, vol. 10, no. 3. pp. 387–391, 2008.

[8] H. Chen, M. C. Roco, X. Li, and Y. Lin, "Trends in nanotechnology patents.," *Nat. Nanotechnol.*, vol. 3, no. 3, pp. 123–125, 2008.

[9] C. Jianrong, M. Yuqing, H. Nongyue, W. Xiaohua, and L. Sijiao, "Nanotechnology and biosensors," *Biotechnology Advances*, vol. 22, no. 7. pp. 505–518, 2004.

[10] A. G. Mamalis, "Recent advances in nanotechnology," *J. Mater. Process. Technol.*, vol. 181, no. 1–3 SPEC. ISS., pp. 52–58, 2007.

[11] J. Ramsden, *Essentials of Nanotechnology*. 2012.

[12] F. Sanchez and K. Sobolev, "Nanotechnology in concrete - A review," *Constr. Build. Mater.*, vol. 24, no. 11, pp. 2060–2071, 2010.

[13] M. S. Dresselhaus, Y.-M. Lin, O. Rabin, M. R. Black, J. Kong, and G. Dresselhaus, *Springer Handbook of Nanotechnology*. 2010.

[14] V. W. Hoyt and E. Mason, "Nanotechnology," *Journal of Chemical Health and Safety*, vol. 15, no. 2. pp. 10–15, 2008.

[15] M. C. Roco, "Nanotechnology: Convergence with modern biology and medicine," *Current Opinion in Biotechnology*, vol. 14, no. 3. pp. 337–346, 2003.

[16] T. Hillie and M. Hlophe, "Nanotechnology and the challenge of clean water.," *Nat. Nanotechnol.*, vol. 2, no. 11, pp. 663–664, 2007.

[17] G. Shen and D. Chen, "One-dimensional nanostructures and devices of II-V group semiconductors," *Nanoscale Research Letters*, vol. 4, no. 8. pp. 779–788, 2009.

[18] X. S. Fang and L. D. Zhang, "One-dimensional (1D) ZnS nanomaterials and nanostructures," *J. Mater. Sci. Technol.*, vol. 22, no. 6, p. 721–+, 2006.

[19] J. Weber, R. Singhal, S. Zekri, and A. Kumar, "One-dimensional nanostructures: fabrication, characterisation and applications," *International Materials Reviews*, vol. 53, no. 4. pp. 235–255, 2008.

[20] Y. Huang, X. F. Duan, Q. Q. Wei, and C. M. Lieber, "Directed assembly of one-dimensional nanostructures into functional networks," *Science (80-.).*, vol. 291, no. 5504, pp. 630–633, 2001.

[21] Y. N. Xia, P. D. Yang, Y. G. Sun, Y. Y. Wu, B. Mayers, B. Gates, Y. D. Yin, F. Kim, and Y. Q. Yan, "One-dimensional nanostructures: Synthesis, characterization, and applications," *Adv. Mater.*, vol. 15, no. 5, pp. 353–389, 2003.

[22] K. J. Choi and H. W. Jang, "One-dimensional oxide nanostructures as gas-sensing materials: Review and issues," *Sensors*, vol. 10, no. 4. pp. 4083–4099, 2010.

[23] G. X. Wang, M. S. Park, H. K. Liu, D. Wexler, and J. Chen, "Synthesis and characterization of one-dimensional CdSe nanostructures," *Appl. Phys. Lett.*, vol. 88, no. 19, 2006.

[24] J. Jie, W. Zhang, I. Bello, C. S. Lee, and S. T. Lee, "One-dimensional II-VI nanostructures: Synthesis, properties and optoelectronic applications," *Nano Today*, vol. 5, no. 4. pp. 313–336, 2010.

[25] T. Q. Nguyen, R. Martel, P. Avouris, M. L. Bushey, L. Brus, and C. Nuckolls, "Molecular Interactions in One-Dimensional Organic Nanostructures," *J. Am. Chem. Soc.*, vol. 126, no. 16, pp. 5234–5242, 2004.

[26] Y. Qi, Z. Wang, M. Zhang, F. Yang, and X. Wang, "Thermoelectric devices based on one-dimensional nanostructures," *J. Mater. Chem. A*, vol. 1, no. 20, p. 6110, 2013.

[27] J. Huang and Q. Wan, "Gas sensors based on semiconducting metal oxide one-dimensional nanostructures," *Sensors*, vol. 9, no. 12. pp. 9903–9924, 2009.

[28] J. Pan, H. Shen, and S. Mathur, "One-Dimensional SnO2 Nanostructures: Synthesis and Applications," *J. Nanotechnol.*, vol. 2012, pp. 1–12, 2012.

[29] G. Shen and D. Chen, "One-dimensional nanostructures for photodetectors.," *Recent Pat. Nanotechnol.*, vol. 4, no. 1, pp. 20–31, 2010.

[30] R. S. Devan, R. A. Patil, J. H. Lin, and Y. R. Ma, "One-dimensional metal-oxide nanostructures: Recent developments in synthesis, characterization, and applications," *Adv. Funct. Mater.*, vol. 22, no. 16, pp. 3326–3370, 2012.

[31] P. M. Rørvik, T. Grande, and M. A. Einarsrud, "One-dimensional nanostructures of ferroelectric perovskites," *Advanced Materials*, vol. 23, no. 35. pp. 4007–4034, 2011.

[32] S. Xu and Z. L. Wang, "One-dimensional ZnO nanostructures: Solution growth and functional properties," *Nano Research*, vol. 4, no. 11. pp. 1013–1098, 2011.

[33] Y. Xia, P. Yang, Y. Sun, Y. Wu, B. Mayers, B. Gates, Y. Yin, F. Kim, and H. Yan, "One-Dimensional Nanostructures: Synthesis, Characterization, and Applications," *Adv. Mater.*, vol. 15, no. 5, pp. 353–389, 2003.

[34] K. L. Ekinci, Y. T. Yang, and M. L. Roukes, "Ultimate limits to inertial mass sensing based upon nanoelectromechanical systems," *J. Appl. Phys.*, vol. 95, no. 5, pp. 2682–2689, 2004.

[35] M. Li, H. X. Tang, and M. L. Roukes, "Ultra-sensitive NEMS-based cantilevers for sensing, scanned probe and very high-frequency applications.," *Nat. Nanotechnol.*, vol. 2, no. 2, pp. 114–120, 2007.

[36] K. L. Ekinci, X. M. H. Huang, and M. L. Roukes, "Ultrasensitive nanoelectromechanical mass detection," *Appl. Phys. Lett.*, vol. 84, no. 22, pp. 4469–4471, 2004.

[37] K. L. Ekinci and M. L. Roukes, “Nanoelectromechanical systems,” *Rev. Sci. Instrum.*, vol. 76, no. 6, 2005.

[38] K. L. Ekinci, “Electromechanical transducers at the nanoscale: Actuation and sensing of motion in nanoelectromechanical systems (NEMS),” *Small*, vol. 1, no. 8–9. pp. 786–797, 2005.

[39] T.-Y. Zhang and W.-H. Xu, “Surface Effects on Nanoindentation,” *Journal of Materials Research*, vol. 17, no. 07. pp. 1715–1720, 2002.

[40] R. Rodríguez and I. Gutierrez, “Correlation between nanoindentation and tensile properties influence of the indentation size effect,” *Mater. Sci. Eng. A*, vol. 361, no. 1–2, pp. 377–384, 2003.

[41] W. C. Oliver and G. M. Pharr, “Nanoindentation in materials research: Past, present, and future,” *MRS Bulletin*, vol. 35, no. 11. pp. 897–907, 2010.

[42] A. M. Minor, J. W. Morris, and E. A. Stach, “Quantitative in situ nanoindentation in an electron microscope,” *Appl. Phys. Lett.*, vol. 79, no. 11, pp. 1625–1627, 2001.

[43] O. L. Warren, Z. Shan, S. A. S. Asif, E. A. Stach, J. W. Morris, and A. M. Minor, “In situ nanoindentation in the TEM,” *Mater. Today*, vol. 10, no. 4, pp. 59–60, 2007.

[44] R. Bassani, R. Solaro, M. Alderighi, C. D. I. Cesare, and M. Allegrini, “Nanoindentation with afm,” in *International conference of Tribology*, 2006, no. September.

[45] T. Burgess and M. Ferry, “Nanoindentation of metallic glasses,” *Materials Today*, vol. 12, no. 1–2. pp. 24–32, 2009.

[46] H. Nili, K. Kalantar-Zadeh, M. Bhaskaran, and S. Sriram, “In situ nanoindentation: Probing nanoscale multifunctionality,” *Prog. Mater. Sci.*, vol. 58, no. 1, pp. 1–29, 2013.

[47] X. Li, H. Gao, C. J. Murphy, and K. K. Caswell, “Nanoindentation of Silver Nanowires,” *Nano Lett.*, vol. 3, no. 11, pp. 1495–1498, 2003.

[48] D. A. Lucca, K. Herrmann, and M. J. Klopfstein, “Nanoindentation: Measuring methods and applications,” *CIRP Annals - Manufacturing Technology*, vol. 59, no. 2. pp. 803–819, 2010.

[49] C. A. Schuh, “Nanoindentation studies of materials,” *Mater. Today*, vol. 9, no. 5, pp. 32–40, 2006.

[50] S. Sundararajan and B. Bhushan, “Development of AFM-based techniques to measure mechanical properties of nanoscale structures,” *Sensors Actuators, A Phys.*, vol. 101, no. 3, pp. 338–351, 2002.

[51] Y. Isono, T. Namazu, and T. Tanaka, “AFM bending testing of nanometric single crystal silicon wire at intermediate temperatures for MEMS,” *Tech. Dig. MEMS 2001. 14th IEEE Int. Conf. Micro Electro Mech. Syst. (Cat. No.01CH37090)*, 2001.

[52] T. Namazu, Y. Isono, and T. Tanaka, “Evaluation of size effect on mechanical properties of single crystal silicon by nanoscale bending test using AFM,” *J. Microelectromechanical Syst.*, vol. 9, no. 4, 2000.

[53] T. Namazu, Y. Isono, and T. Tanaka, “Plastic deformation of nanometric single crystal silicon wire in AFM bending test at intermediate temperatures,” *J. Microelectromechanical Syst.*, vol. 11, no. 2, pp. 125–135, 2002.

[54] T. Namazu and Y. Isono, “Quasi-static bending test of nano-scale SiO2 wire at intermediate temperatures using AFM-based technique,” *Sensors Actuators, A Phys.*, vol. 104, no. 1, pp. 78–85, 2003.

[55] T. Namazu, Y. Isono, and T. Tanaka, “Evaluation of size effect on mechanical properties of single crystal silicon by nanoscale bending test using AFM,” *J Microelectromech S*, vol. 9, pp. 450–459, 2000.

[56] C. M. Lieber, “One-dimensional nanostructures: Chemistry, physics & applications,” *Solid State Communications*, vol. 107, no. 11. pp. 607–616, 1998.

[57] T. Zhai, L. Li, Y. Ma, M. Liao, X. Wang, X. Fang, J. Yao, Y. Bando, and D. Golberg, “One-dimensional inorganic nanostructures: synthesis, field-emission and photodetection.,” *Chem. Soc. Rev.*, vol. 40, no. 5, pp. 2986–3004, 2011.

[58] B. Erdem Alaca, “Integration of one-dimensional nanostructures with microsystems: an overview,” *International Materials Reviews*, vol. 54, no. 5. pp. 245–282, 2009.

[59] X. T. Zhou, J. Q. Hu, C. P. Li, D. D. D. Ma, C. S. Lee, and S. T. Lee, “Silicon nanowires as chemical sensors,” *Chemical Physics Letters*, vol. 369, no. 1–2. pp. 220–224, 2003.

[60] X. T. Zhou, J. Q. Hu, C. P. Li, D. D. D. Ma, C. S. Lee, and S. T. Lee, “Silicon nanowires as chemical sensors,” *Chem. Phys. Lett.*, vol. 369, no. 1–2, pp. 220–224, 2003.

[61] X.-J. Huang and Y.-K. Choi, “Chemical sensors based on nanostructured materials,” *Sensors and Actuators B: Chemical*, vol. 122, no. 2. pp. 659–671, 2007.

[62] A. Liu, “Towards development of chemosensors and biosensors with metal-oxide-based nanowires or nanotubes,” *Biosensors and Bioelectronics*, vol. 24, no. 2. pp. 167–177, 2008.

[63] N. S. Ramgir, Y. Yang, and M. Zacharias, “Nanowire-based sensors,” *Small*, vol. 6, no. 16. pp. 1705–1722, 2010.

[64] R. M. Penner, “Chemical Sensing with Nanowires,” *Annual Review of Analytical Chemistry*, vol. 5, no. 1. pp. 461–485, 2012.

[65] R. Agarwal and C. M. Lieber, “Semiconductor nanowires: Optics and optoelectronics,” *Appl. Phys. A Mater. Sci. Process.*, vol. 85, no. 3, pp. 209–215, 2006.

[66] Y. Kim, Q. Gao, H. J. Joyce, H. H. Tan, C. Jagadish, M. Paladugu, and J. Zou, “III-V nanowires for optoelectronics,” in *Proc. of SPIE*, 2006, vol. 6352, p. 635226.

[67] Y. T. Yang, C. Callegari, X. L. Feng, K. L. Ekinci, and M. L. Roukes, “Zeptogram-scale nanomechanical mass sensing,” *Nano Lett.*, vol. 6, no. 4, pp. 583–586, 2006.

[68] W. Hiebert, “Mass sensing: Devices reach single-proton limit,” *Nature Nanotechnology*, vol. 7, no. 5. pp. 278–280, 2012.

[69] J. Xiang, W. Lu, Y. Hu, Y. Wu, H. Yan, and C. M. Lieber, “Ge/Si nanowire heterostructures as high-performance field-effect transistors.,” *Nature*, vol. 441, no. 7092, pp. 489–493, 2006.

[70] Y.-S. Sohn, J. Park, G. Yoon, J. Song, S.-W. Jee, J.-H. Lee, S. Na, T. Kwon, and K. Eom, “Mechanical Properties of Silicon Nanowires.,” *Nanoscale Res. Lett.*, vol. 5, no. 1, pp. 211–216, 2009.

[71] D.-M. Tang, C.-L. Ren, M.-S. Wang, X. Wei, N. Kawamoto, C. Liu, Y. Bando, M. Mitome, N. Fukata, and D. Golberg, “Mechanical properties of Si nanowires

as revealed by in situ transmission electron microscopy and molecular dynamics simulations.," *Nano Lett.*, vol. 12, no. 4, pp. 1898–1904, 2012.

[72] B. Wu, A. Heidelberg, and J. J. Boland, "Mechanical properties of ultrahigh-strength gold nanowires.," *Nat. Mater.*, vol. 4, no. 7, pp. 525–529, 2005.

[73] D. Zhang, J. M. Breguet, R. Clavel, V. Sivakov, S. Christiansen, and J. Michler, "In situ electron microscopy mechanical testing of silicon nanowires using electrostatically actuated tensile stages," *J. Microelectromechanical Syst.*, vol. 19, no. 3, pp. 663–674, 2010.

[74] Z. L. Wang, Z. R. Dai, R. P. Gao, and J. L. Gole, "Measuring the Young's modulus of solid nanowires by in situ TEM," *J. Electron Microsc. (Tokyo).*, vol. 51, no. 90001, p. 79S–85, 2002.

[75] B. Chen, J. Wang, Q. Gao, Y. Chen, X. Liao, C. Lu, H. H. Tan, Y. W. Mai, J. Zou, S. P. Ringer, H. Gao, and C. Jagadish, "Strengthening brittle semiconductor nanowires through stacking faults: Insights from in situ mechanical testing," *Nano Lett.*, vol. 13, no. 9, pp. 4369–4373, 2013.

[76] E. Celik, I. Guven, and E. Madenci, "Mechanical characterization of nickel nanowires by using a customized atomic force microscope.," *Nanotechnology*, vol. 22, no. 15, p. 155702, 2011.

[77] G. Richter, K. Hillerich, D. S. Gianola, R. Mönig, O. Kraft, and C. A. Volkert, "Ultrahigh strength single crystalline nanowhiskers grown by physical vapor deposition," *Nano Lett.*, vol. 9, no. 8, pp. 3048–3052, 2009.

[78] J. H. Seo, Y. Yoo, N. Y. Park, S. W. Yoon, H. Lee, S. Han, S. W. Lee, T. Y. Seong, S. C. Lee, K. B. Lee, P. R. Cha, H. S. Park, B. Kim, and J. P. Ahn, "Superplastic deformation of defect-free Au nanowires via coherent twin propagation," *Nano Lett.*, vol. 11, no. 8, pp. 3499–3502, 2011.

[79] G. Galilei and S. Drake, *Two new sciences: including centers of gravity and force of percussion*. 1989.

[80] W. B. Parsons, *Engineers and Engineering in the Renaissance*. 1976.

[81] a. a. Griffith, "The Phenomena of Rupture and Flow in Solids," *Philos. Trans. R. Soc. A Math. Phys. Eng. Sci.*, vol. 221, no. 582–593, pp. 163–198, 1921.

[82] W. Weibull and W. Weibull, *A statistical theory of the strength of materials*, vol. 149. 1939.

[83] L. N. Davidenkov, E. Shevandin, F. Wittmann, “The Influence of Size on the Brittle Strength of Steel,” *J. Appl. Mech.*, pp. 63–67, 1947.

[84] J. Han, L. Fang, J. Sun, Y. Han, and K. Sun, “Length-dependent mechanical properties of gold nanowires,” *J. Appl. Phys.*, vol. 112, no. 11, 2012.

[85] M. Lucas, A. M. Leach, M. T. McDowell, S. E. Hunyadi, K. Gall, C. J. Murphy, and E. Riedo, “Plastic deformation of pentagonal silver nanowires: Comparison between AFM nanoindentation and atomistic simulations,” *Phys. Rev. B - Condens. Matter Mater. Phys.*, vol. 77, no. 24, 2008.

[86] A. Asthana, K. Momeni, A. Prasad, Y. K. Yap, and R. S. Yassar, “In situ observation of size-scale effects on the mechanical properties of ZnO nanowires.,” *Nanotechnology*, vol. 22, no. 26, p. 265712, 2011.

[87] B. Wen, J. Sader, and J. Boland, “Mechanical Properties of ZnO Nanowires,” *Physical Review Letters*, vol. 101, no. 17. 2008.

[88] A. V. Desai and M. A. Haque, “Mechanical properties of ZnO nanowires,” *Sensors and Actuators A: Physical*, vol. 134, no. 1. pp. 169–176, 2007.

[89] Y. Zhu, F. Xu, Q. Qin, W. Y. Fung, and W. Lu, “Mechanical properties of vapor-liquid-solid synthesized silicon nanowires.,” *Nano Lett.*, vol. 9, no. 11, pp. 3934–3939, 2009.

[90] X. Wu, J. S. Kulkarni, G. Collins, N. Petkov, D. Almécija, J. J. Boland, D. Erts, and J. D. Holmes, “Synthesis and electrical and mechanical properties of silicon and germanium nanowires,” *Chemistry of Materials*, vol. 20, no. 19. pp. 5954–5967, 2008.

[91] P.-C. Chang, Z. Fan, C.-J. Chien, D. Stichtenoth, C. Ronning, and J. G. Lu, “High-performance ZnO nanowire field effect transistors,” *Appl. Phys. Lett.*, vol. 89, no. 13, p. 133113, 2006.

[92] S. N. Cha, J. E. Jang, Y. Choi, G. A. J. Amaratunga, G. W. Ho, M. E. Welland, D. G. Hasko, D. J. Kang, and J. M. Kim, “High performance ZnO nanowire field effect transistor using self-aligned nanogap gate electrodes,” *Appl. Phys. Lett.*, vol. 89, no. 26, 2006.

[93] K. E. Moselund, M. T. Björk, H. Schmid, H. Ghoneim, S. Karg, E. Lörtscher, W. Riess, and H. Riel, “Silicon nanowire tunnel FETs: Low-temperature operation and influence of high-k gate dielectric,” *IEEE Transactions on Electron Devices*, vol. 58, no. 9. pp. 2911–2916, 2011.

[94] P. Xie, Q. Xiong, Y. Fang, Q. Qing, and C. M. Lieber, “Local electrical potential detection of DNA by nanowire–nanopore sensors,” *Nature Nanotechnology*, vol. 7, no. 2. pp. 119–125, 2011.

[95] M. Sakurai, Y. G. Wang, T. Uemura, and M. Aono, “Electrical properties of individual ZnO nanowires.,” *Nanotechnology*, vol. 20, no. 15, p. 155203, 2009.

[96] J. Y. Huang, H. Zheng, S. X. Mao, Q. Li, and G. T. Wang, “In situ nanomechanics of GaN nanowires,” *Nano Lett.*, vol. 11, no. 4, pp. 1618–1622, 2011.

[97] X. Teng, M. Feygenson, Q. Wang, J. He, W. Du, A. I. Frenkel, W. Han, and M. Aronson, “Electronic and magnetic properties of ultrathin Au/Pt nanowires,” *Nano Lett.*, vol. 9, no. 9, pp. 3177–3184, 2009.

[98] X. Teng, W. Q. Han, W. Ku, and M. Hücker, “Synthesis of ultrathin palladium and platinum nanowires and a study of their magnetic properties,” *Angew. Chemie - Int. Ed.*, vol. 47, no. 11, pp. 2055–2058, 2008.

[99] D. A. LaVan and W. N. Sharpe, “Tensile testing of microsamples,” *Experimental Mechanics*, vol. 39, no. 3. pp. 210–216, 1999.

[100] W. N. Sharpe, J. Bagdahn, K. Jackson, and G. Coles, “Tensile testing of MEMS materials - recent progress,” *J. Mater. Sci.*, vol. 38, pp. 4075–4079, 2003.

[101] M. A. Haque and M. T. A Saif, “Mechanical behavior of 30-50 nm thick aluminum films under uniaxial tension,” *Scr. Mater.*, vol. 47, no. 12, pp. 863–867, 2002.

[102] Y. Zhu, C. Ke, and H. D. Espinosa, “Experimental techniques for the mechanical characterization of one-dimensional nanostructures,” *Experimental Mechanics*, vol. 47, no. 1. pp. 7–24, 2007.

[103] D. Nakabayashi, P. C. Silva, J. C. González, V. Rodrigues, and D. Ugarte, “Low-cost nanomanipulator for in situ experiments in a SEM.,” *Microsc. Microanal.*, vol. 12, no. 4, pp. 311–316, 2006.

[104] B. Moser, J. Kuebler, H. Meinhard, W. Muster, and J. Michler, “Observation of instabilities during plastic deformation by in-situ SEM indentation experiments,” *Adv. Eng. Mater.*, vol. 7, no. 5, pp. 388–392, 2005.

[105] J. Xiao, S. Y. Ryu, Y. Huang, K.-C. Hwang, U. Paik, and J. A. Rogers, "Mechanics of nanowire/nanotube in-surface buckling on elastomeric substrates.," *Nanotechnology*, vol. 21, no. 8, p. 85708, 2010.

[106] H. S. Park, "Surface stress effects on the critical buckling strains of silicon nanowires," *Comput. Mater. Sci.*, vol. 51, no. 1, pp. 396–401, 2012.

[107] S. J. Young, L. W. Ji, S. J. Chang, T. H. Fang, and T. J. Hsueh, "Nanoindentation of vertical ZnO nanowires," *Phys. E Low-Dimensional Syst. Nanostructures*, vol. 39, no. 2, pp. 240–243, 2007.

[108] J. Song, X. Wang, E. Riedo, and Z. L. Wang, "Elastic property of vertically aligned nanowires," *Nano Lett.*, vol. 5, no. 10, pp. 1954–1958, 2005.

[109] J. Liu, S. Lee, K. Lee, Y. H. Ahn, J.-Y. Park, and K. H. Koh, "Bending and bundling of metal-free vertically aligned ZnO nanowires due to electrostatic interaction.," *Nanotechnology*, vol. 19, no. 18, p. 185607, 2008.

[110] Y. Huang, Y. Zhang, X. Wang, X. Bai, Y. Gu, X. Yan, Q. Liao, J. Qi, and J. Liu, "Size independence and doping dependence of bending modulus in znO nanowires," *Cryst. Growth Des.*, vol. 9, no. 4, pp. 1640–1642, 2009.

[111] G. Feng, W. D. Nix, Y. Yoon, and C. J. Lee, "A study of the mechanical properties of nanowires using nanoindentation," *J. Appl. Phys.*, vol. 99, no. 7, 2006.

[112] D. M. Ebenstein and L. A. Pruitt, "Nanoindentation of biological materials," *Nano Today*, vol. 1, no. 3, pp. 26–33, 2006.

[113] N. K. Chang, Y. S. Lin, C. Y. Chen, and S. H. Chang, "Size effect of indenter on determining modulus of nanowires using nanoindentation technique," *Thin Solid Films*, vol. 517, no. 13, pp. 3695–3697, 2009.

[114] P. E. Allain, A. Bosseboeuf, F. Parrain, S. Maaroufi, P. Coste, and A. Walther, "Large range MEMS motion detection using integrated piezo-resistive silicon nanowire," in *Proceedings of the IEEE International Conference on Micro Electro Mechanical Systems (MEMS)*, 2012, pp. 1320–1323.

[115] K. A. Shaw, Z. L. Zhang, and N. C. MacDonald, "SCREAM I: A single mask, single-crystal silicon process for microelectromechanical structures," *[1993] Proc. IEEE Micro Electro Mech. Syst.*, 1993.

[116] K. A. Shaw, Z. L. Zhang, and N. C. MacDonald, “SCREAM I: a single mask, single-crystal silicon, reactive ion etching process for microelectromechanical structures,” *Sensors Actuators A Phys.*, vol. 40, pp. 63–70, 1994.

[117] G. H. P. Zhang W, Zhang W, Turner K, “Scream’03: A Single Mask Process For High-Q Single Crystal Silicon MEMS,” in *Proceedings of IMECE04*, 2004.

[118] a. N. Cleland and M. L. Roukes, “Fabrication of high frequency nanometer scale mechanical resonators from bulk Si crystals,” *Appl. Phys. Lett.*, vol. 69, p. 2653, 1996.

[119] O. Ozsun, B. E. Alaca, Y. Leblebici, A. D. Yalcinkaya, I. Yildiz, M. Yilmaz, and M. Zervas, “Monolithic integration of silicon nanowires with a microgripper,” *J. Microelectromechanical Syst.*, vol. 18, pp. 1335–1344, 2009.

[120] T. H. P. Chang, “Proximity effect in electron-beam lithography,” *Journal of Vacuum Science and Technology*, vol. 12. p. 1271, 1975.

[121] G. Binnig, C. Quate, and C. Gerber, “Atomic Force Microscope,” *Phys. Rev. Lett.*, vol. 56, no. 9, pp. 930–933, 1986.

[122] E. Meyer, “Atomic force microscopy,” *Progress in Surface Science*, vol. 41, no. 1. pp. 3–49, 1992.

[123] A. Trache and G. A. Meininger, “Atomic force microscopy (AFM),” *Curr Protoc Microbiol*, vol. Chapter 2, p. Unit 2C 2, 2008.

[124] A. Trache and G. A. Meininger, “Atomic force microscopy (AFM),” *Current Protocols in Microbiology*, no. SUPPL. 8. 2008.

[125] C. R. Blanchard, “Atomic Force Microscopy–AFM,” *Chem. Educ.*, vol. 1, pp. 1–8, 2000.

[126] B. Wen, J. Sader, and J. Boland, “Mechanical Properties of ZnO Nanowires,” *Phys. Rev. Lett.*, vol. 101, p. 175502, 2008.

[127] J. L. Hutter and J. Bechhoefer, “Calibration of atomic-force microscope tips,” *Rev. Sci. Instrum.*, vol. 64, no. 7, p. 1868, 1993.

[128] H. Butt and M. Jaschke, “Calculation of thermal noise in atomic force microscopy,” *Nanotechnology*, vol. 1, 1995.

[129] D. a. Walters, J. P. Cleveland, N. H. Thomson, P. K. Hansma, M. a. Wendman, G. Gurley, and V. Elings, "Short cantilevers for atomic force microscopy," *Rev. Sci. Instrum.*, vol. 67, no. 10, p. 3583, 1996.

[130] J. L. Hutter, "Comment on Tilt of Atomic Force Microscope Cantilevers - Effect on Spring Constant and Adhesion Measurements," *Langmuir*, pp. 2630–2632, 2005.

[131] H. J. Butt, B. Cappella, and M. Kappl, "Force measurements with the atomic force microscope: Technique, interpretation and applications," *Surf. Sci. Rep.*, vol. 59, no. 1–6, pp. 1–152, 2005.

[132] B. Cappella, P. Baschieri, C. Frediani, P. Miccoli, and C. Ascoli, "Force-distance curves by AFM," *IEEE Engineering in Medicine and Biology Magazine*, vol. 16, no. 2. pp. 58–65, 1997.

[133] C. S. Hodges, "Measuring forces with the AFM: Polymeric surfaces in liquids," *Advances in Colloid and Interface Science*, vol. 99, no. 1. pp. 13–75, 2002.

[134] M. Pfreundschuh, D. Martinez-Martin, E. Mulvihill, S. Wegmann, and D. J. Muller, "Multiparametric high-resolution imaging of native proteins by force-distance curve-based AFM.," *Nat. Protoc.*, vol. 9, no. 5, pp. 1113–30, 2014.

[135] M. Radmacher, "Measuring the elastic properties of biological samples with the AFM," *Eng. Med. Biol.*, vol. 16, no. 2, pp. 47–57, 1997.

[136] W. Heinz, A. Emad, J. Hassn, and F. Serry, "Applications of Force Volume Imaging with Atomic Force Microscopes," *Veeco application note AN20, …*, vol. Im. pp. 1–4, 2004.

[137] C. T. Gibson, B. L. Weeks, C. Abell, T. Rayment, and S. Myhra, "Calibration of AFM cantilever spring constants," *Ultramicroscopy*, vol. 97, no. 1–4, pp. 113–118, 2003.

[138] B. Pittenger, N. Erina, and C. Su, "Application Note # 128 Quantitative Mechanical Property Mapping at the Nanoscale with PeakForce QNM," 2012.

[139] Bruker AFM Probes, "FASTSCAN-A," 2015. [Online]. Available: http://www.brukerafmprobes.com/p-3759-fastscan-a.aspx.

[140] B. D. Cullity, "Elements of X-Ray Diffraction," *American Journal of Physics*, vol. 25, no. 6. p. 394, 1957.

[141] A. Dommann, A. Enzler, and N. Onda, “Advanced X-ray analysis techniques to investigate aging of micromachined silicon actuators for space application,” in *Microelectronics Reliability*, 2003, vol. 43, no. 7, pp. 1099–1103.

[142] A. Sakdinawat and D. Attwood, “Nanoscale X-ray imaging,” *Nature Photonics*, vol. 4, no. 12. pp. 840–848, 2010.

[143] M. A. Capano, B. C. Kim, A. R. Smith, E. P. Kvam, S. Tsoi, and A. K. Ramdas, “Residual strains in cubic silicon carbide measured by Raman spectroscopy correlated with x-ray diffraction and transmission electron microscopy,” *J. Appl. Phys.*, vol. 100, no. 8, 2006.

[144] C. Men and C. Lin, “Characterization of bonded silicon-on-aluminum-nitride wafers with RBS, TEM and HRXRD techniques,” *Microelectron. Eng.*, vol. 85, no. 8, pp. 1807–1810, 2008.

[145] A. Setiawan, I. Hamidah, S. Maryanto, S. Aisyah, and T. Yao, “Dislocations in P-MBE grown ZnO layers characterized by HRXRD and TEM,” in *AIP Conference Proceedings*, 2008, vol. 989, pp. 138–142.

[146] E. Mukhamedzhanov, M. Kummer, and A. Dommann, “Triple-crystal diffractometry, x-ray standing wave and reciprocal space mapping study of homoepitaxial grown Si layers,” *Journal of Physics D: Applied Physics*, vol. 33, no. 17. pp. 2087–2091, 2000.

[147] A. Neels, A. Dommann, P. Niedermann, C. Farub, and H. Von Känel, “Advanced stress, strain and geometrical analysis in semiconductor devices,” in *AIP Conference Proceedings*, 2010, vol. 1300, pp. 114–119.

[148] A. Neels, A. Dommann, A. Schifferle, O. Papes, and E. Mazza, “Reliability and failure in single crystal silicon MEMS devices,” *Microelectron. Reliab.*, vol. 48, no. 8–9, pp. 1245–1247, 2008.

[149] Y. Lu and J. Lou, “Quantitative in-situ nanomechanical characterization of metallic nanowires,” *JOM*, vol. 63, no. 9. pp. 35–42, 2011.

[150] M. Radmacher, “Measuring the elastic properties of biological samples with the AFM,” *IEEE Eng. Med. Biol.*, vol. 16, no. 2, pp. 47–57, 1997.

[151] J. R. Withers and D. E. Aston, “Nanomechanical measurements with AFM in the elastic limit,” *Advances in Colloid and Interface Science*, vol. 120, no. 1–3. pp. 57–67, 2006.

[152] J. J. Roa, G. Oncins, J. Diaz, F. Sanz, and M. Segarra, “Calculation of Young’s modulus value by means of AFM.,” *Recent Pat. Nanotechnol.*, vol. 5, no. 1, pp. 27–36, 2011.

[153] S. Vlassov, B. Polyakov, L. M. Dorogin, M. Antsov, M. Mets, M. Umalas, R. Saar, R. Lõhmus, and I. Kink, “Elasticity and yield strength of pentagonal silver nanowires: In situ bending tests,” *Mater. Chem. Phys.*, vol. 143, no. 3, pp. 1026–1031, 2014.

[154] Y. Chen, B. L. Dorgan, D. N. McIlroy, and D. E. Aston, “On the importance of boundary conditions on nanomechanical bending behavior and elastic modulus determination of silver nanowires,” *J. Appl. Phys.*, vol. 100, no. 10, 2006.

[155] G. Jing, H. Duan, X. Sun, Z. Zhang, J. Xu, Y. Li, J. Wang, and D. Yu, “Surface effects on elastic properties of silver nanowires: Contact atomic-force microscopy,” *Physical Review B*, vol. 73, no. 23. 2006.

[156] M. T. McDowell, A. M. Leach, and K. Gall, “Bending and tensile deformation of metallic nanowires,” *Modelling and Simulation in Materials Science and Engineering*, vol. 16, no. 4. p. 045003, 2008.

[157] G. Yun and H. S. Park, “Surface stress effects on the bending properties of fcc metal nanowires,” *Phys. Rev. B*, vol. 79, no. 19, p. 195421, 2009.

[158] G. Yun and H. Park, “Surface stress effects on the bending properties of fcc metal nanowires,” *Physical Review B*, vol. 79, no. 19. 2009.

[159] G. Yun and H. S. Park, “Surface stress effects on the bending properties of fcc metal nanowires,” *Phys. Rev. B*, vol. 79, no. 19, p. 15, 2009.

[160] A. W. Hassel, V. Cimalla, C. C. Röhlig, J. Pezoldt, M. Niebelschütz, O. Ambacher, K. Brückner, M. Hein, J. Weber, S. Milenkovic, and A. J. Smith, “Nanomechanics of single crystalline tungsten nanowires,” *J. Nanomater.*, vol. 2008, no. 1, 2008.

[161] S. Hoffmann, F. Östlund, J. Michler, H. J. Fan, M. Zacharias, S. H. Christiansen, and C. Ballif, “Fracture strength and Young’s modulus of ZnO nanowires,” *Nanotechnology*, vol. 18, no. 20. p. 205503, 2007.

[162] R. Erdlyi, M. Hannibal Madsen, G. Sfrn, Z. Hajnal, I. Endre Lukcs, G. Flp, S. Csonka, J. Nygrd, and J. Volk, “In-situ mechanical characterization of wurtzite InAs nanowires,” *Solid State Commun.*, vol. 152, no. 19, pp. 1829–1833, 2012.

[163] C. Lu, “On the bending strength of ZnO nanowires,” *Physics Letters A*, vol. 372, no. 39. pp. 6113–6115, 2008.

[164] B. Wen, J. Sader, and J. Boland, “Mechanical Properties of ZnO Nanowires,” *Phys. Rev. Lett.*, vol. 101, no. 17, p. 175502, 2008.

[165] H. Ni, X. Li, G. Cheng, and R. Klie, “Elastic modulus of single-crystal GaN nanowires,” *Journal of Materials Research*, vol. 21, no. 11. pp. 2882–2887, 2006.

[166] S. Yang, L. Wang, X. Tian, Z. Xu, W. Wang, X. Bai, and E. Wang, “Piezotronic Effect of Zinc Oxide Nanowires Studied by In Situ TEM.,” *Adv. Mater.*, pp. 1–7, 2012.

[167] B. Polyakov, L. M. Dorogin, S. Vlassov, I. Kink, A. E. Romanov, and R. Lohmus, “Simultaneous measurement of static and kinetic friction of ZnO nanowires in situ with a scanning electron microscope,” *Micron*, vol. 43, no. 11, pp. 1140–1146, 2012.

[168] S. Yang, L. Wang, X. Tian, Z. Xu, W. Wang, X. Bai, and E. Wang, “The piezotronic effect of zinc oxide nanowires studied by in situ TEM,” *Adv. Mater.*, vol. 24, no. 34, pp. 4676–4682, 2012.

[169] Y. Huang, X. Bai, and Y. Zhang, “In situ mechanical properties of individual ZnO nanowires and the mass measurement of nanoparticles,” *J. Phys. Condens. Matter*, vol. 18, no. 15, pp. L179–L184, 2006.

[170] K. H. Liu, P. Gao, Z. Xu, X. D. Bai, and E. G. Wang, “In situ probing electrical response on bending of ZnO nanowires inside transmission electron microscope,” *Appl. Phys. Lett.*, vol. 92, no. 21, 2008.

[171] C. Q. Chen and J. Zhu, “Bending strength and flexibility of ZnO nanowires,” *Appl. Phys. Lett.*, vol. 90, no. 4, 2007.

[172] A. Kushima, J. Y. Huang, and J. Li, “Quantitative fracture strength and plasticity measurements of lithiated silicon nanowires by in situ TEM tensile experiments,” *ACS Nano*, vol. 6, no. 11, pp. 9425–9432, 2012.

[173] G. Stan, S. Krylyuk, A. V. Davydov, I. Levin, and R. F. Cook, “Ultimate bending strength of Si nanowires,” *Nano Lett.*, vol. 12, no. 5, pp. 2599–2604, 2012.

[174] A. Heidelberg, L. T. Ngo, B. Wu, M. A. Phillips, S. Sharma, T. I. Kamins, J. E. Sader, and J. J. Boland, “A generalized description of the elastic properties of nanowires,” *Nano Lett.*, vol. 6, no. 6, pp. 1101–1106, 2006.

[175] S. Hoffmann, I. Utke, B. Moser, J. Michler, S. H. Christiansen, V. Schmidt, S. Senz, P. Werner, U. Gösele, and C. Ballif, “Measurement of the bending strength of vapor-liquid-solid grown silicon nanowires,” *Nano Lett.*, vol. 6, no. 4, pp. 622–625, 2006.

APPENDIX

Appendix A: Micro/Nanofabrication- Recipe Development Efforts

Process Steps	Sample No: 1	Sample No: 2	Sample No:3	Sample No: 4	Sample No: 5	Sample No: 6	Sample No: 7	Sample No: 8	Sample No: 9	Sample No: 10	Sample No: 11	Sample No: 12	Sample No: 13	Sample No: 14	Sample No: 15
STS time(sec.s)	35	17	17	17	35	35	35	35	35	35	35	35	35	35	35
RIE Step	single step	double step	double step	double step	single step	double step	single step	double step	single step	double step	single step	double step	single step	double step	single step
Final Trench Depth (μm)	7, 250	7, 000	7, 550	10, 000	7, 400	10, 000	5, 800	6, 800	7, 500	7, 500	12, 500	12, 500	10, 000	10, 000	11, 500
Result	OK	OK	OK	X	X	X	X	OK	OK	OK	X	X	OK	X	X

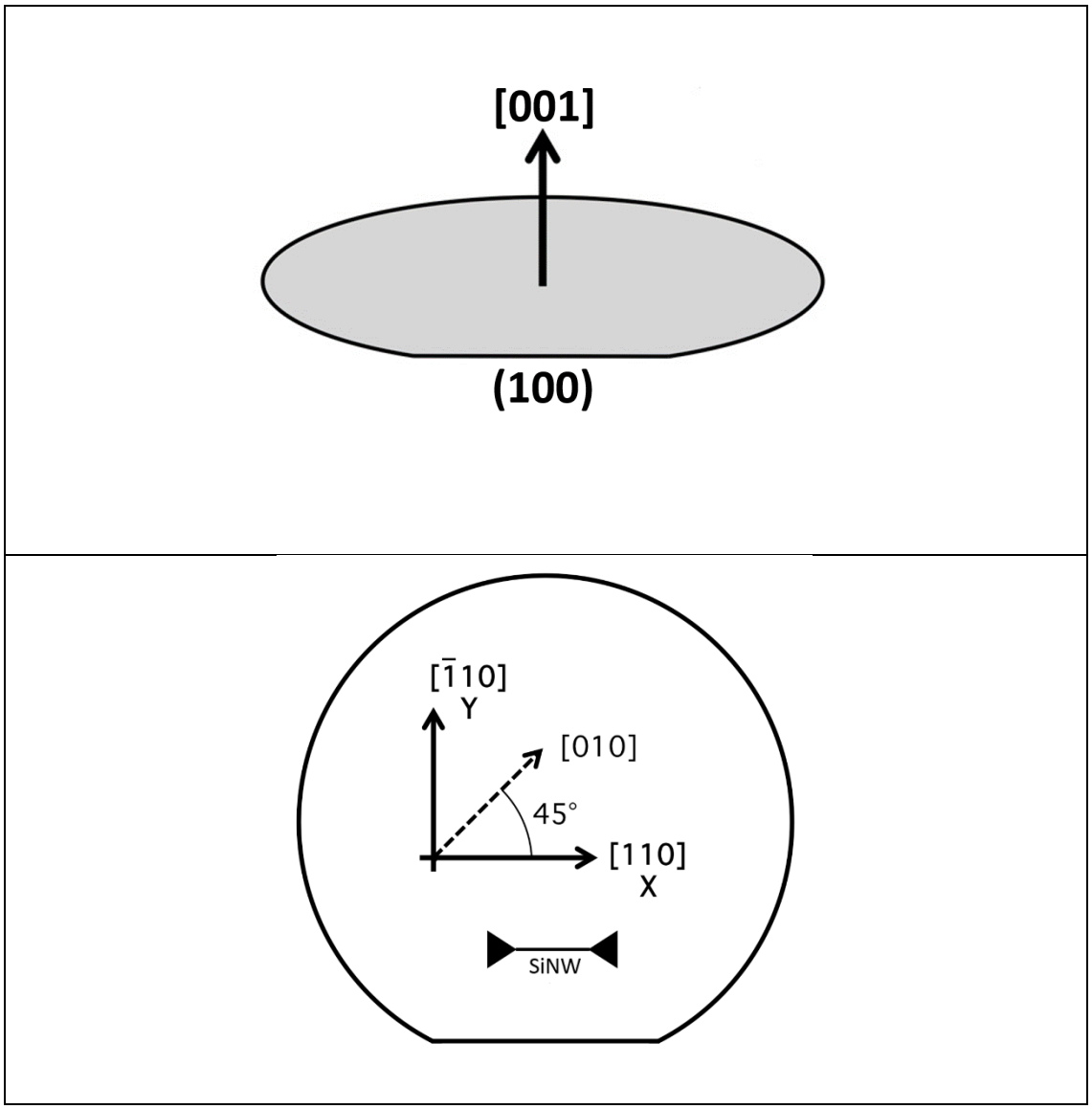
[001]
(100)
[1̄10]
Y
[010]
45°
[110]
X
SiNW

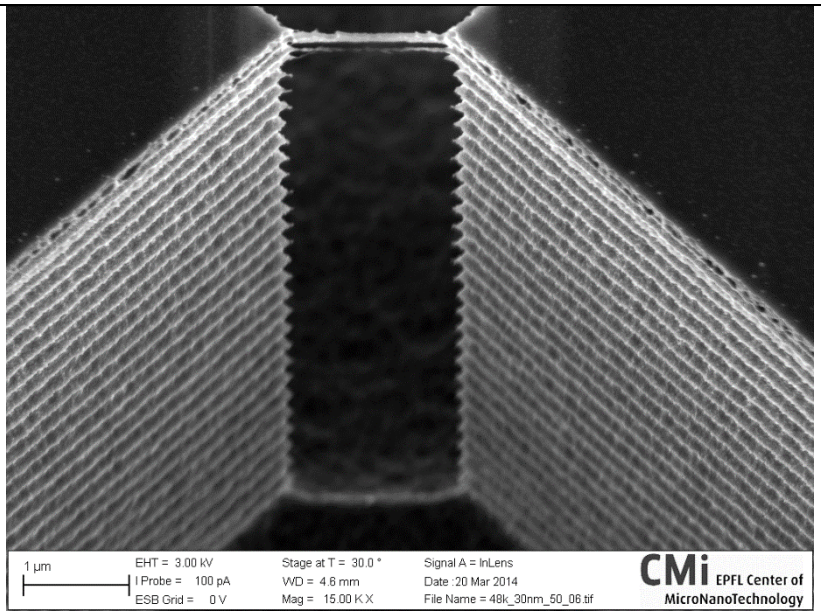
1 µm
EHT = 3.00 kV
I Probe = 100 pA
ESB Grid = 0 V
Stage at T = 30.0 °
WD = 4.6 mm
Mag = 15.00 K X
Signal A = InLens
Date :20 Mar 2014
File Name = 48k_30nm_50_06.tif
CMi EPFL Center of MicroNanoTechnology

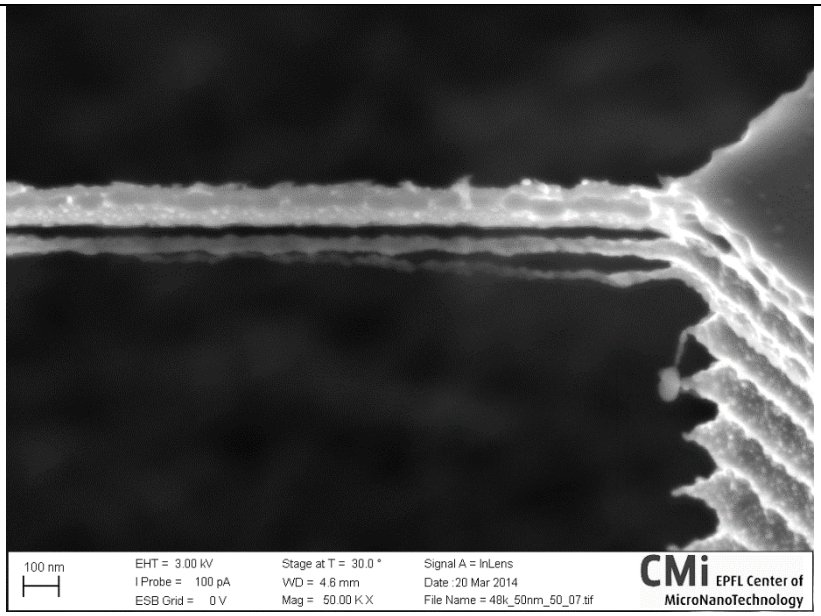
100 nm
EHT = 3.00 kV
I Probe = 100 pA
ESB Grid = 0 V
Stage at T = 30.0 °
WD = 4.6 mm
Mag = 50.00 K X
Signal A = InLens
Date :20 Mar 2014
File Name = 48k_50nm_50_07.tif
CMi EPFL Center of MicroNanoTechnology

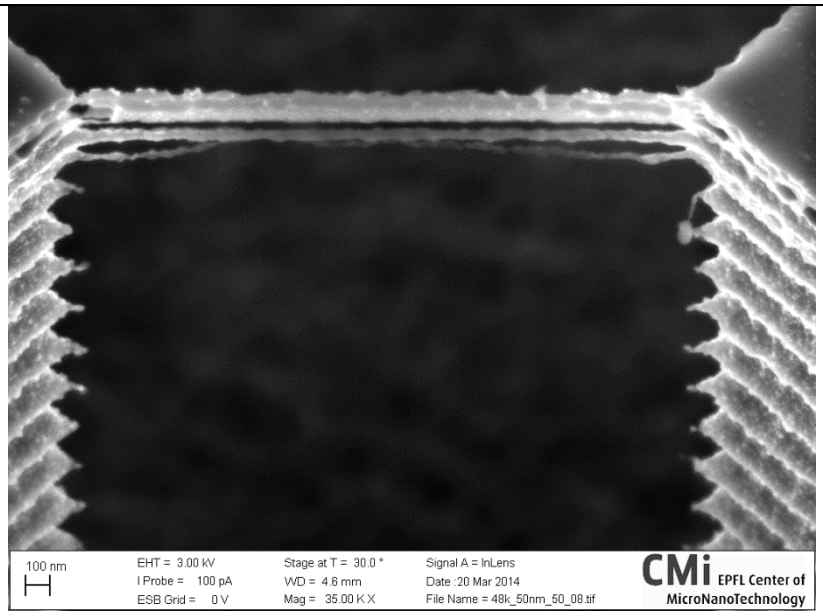
100 nm
EHT = 3.00 kV
I Probe = 100 pA
ESB Grid = 0 V
Stage at T = 30.0 °
WD = 4.6 mm
Mag = 35.00 K X
Signal A = InLens
Date :20 Mar 2014
File Name = 48k_50nm_50_08.tif
CMi EPFL Center of MicroNanoTechnology

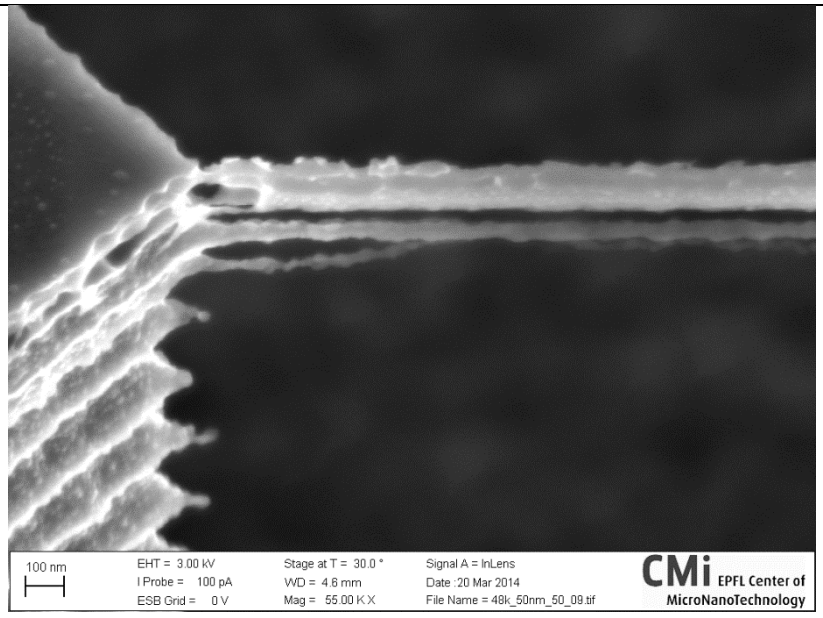
100 nm
EHT = 3.00 kV
I Probe = 100 pA
ESB Grid = 0 V
Stage at T = 30.0 °
WD = 4.6 mm
Mag = 55.00 K X
Signal A = InLens
Date :20 Mar 2014
File Name = 48k_50nm_50_09.tif
CMi EPFL Center of MicroNanoTechnology

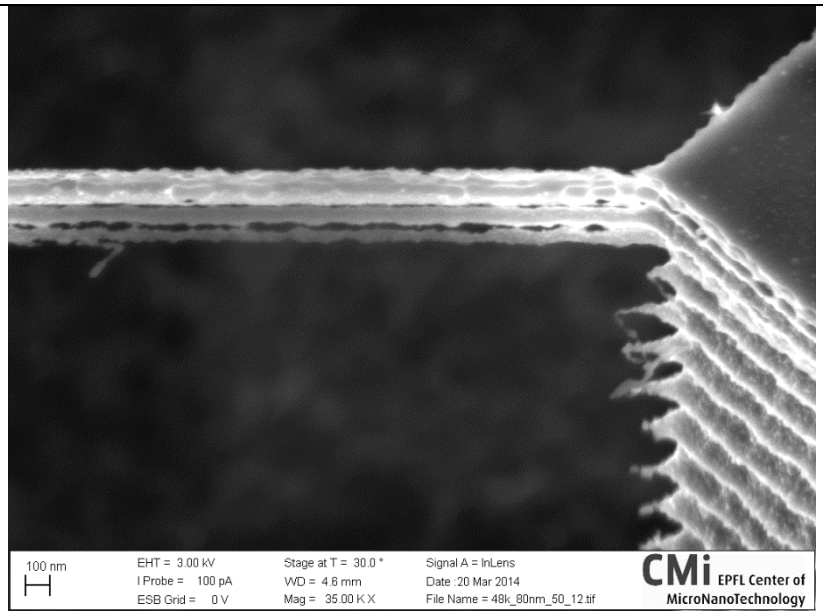
100 nm
EHT = 3.00 kV
I Probe = 100 pA
ESB Grid = 0 V
Stage at T = 30.0 °
WD = 4.6 mm
Mag = 35.00 K X
Signal A = InLens
Date :20 Mar 2014
File Name = 48k_80nm_50_12.tif
CMi EPFL Center of MicroNanoTechnology

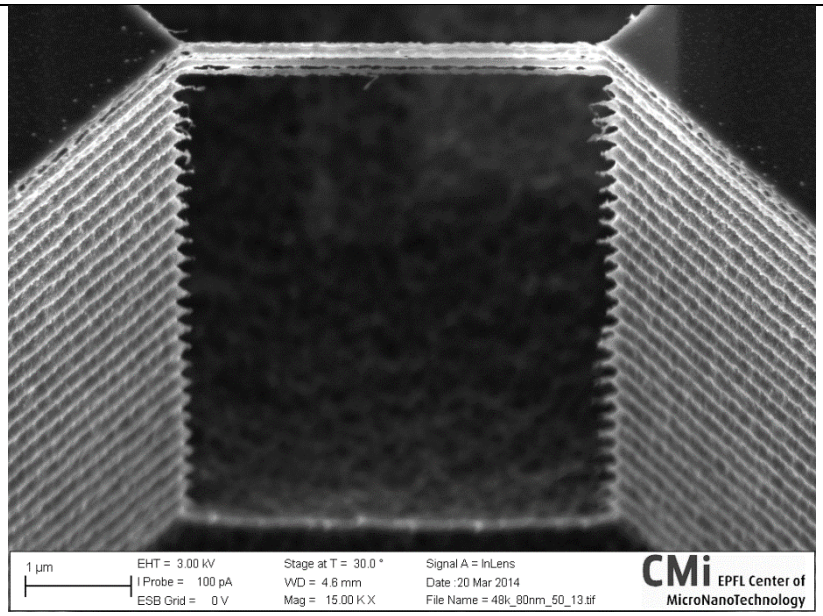
1 µm
EHT = 3.00 kV
I Probe = 100 pA
ESB Grid = 0 V
Stage at T = 30.0 °
WD = 4.6 mm
Mag = 15.00 K X
Signal A = InLens
Date :20 Mar 2014
File Name = 48k_80nm_50_13.tif
CMi EPFL Center of MicroNanoTechnology

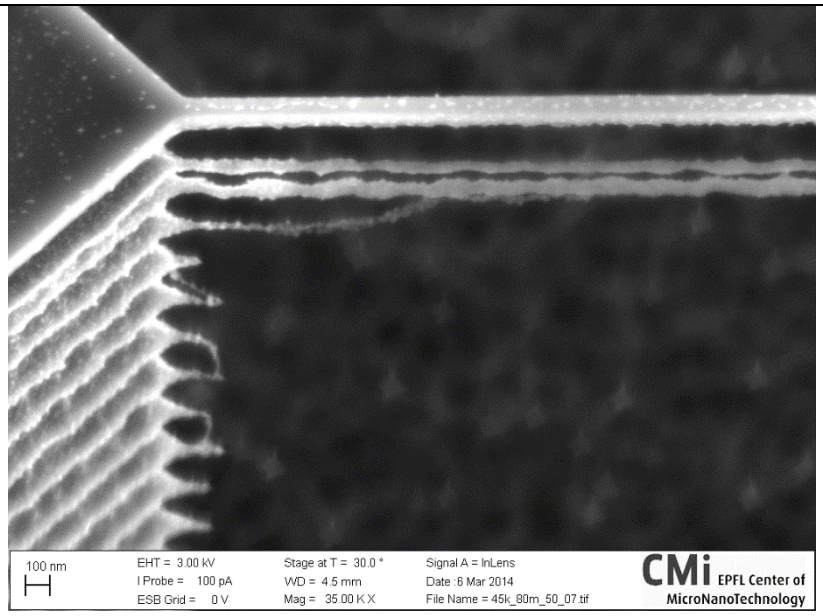
100 nm
EHT = 3.00 kV
I Probe = 100 pA
ESB Grid = 0 V
Stage at T = 30.0 °
WD = 4.5 mm
Mag = 35.00 K X
Signal A = InLens
Date :6 Mar 2014
File Name = 45k_80m_50_07.tif
CMi EPFL Center of MicroNanoTechnology

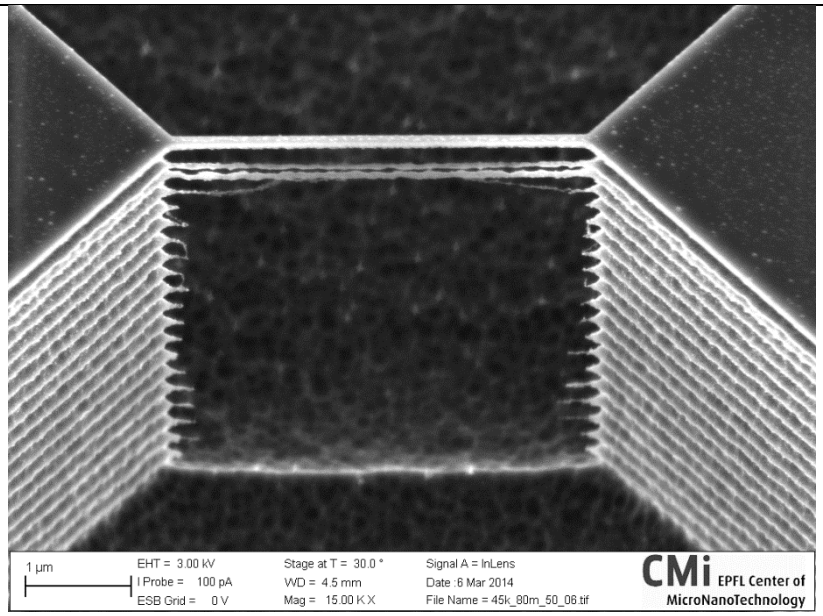
1 µm
EHT = 3.00 kV
I Probe = 100 pA
ESB Grid = 0 V
Stage at T = 30.0 °
WD = 4.5 mm
Mag = 15.00 K X
Signal A = InLens
Date :6 Mar 2014
File Name = 45k_80m_50_08.tif
CMi EPFL Center of MicroNanoTechnology

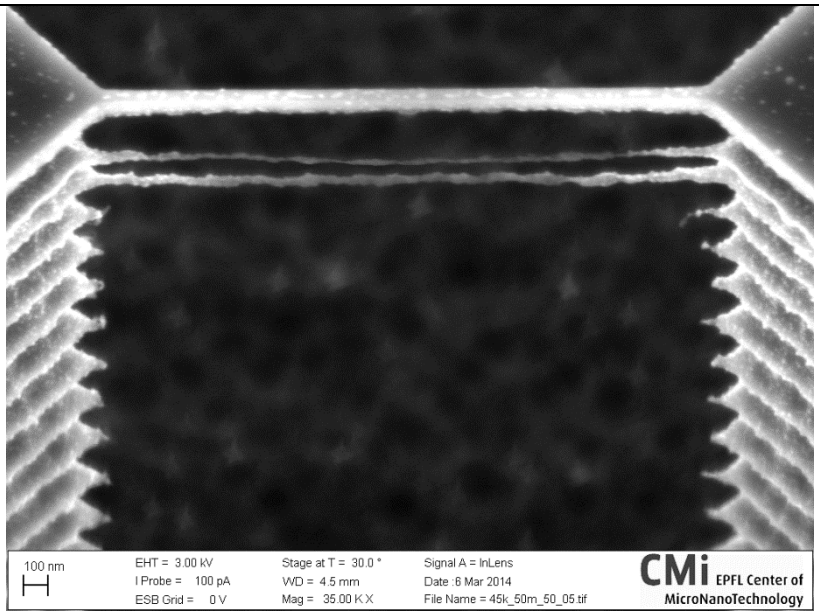
100 nm
EHT = 3.00 kV
I Probe = 100 pA
ESB Grid = 0 V
Stage at T = 30.0 °
WD = 4.5 mm
Mag = 35.00 K X
Signal A = InLens
Date :6 Mar 2014
File Name = 45k_50m_50_05.tif
CMi EPFL Center of MicroNanoTechnology

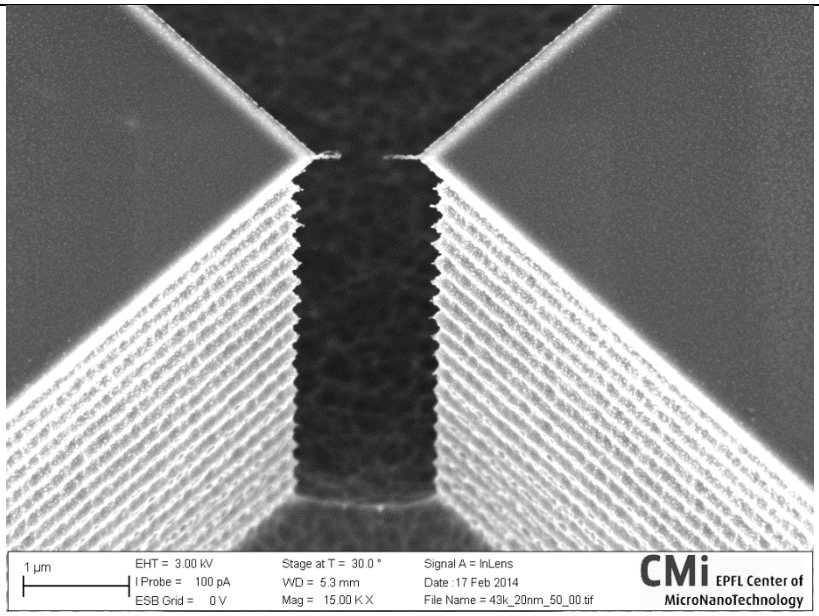
1 µm
EHT = 3.00 kV
I Probe = 100 pA
ESB Grid = 0 V
Stage at T = 30.0 °
WD = 5.3 mm
Mag = 15.00 K X
Signal A = InLens
Date :17 Feb 2014
File Name = 43k_20nm_50_00.tif
CMi EPFL Center of MicroNanoTechnology

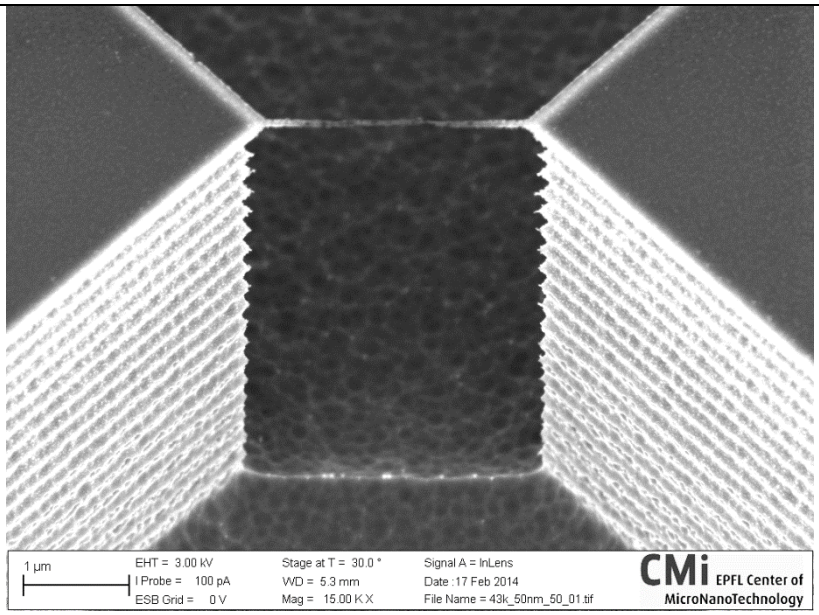
1 µm
EHT = 3.00 kV
I Probe = 100 pA
ESB Grid = 0 V
Stage at T = 30.0 °
WD = 5.3 mm
Mag = 15.00 K X
Signal A = InLens
Date :17 Feb 2014
File Name = 43k_50nm_50_01.tif
CMi EPFL Center of MicroNanoTechnology

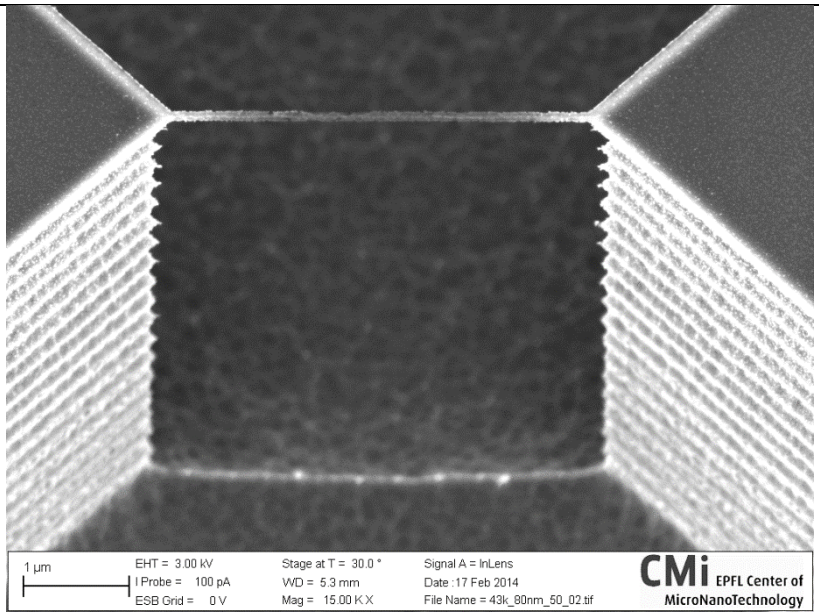
1 µm
EHT = 3.00 kV
I Probe = 100 pA
ESB Grid = 0 V
Stage at T = 30.0 °
WD = 5.3 mm
Mag = 15.00 K X
Signal A = InLens
Date :17 Feb 2014
File Name = 43k_80nm_50_02.tif
CMi EPFL Center of MicroNanoTechnology

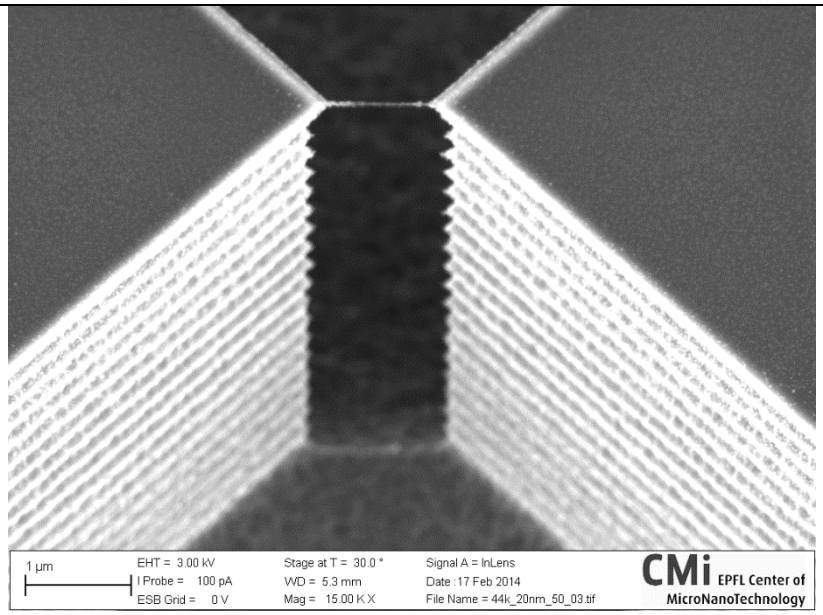
1 µm
EHT = 3.00 kV
I Probe = 100 pA
ESB Grid = 0 V
Stage at T = 30.0 °
WD = 5.3 mm
Mag = 15.00 K X
Signal A = InLens
Date :17 Feb 2014
File Name = 44k_20nm_50_03.tif
CMi EPFL Center of MicroNanoTechnology

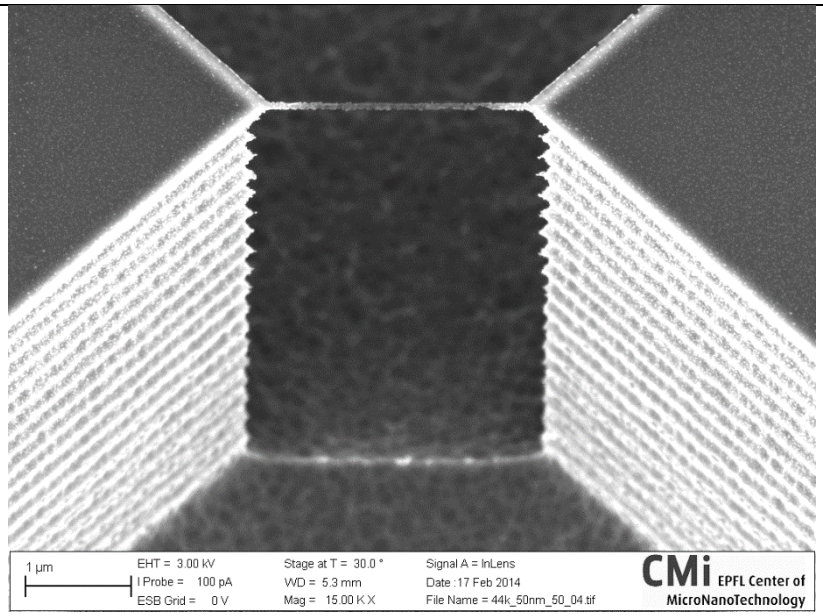
1 µm
EHT = 3.00 kV
I Probe = 100 pA
ESB Grid = 0 V
Stage at T = 30.0 °
WD = 5.3 mm
Mag = 15.00 K X
Signal A = InLens
Date :17 Feb 2014
File Name = 44k_50nm_50_04.tif
CMi EPFL Center of MicroNanoTechnology

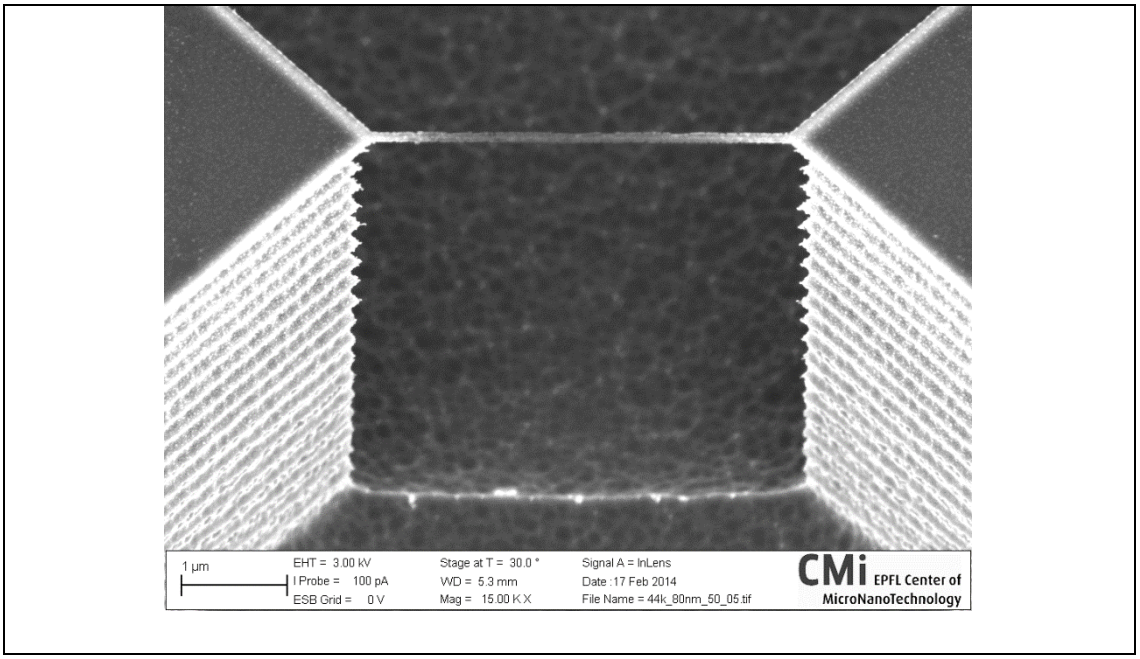

E-Beam Lithography Dose Calibration Study

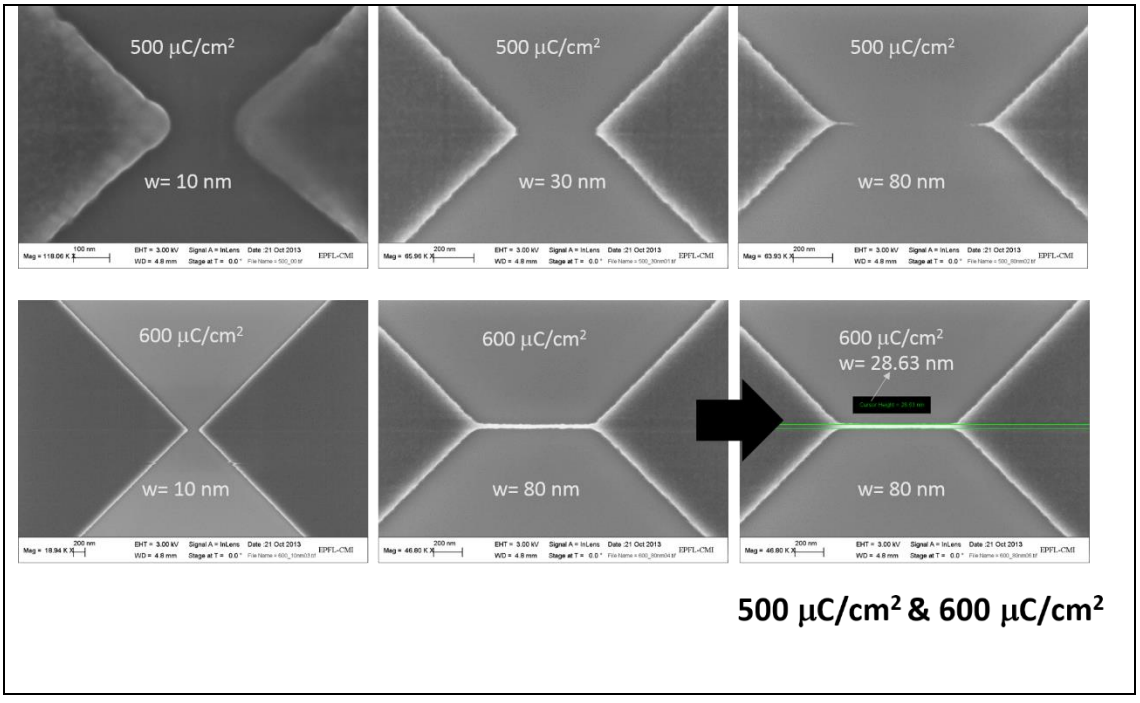

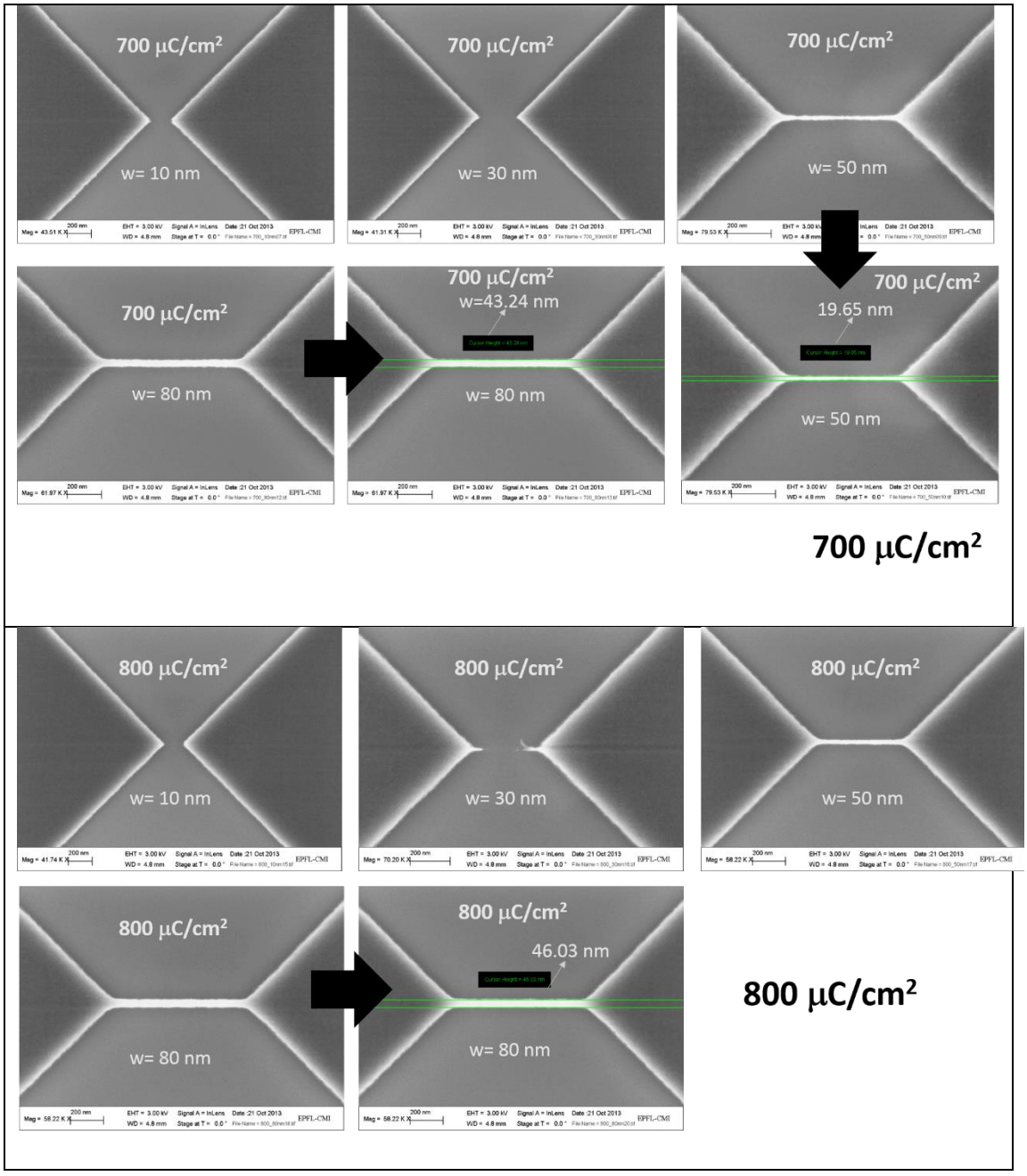
700 μC/cm²
w= 10 nm
700 μC/cm²
w= 30 nm
700 μC/cm²
w= 50 nm
700 μC/cm²
w= 80 nm
700 μC/cm²
w=43.24 nm
w= 80 nm
700 μC/cm²
19.65 nm
w= 50 nm
700 μC/cm²
800 μC/cm²
w= 10 nm
800 μC/cm²
w= 30 nm
800 μC/cm²
w= 50 nm
800 μC/cm²
w= 80 nm
800 μC/cm²
46.03 nm
w= 80 nm
800 μC/cm²

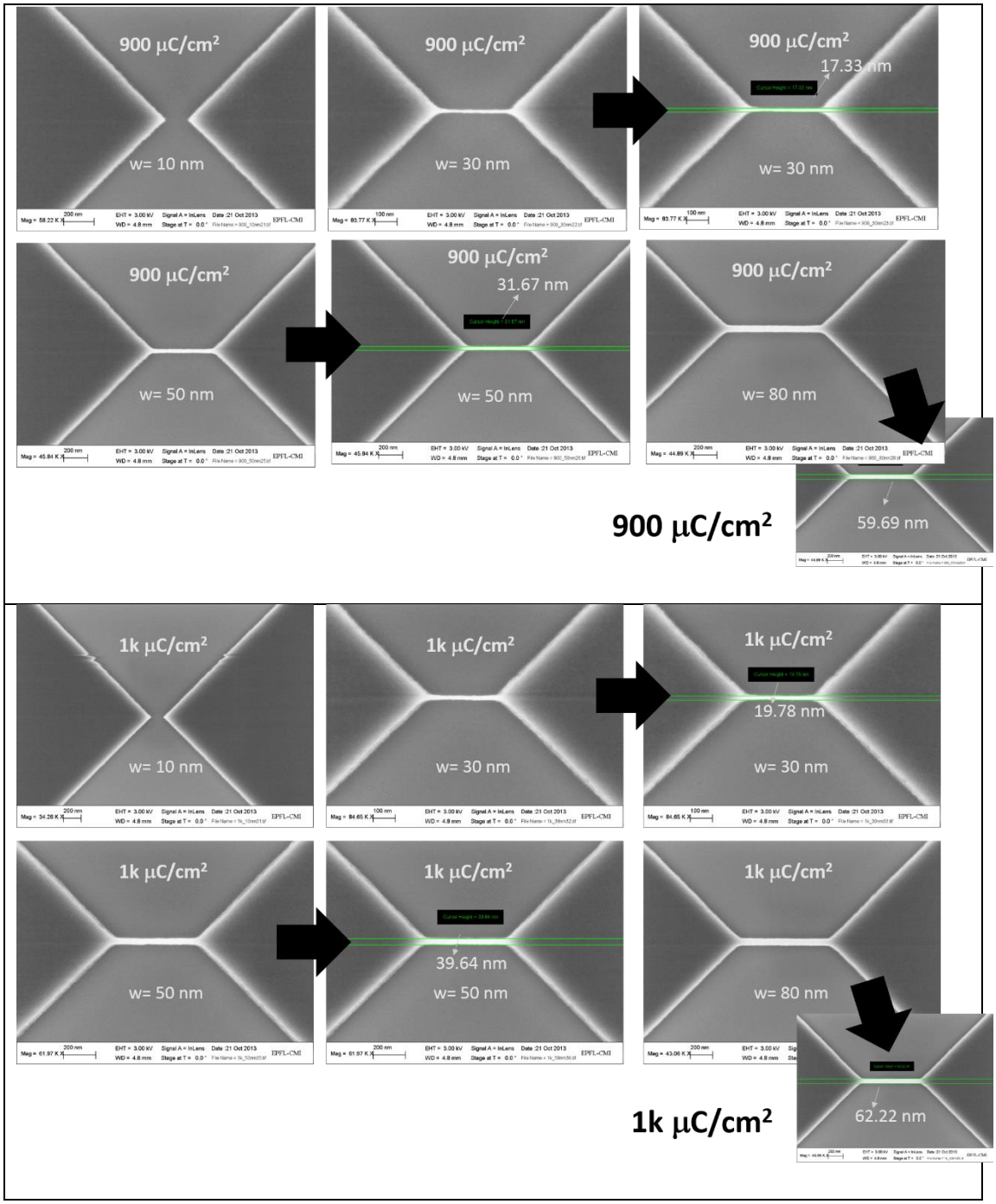
900 μC/cm²
w= 10 nm
900 μC/cm²
w= 30 nm
900 μC/cm²
17.33 nm
w= 30 nm
900 μC/cm²
w= 50 nm
900 μC/cm²
31.67 nm
w= 50 nm
900 μC/cm²
w= 80 nm
59.69 nm
900 μC/cm²
1k μC/cm²
w= 10 nm
1k μC/cm²
w= 30 nm
1k μC/cm²
19.78 nm
w= 30 nm
1k μC/cm²
w= 50 nm
1k μC/cm²
39.64 nm
w= 50 nm
1k μC/cm²
w= 80 nm
62.22 nm
1k μC/cm²

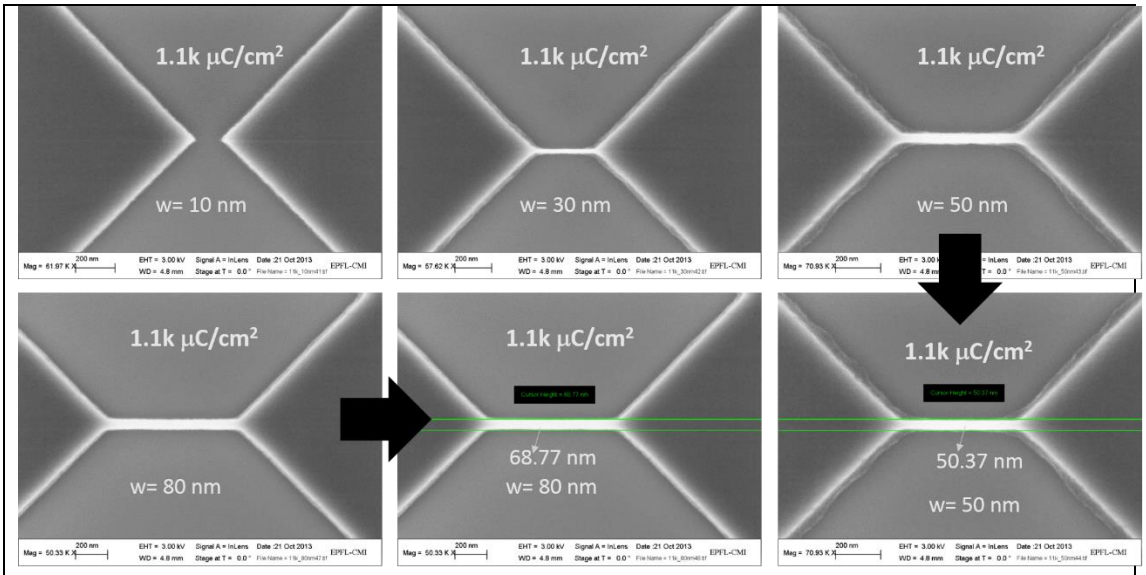

1.1k μC/cm²

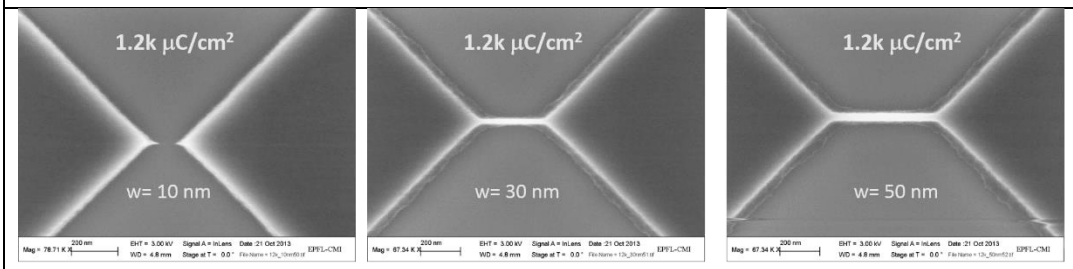

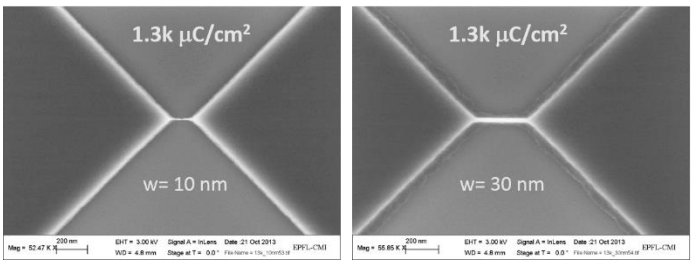

1.2k μC/cm² & 1.3k μC/cm²

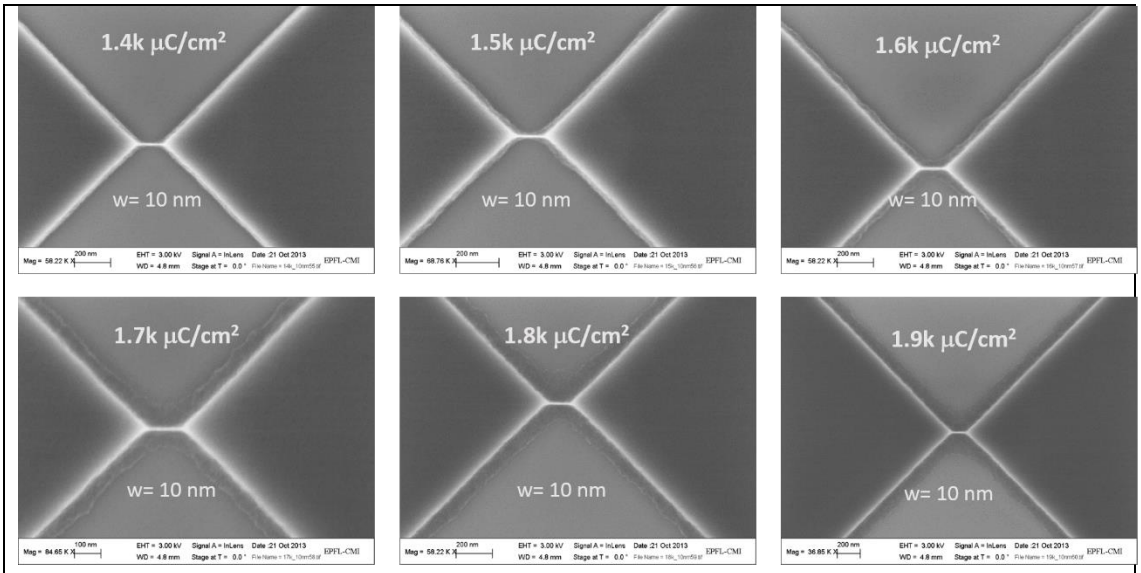

1.4k μC/cm² - 1.9k μC/cm²

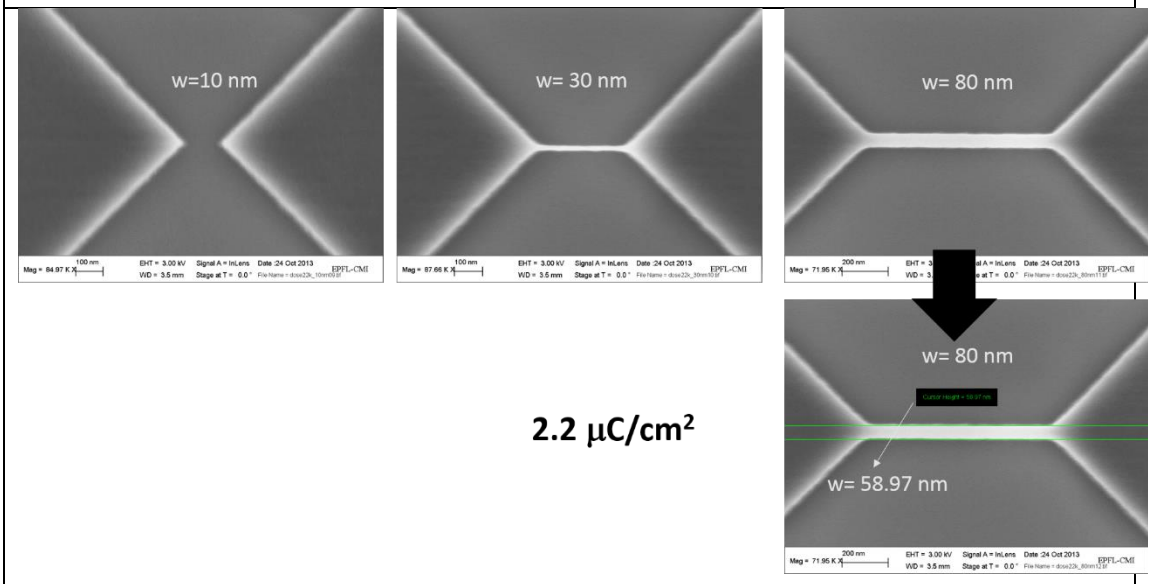

2.2 μC/cm²

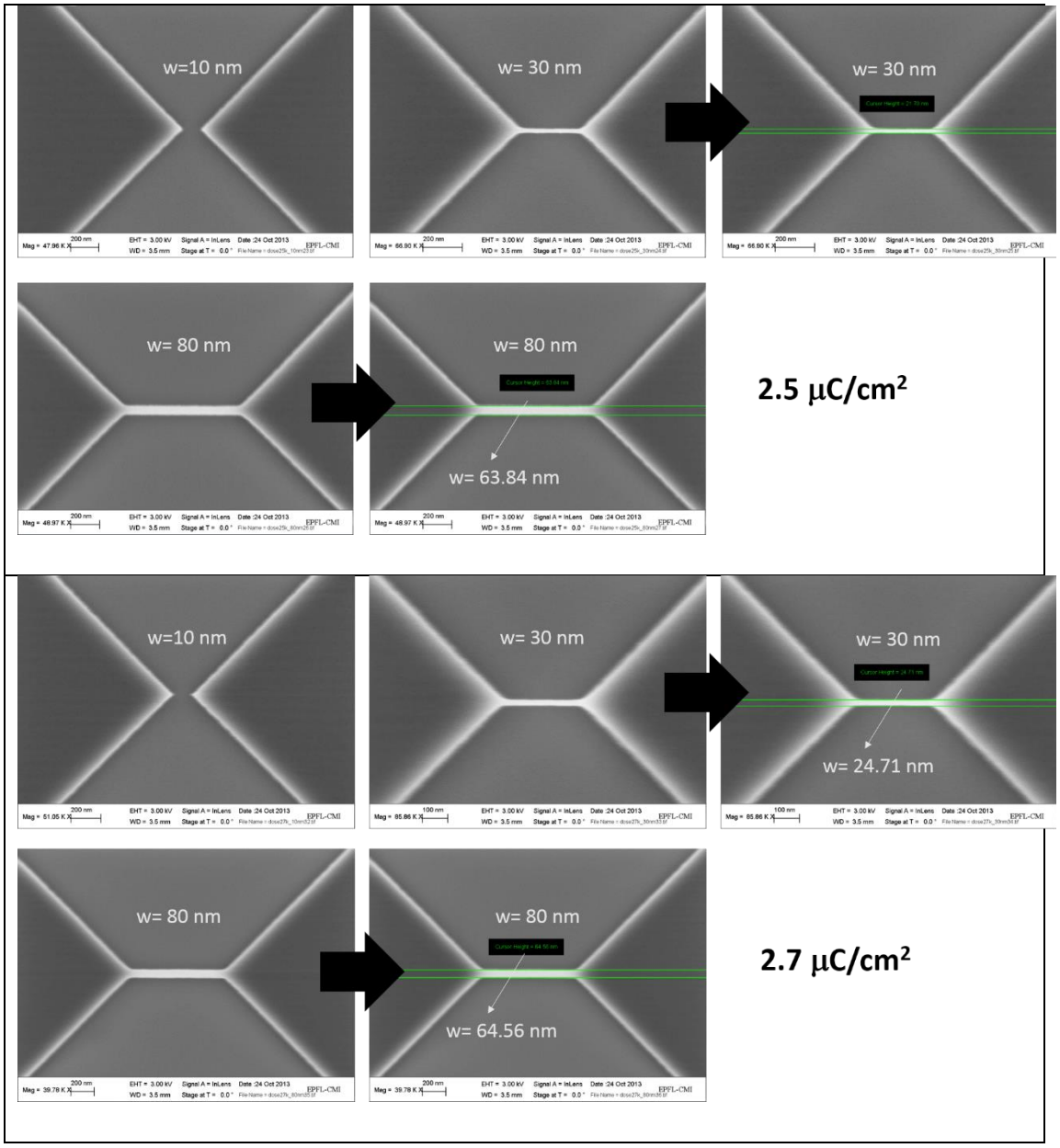
w=10 nm
w= 30 nm
w= 30 nm
w= 80 nm
w= 80 nm
w= 63.84 nm
2.5 µC/cm²
w=10 nm
w= 30 nm
w= 30 nm
w= 24.71 nm
w= 80 nm
w= 80 nm
w= 64.56 nm
2.7 µC/cm²

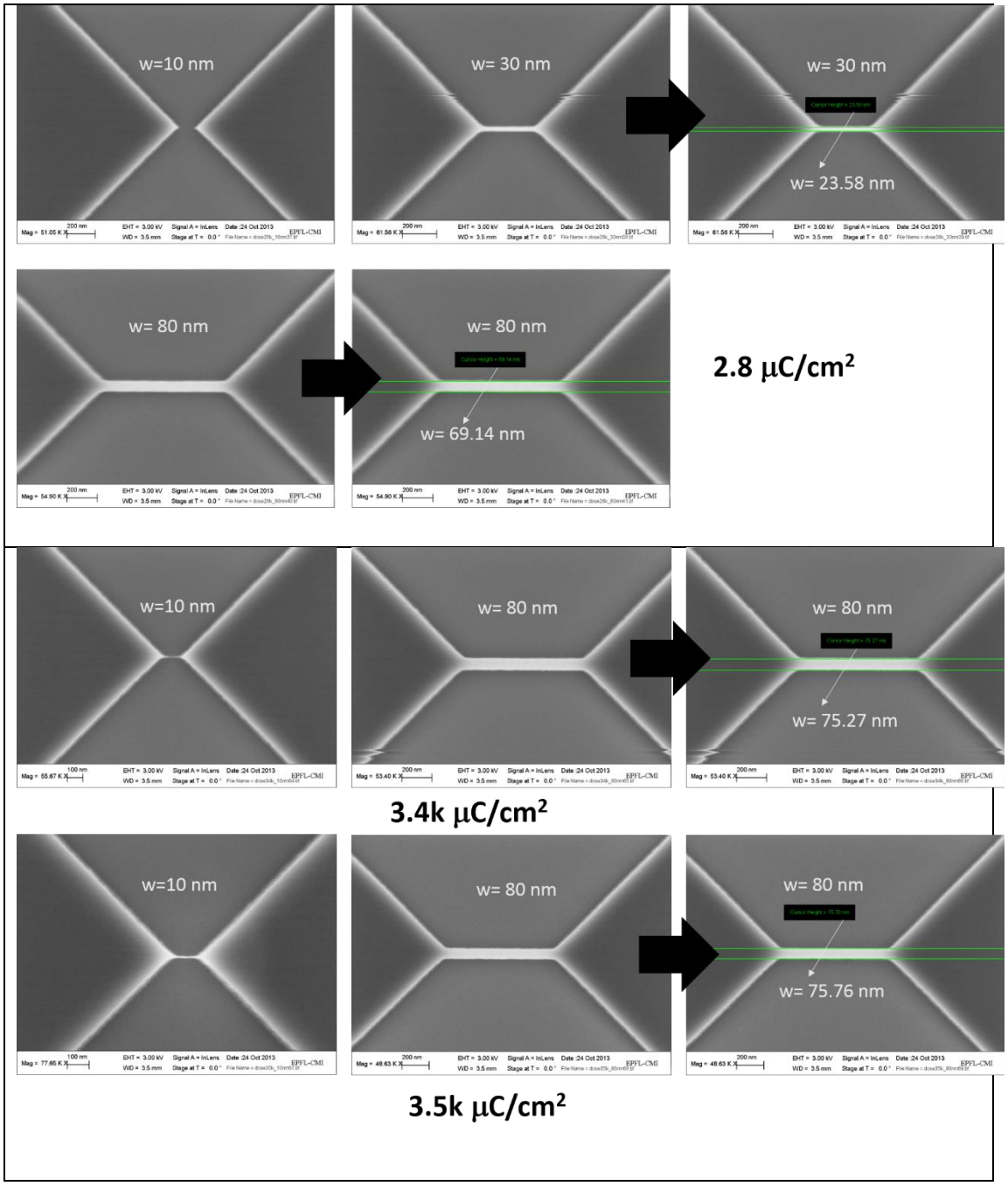
w=10 nm
w= 30 nm
w= 30 nm
w= 23.58 nm
w= 80 nm
w= 80 nm
w= 69.14 nm
2.8 μC/cm²
w=10 nm
w= 80 nm
w= 80 nm
w= 75.27 nm
3.4k μC/cm²
w=10 nm
w= 80 nm
w= 80 nm
w= 75.76 nm
3.5k μC/cm²

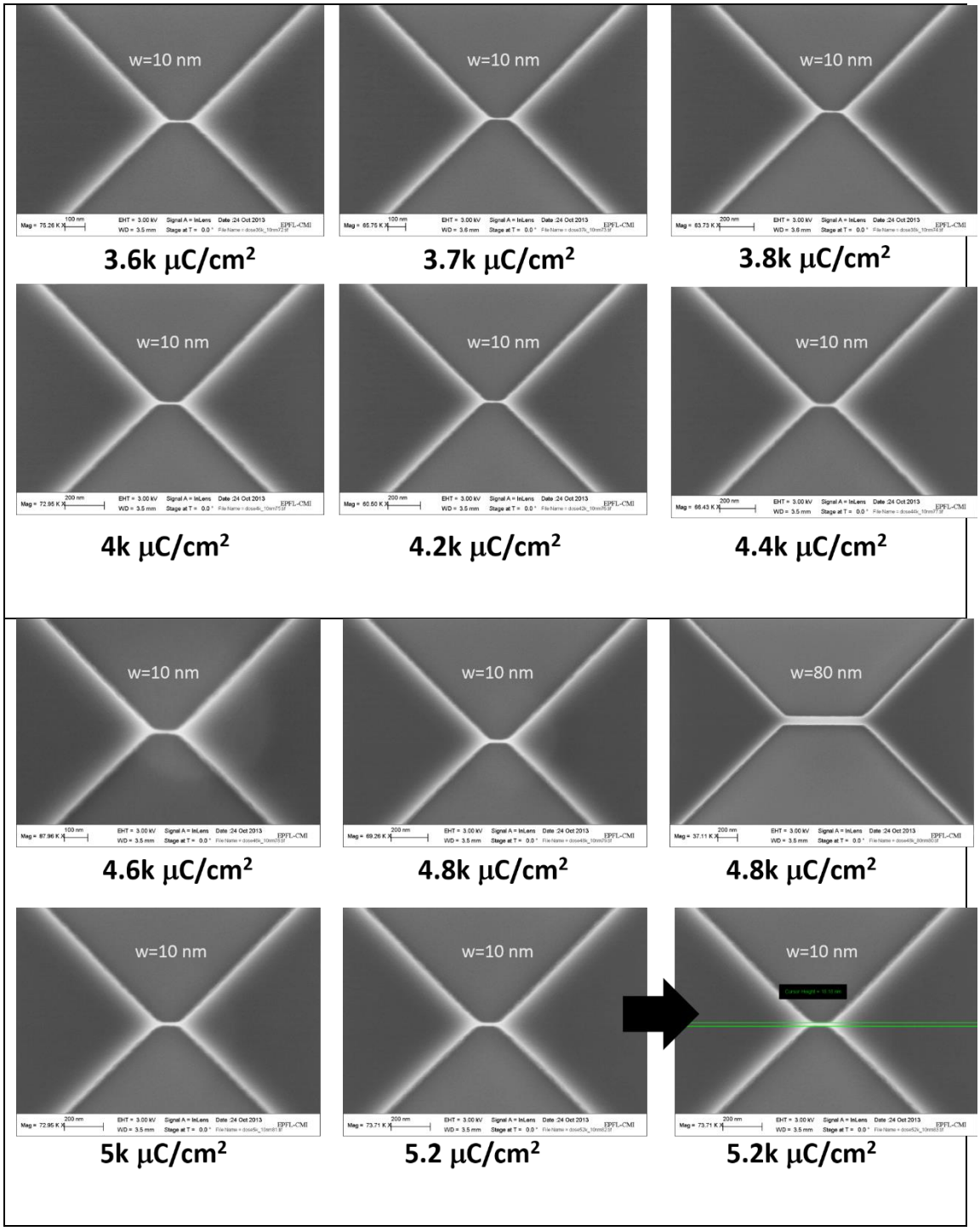
w=10 nm
3.6k μC/cm²
w=10 nm
3.7k μC/cm²
w=10 nm
3.8k μC/cm²
w=10 nm
4k μC/cm²
w=10 nm
4.2k μC/cm²
w=10 nm
4.4k μC/cm²
w=10 nm
4.6k μC/cm²
w=10 nm
4.8k μC/cm²
w=80 nm
4.8k μC/cm²
w=10 nm
5k μC/cm²
w=10 nm
5.2 μC/cm²
w=10 nm
5.2k μC/cm²

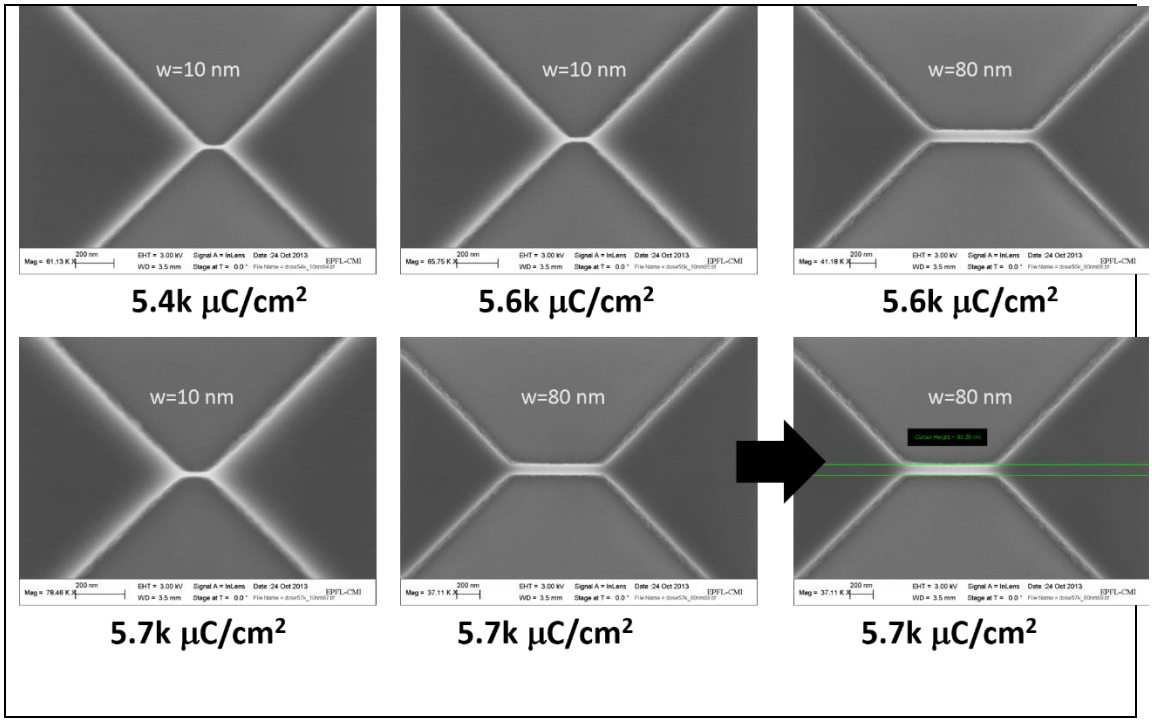
w=10 nm
w=10 nm
w=80 nm
5.4k μC/cm²
5.6k μC/cm²
5.6k μC/cm²
w=10 nm
w=80 nm
w=80 nm
5.7k μC/cm²
5.7k μC/cm²
5.7k μC/cm²

Appendix B: Nano-Mechanical Characterization Efforts

Dimension of the nanowires being tested by the AFM								
Width (nm)	30	50	50	50	80	80	80	80
Length (µm)	4.5	2.5	3.75	5	4	6	8	12

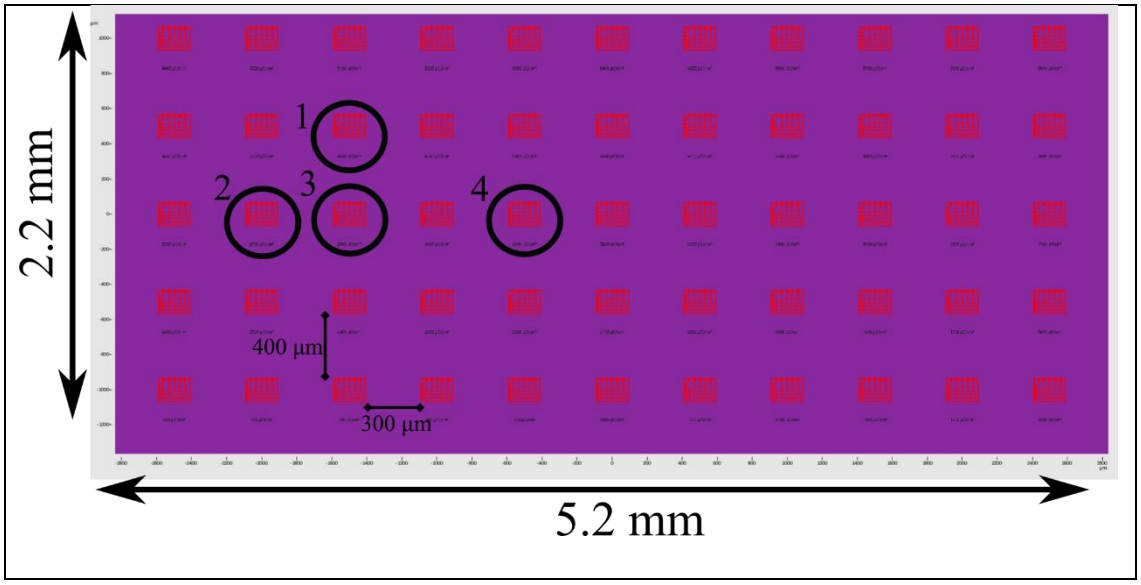

Dose 2800	Dose 2900
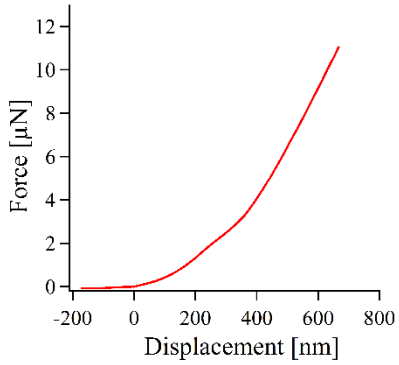	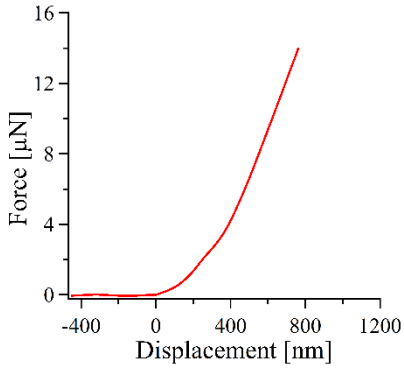
Dose 3100	**Dose 4600**
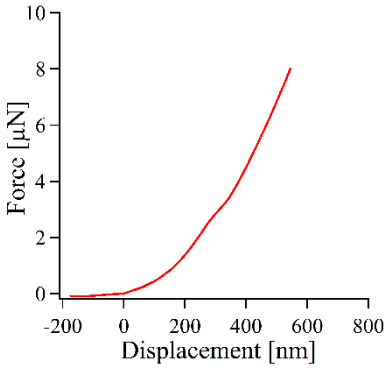	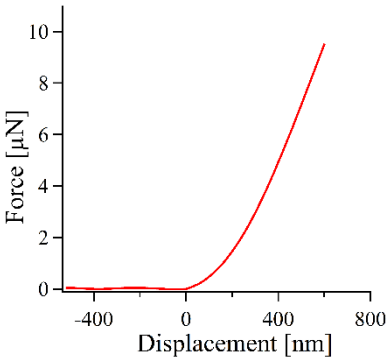
Dose 4700	**Dose 4900**
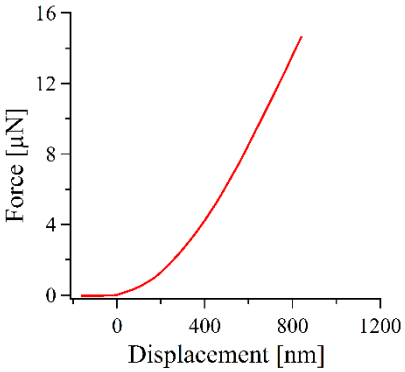	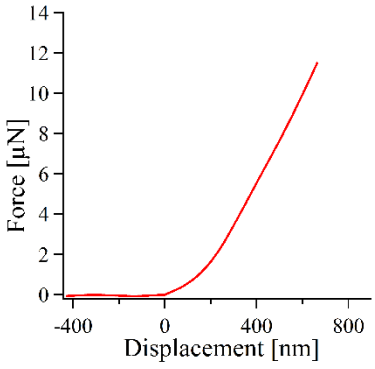

Dose 5700	Dose 5800
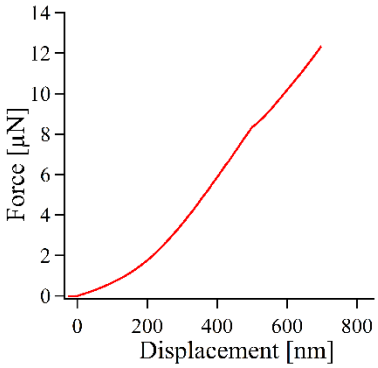	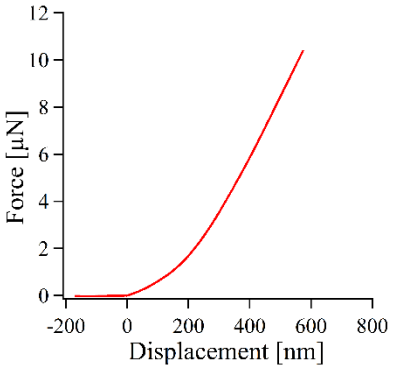
Dose 5800	
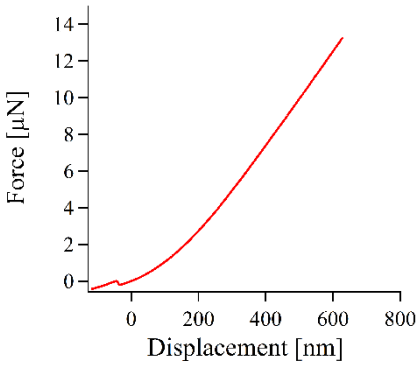	

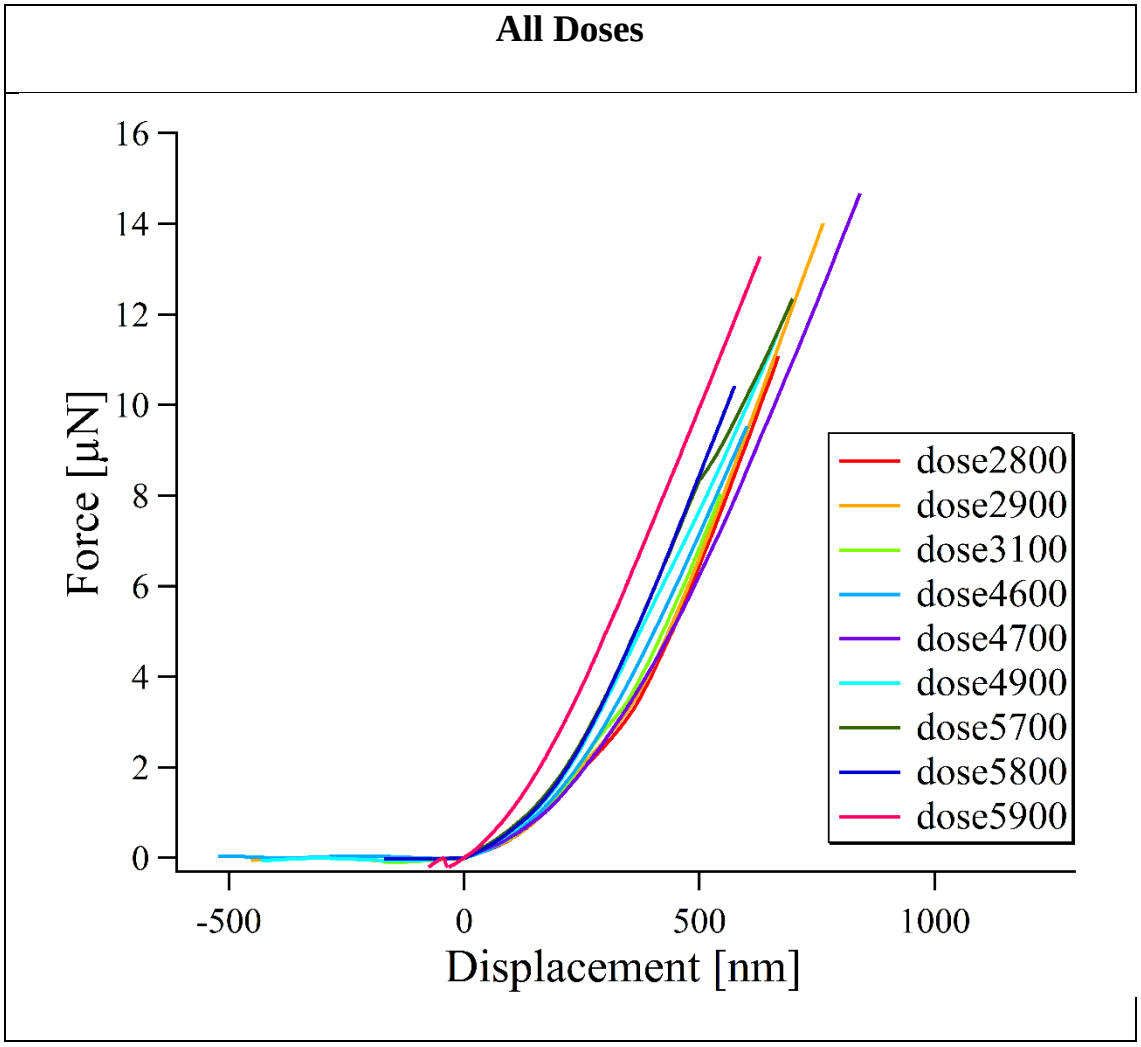
All Doses
16
14
12
10
8
6
4
2
0
Force [µN]
-500
0
500
1000
Displacement [nm]
dose2800
dose2900
dose3100
dose4600
dose4700
dose4900
dose5700
dose5800
dose5900

Appendix C: HRXRD Measurements- Deformation at the atomic scale

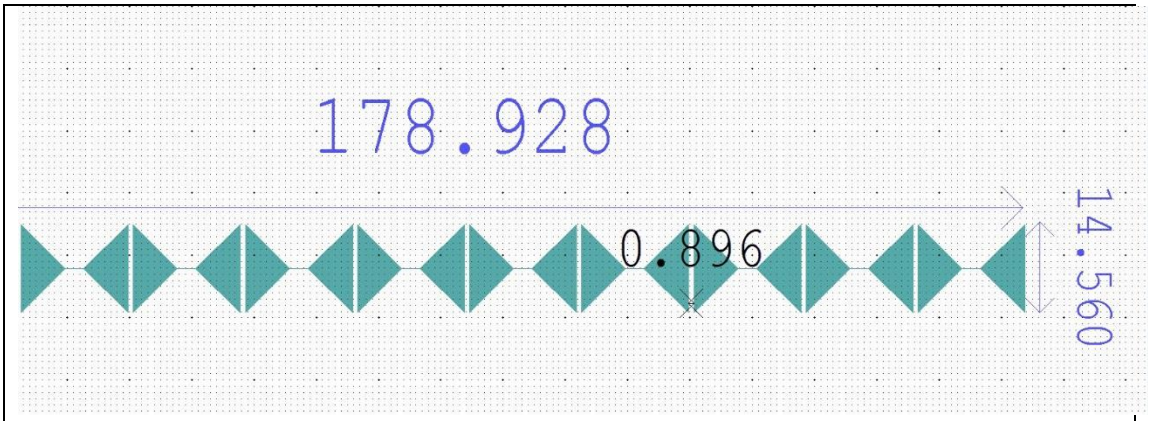

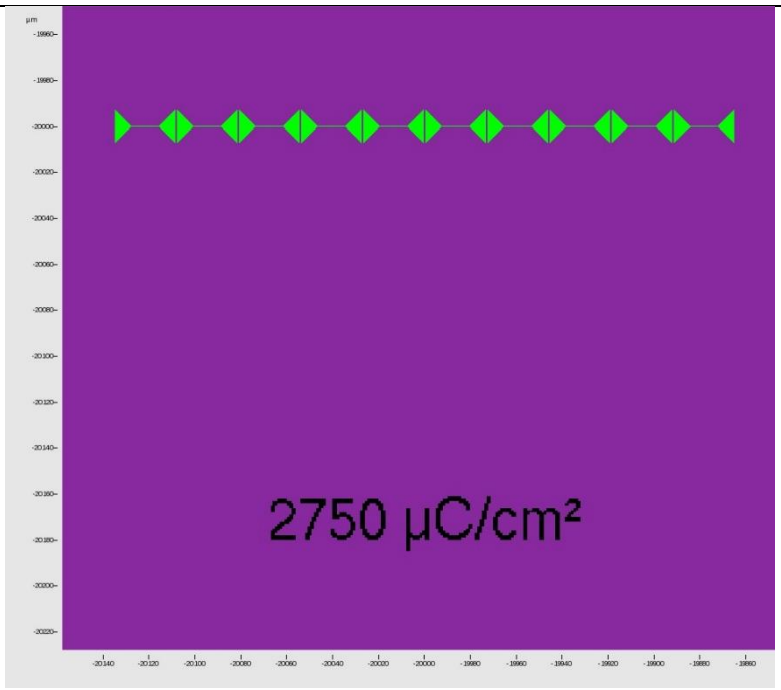

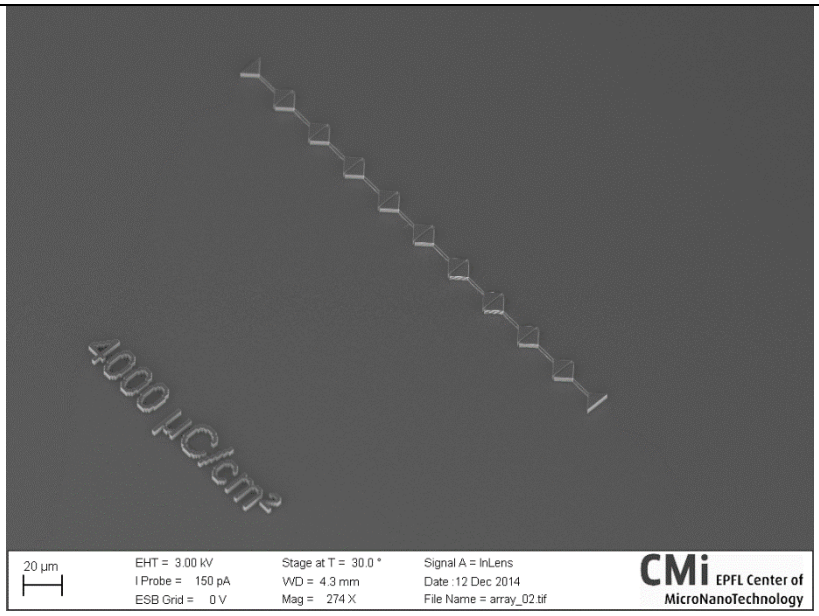
4000 μC/cm²
20 μm
EHT = 3.00 kV
I Probe = 150 pA
ESB Grid = 0 V
Stage at T = 30.0 °
WD = 4.3 mm
Mag = 274 X
Signal A = InLens
Date :12 Dec 2014
File Name = array_02.tif
CMi EPFL Center of MicroNanoTechnology

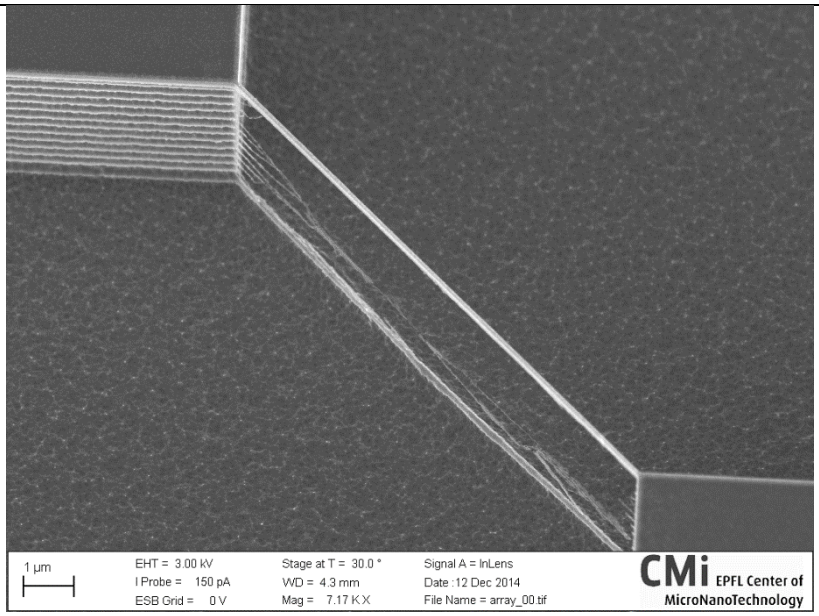
1 μm
EHT = 3.00 kV
I Probe = 150 pA
ESB Grid = 0 V
Stage at T = 30.0 °
WD = 4.3 mm
Mag = 7.17 K X
Signal A = InLens
Date :12 Dec 2014
File Name = array_00.tif
CMi EPFL Center of MicroNanoTechnology